DEPTH PROFILES OF THE "TOP" AND "WHEEL" SIDE OF $Fe_{40}Ni_{40}Si_4B_{16}$ (GLASSY METAL) BY X-RAY PHOTOELECTRON SPECTROSCOPY

A THESIS

PRESENTED TO THE SCHOOL OF GRADUATE STUDIES

AND

THE FACULTY OF SCIENCE

ADDIS ABABA UNIVERSITY

IN PARTIAL FULFILLMENT OF THE REQUIPEMENTS FOR

THE DEGREE MASTER OF SCIENCE IN PHYSICS

by

Solomon Bililign

June, 1985

This work is dedicated to my instructor and friend Mulugeta Bekele who has inspired me to carry on as a physics student.

And my sister yesherhareg.

ADDIS ABABA UNIVERSITY LIBRARY

ACKNOLEDGEMENT.

I offer my deepest gratitude to my advisor and instructor Dr.Peter Mikusik for his dedication and limitless effort in guiding and supervising this work. His rich experience in the field, without which this thesis would not have materialized, helped me facilitate my progress in this work and aroused my interest in the field, for further research.

I would like to express my deep indeptedness to W/t Hiwot Berhane who devoted her valuable and free time in assisting me in the technical preparation of the thesis so neatly.

I would also like to thank prof. Tosi of the ICTP and the Librarian of the ICTP for their help in supplying me with materials I badly needed.

Lastely I would like to thank the Acqusition Department of AAU Library for its kind collaboration in ordering articles not available here from abroad.

ABSTRACT

X-ray photoelectron Spectroscopy is applied to the study of a metallic glass $Fe_{40}Ni_{40}Si_4B_{16}$ prepared by melt spinning method. Spectra of the sample were taken elsewhere by ESCA 3 MARK II spectrometer on the top side and wheel side, in its as recieved form, after sputtering for 5, 15 and 30 minutes respectively and when the sample crystallizes by heating to 580°C. These spectra were recorded for two detection angles 15° and 55° from the surface normal. The core level and valence band spectra are interpreted, and the surface concentration of the top and the wheel sides are calculated after each sample treatment. It is found that the surface is highly contaminated with oxygen and Carbon and these contaminants form rather complicated chemical compounds with the matrix elements. Surface composition after all treatments is discussed and conclusion concerning concentration changes are drawn, eg. it has been observed that the surface is enriched by Boron and Iron after Sputtering. The electronic structures of the amorphous and crystalline samples are found to be similar.

CONTENTS

INTRODUCTION

Metallic glasses (MG) are now-a-days a subject of increasing research effort. They represent a newly recognized and interesting class of metastable solids. MG's prepared on the base of transition metals exhibit technologically interesting properties quite unexpected for solid metals [1].

The theory of crystalline matter based on crystal periodicity and translational invariance is extensively studied, but no such theory is developed for the disordered state.

The motivation to study MG's is two fold. From the technological point of view their good corrosion resistance, high mechanical strength and ductility, great stability against crystallization, superconductivity and interesting magnetic properties have made the study of these materials of great technological importance. From the theoretical point of view they offer the opportunity to study alloy compositions which may not be stable in the crystalline form and to study electronic band structure under the influence of lack of periodicity. Especially MG's formed from simple metals are the ideal testing ground for the microscopic theory of the amorphous state.

Various techniques are employed to study the properties of MG's and probe their structure. But there are many interesting phenomena related to the surface properties of MG's like corrosion resistance, segregation, catalysis and wear, for which electron spectroscopy being surface sensitive could make important contributions.

In electron spectroscopy experiments the electrons emitted from a solid are detected in an electron energy analyzer. In photoemission the electrons are emitted as a consequence of the excitation by bombarding the sample surface by photons. For excitation energies of the order of 1-2 KeV we have X-ray photoelectron spectroscopy (XPS)

Electrons that contribute to the photoelectron line are those that have not undergone any inelastic collsions, they are effectively created within a distance from the surface equal to the electron mean free path. This so called escape depth is generally within 10 to 50 A^{O} for electron kinetic energies relevent in electron spectroscopy [2]. This makes XPS a surface technique, with high sensetivity to the detailed conditions of the outermost atomic layers.

In XPS experiments excitation energy is high enough to ionize inner electron shells as well, and information about the core electrons may be obtained in addition to valence band spectra. From analysis of core line XPS spectra important information may be obtained. Elemental composition of the sample surface within the escape depth of the photoelectrons, can be obtained from XPS since the binding energies of core electrons are measurable for each element. Using the energy dependence of the escape depth of photoelectrons information about the concentration depth profiles can be obtained by measuring the intensities of core electrons with different binding energies of the same element. The change in surface composition can be monitored, and from the knowledge of photoionization cross section absolute composition of alloy surfaces can be determined.

By applying XPS with Ar^+ ion bombardment on MG $Fe_{40}Ni_{40}Si_4B_{16}$ we shall investigate the surface composition of the top-side and wheel-side of the sample. We shall study and interprate the XPS spectra of the sample which has undergone several treatments (sputtering and annealing) and finally we shall study the electronic density around the Fermi level of the amorphous and crystalline sample.

The sample of MG was prepared in KOSICE[+] and photoelectron spectra were recorded in Prague[++]. Aim of this thesis is to (a) determine surface and under surface concentration, of elements contained at the surface of MG. (b) calculate and compare the concentrations between the "wheel-side" and the "top- side" surface, (c) interperate the changes in the chemical composition and (d) determine concentration of elements for five sample surface treatments.

+ Faculty of Sciences: P.J. Safarik university, Kosice, Czechoslovakia.
++ Center of Electron Spectroscopy, Czechoslovak Academy of Science, Prague, Czechoslovakia.

CHAPTER I

METALLIC GLASSES.

By definition a glass is a material obtained from the liquid which does not crystallize during solidification and it is there fore an amorphous solid. The glass is metallic when it contains enough metal atoms so that its physical properties such as electrical and thermal conductivities are similar to those of the crystalline material of the same composition [3].

Amorphous materials are prepared by different methods and metallic glasses (MG's) are amorphous materials prepared by rapid quenching from the liquid state.

Metallic glasses are characterized by the following properties. They show strong similarites to ordinary glass and liquid metals, but in contrast to ordinary glasses, the volume of the glass is nearly the same in the glassy and crystalline state, they show a reversible glass-liquid transition at the glass temperature T_g. At a temperature T slightly higher than Tg they undergo recrystallization. They are metastable with respect to the thermodynamic ground state.

Most of the metallic glass alloys fall into two groups. The transition -transition metal alloys (T-T alloys) and alloys containing at least one transition metal and a metalloid. (T-M alloys) The metalloid is usually P, Si, C or B and they are called glass formers.

The glass forming tendency (for a given rate of cooling and for substances of a given molecular type) is greater the lower is the reduced melting temperature T_r[4].

$$\tau_m \simeq \frac{k T_m}{H_v} \qquad (1)$$

T_m = Thermodynamic crystallization temperature

H_V = Molecular heat of vaporization.

1-1 PREPARATION.

Metallic glasses are prepared by rapid quenching from the melt. The liquid is converted rapidly from a jet or a droplet into a thin layer in contact with a thermal conductor. The cooling rate is usually 10^6 K/sec. Two methods of preparation are in common use [5].

a) Splat cooling: The liquid alloy is squeezed between a rapidly moving piston and a fixed anvil.

b) Melt spinning: A rapidly spinning copper or steel is used to conduct heat away from the melt. The ribbons produced by this technique are 1cm wide and 10μm thick.

1.2 STRUCTURE OF METALLIC GLASSES.

In spite of the absence of a long range order, an essential property of a crystal, the structure of metallic glasses is defined by the local order in a group of atoms involving the first, second and third neighbours of any given atom. From diffraction studies it is accepted that there is no long range order in these solids. But there is a considerable short range order (SRO) [6].

The dense random packing (DRP) of hard spheres is the most widely accepted model to describe metallic glasses. This model gives quite accurate discription of metallic glasses containing only one element. But most metallic glasses are alloys of two or more elements, random packing of atoms is not just possible to built up a model. Since the properties of MG's depend on SRO it is very important to be careful in selecting the initial cluster of a critical number of atoms which then serves as a motive which repeates itself to fill space without being systematically translated in three directions. The choice of the packing in the original cluster is guided by the results of scattering experiments. Of this methods EXAFS (extended x-ray absorption fine structure) has a unique capability of probing the near neighbour environment in multicomponent-systems where the EXAFS for each element can be studied.

In the case of TM alloys experimental data of several techniques suggest two features about their local structure [7].

(a) The first coordination shell around the metalloid is well defined with a narrow distribution of bond lengths, further there is little evidence for coordination number which departs significantly from 8 or 9.

(b) The environment around the metalloid is similar to that observed in the corresponding crystalline phase.The distinctive properties of two similar crystalline structures are observable in glasses also.

In conclusion, DRP models are conditionally acceptable as models for amorphous T-M alloys. And present day knowledge on the models of metallic glasses show a strong evidence that the structure of T-M alloys, requires models with greater complexity than that required by DRP model.

1-3. ELECTRONIC STRUCTURE AND TRANSPORT.

Knowledge and information on the electronic transport properties comes from measurements in electrical resistivity, thermopower and the hall coefficient.

MG s have two important characteristics of electrical conductivity, (a) their resistivity is relatively high, greater than 100$\mu\Omega$cm at room temperature . (b) Thier temperature coefficient is very small and can be zero or negative. ($\pm 10^{-4}K^{-1}$)

The high resistivity of amorphous alloys as compared to the crystalline state is related to the increased scattering of the conduction electrons due to a random atomic arrangement. In such a random structure the phonon contribution to the scattering of electrons is very small causing the small temperature coefficient of resistivity.

The observation of small, zero or negative temperature coefficient of resistivity depends on the concentration and it can be varied on alloying continuously.

The Hall coefficient of simple MG s shows a nearly free electron metal behavior, but the +ve Hall coefficient of Transition metal based glassy alloy's is not yet explained.

Most MG s also show superconductivity.

1-4. MAGNETIC PROPERTIES.

T-M alloys are mostly ferromagnetic with curie temperature T_c above room temperature. They are extremely soft magnetic materials with very high initial and maximum permeabilities and very low coercive fields. They have very low power loses at 50-60 HZ.

In amorphous ferromagnetic alloys the characteristic properties of

magnetization processes and the hysterisis loops are sensitvely affected by fluctuations of material properties and defect structure [8].

It is also shown that the processing condition doesnot affect crystallization, T_c, saturation magnetization and hardness, But the coercive force varies greatly and increases monotonically with an increase in melt temperature and decrease with rotating speed [9].

In the case of TM alloys, the magnetic properties are dominated by the transition metal elements [10].

The megnetic moment and Tc are largely affected by structural disorder when Fe content increases in Fe based MG's, while the effects are small for Ni based MG's .

Further an inhomogenous character of the appearance of magnetism has been evidenced in many MG's. And it has been proved that fluctuations in environmental conditions (coordination number, interatomic distances) favour the inhomogeneous nature of the onset of magnetism in amorphous alloys [11].

1-5. MECHANICAL PROPERTIES.

MG's are very stiff and strong. They are capable of plastic deformation, They have high fracture toughness, high hardness and good wear resistance. They have an exceptionally high bend fatigue strength and very high corrosion resistance.

1-6. APPLICATIONS.

The main interest on MG's is based on their possible technological applications based on their magnetic, electrical and mechanical properties.

The mechanical properties suggest applications as strengthening fibers in composite materials, for structural and aeronautical uses, reinforcement of concrete etc. Owing to their hardness they can be used as cutting edges for cutting tools.

Their interesting magnetic properties, as their small coercive force which results in very low hysteresis loses makes them a good candidate in power transformers. They can also be used as core material in inductive components for electronic circuits.

The high value of resistivity combined with very small temperature coefficient might be of interest in electrical circutery of measuring instruments requiring resistance components insensitive to temperature.

Their very high corrosion resistance suggest chemical,surgical and biomedical uses.

There are other possible applications such as brazing foils, emission cathodes, electrical fusses and hydrogen storage.

CHAPTER II

X-RAY PHOTOELECTRON SPECTROSCOPY (XPS)*

2.1. PRINCIPLES OF PHOTOEMISSION.

In photoelectron spectroscopy photons in a more or less well defined state (energy, direction of propogation, etc) impinges on the surface. Given a sufficiently high energy photon, they excite electrons directly out of the valence band or core levels.

The basis of photoelectron spectroscopy is thus the measurement of energies of electrons emitted from a sample in vacuum following ionization by incident photons. The binding energy of emitted electrons originating from a particular state is obtained from the energy balance equation:

$$E_B = \hbar\omega - E_k \qquad (1)$$

if energy is referred to the vacuum level and:

$$E_B = \hbar\omega - E_k - \phi \qquad (2)$$

if referred from the fermi level where ϕ is the work function of the sample and $\hbar\omega$, energy of the incident particle.

---

* Sometimes the more general name is used, namely ESCA - electron spectroscopy for chemical analysis.

In XPS X-ray photons are the incoming and electrons the outgoing particles to be analyzed, and in such an experiment the sample is actually left in an ionized state after the electron emission hence the sample and photoemitted electrons may be viewed in a one electron picture where the electrons are considered to come from a one electron orbital within the sample without suffering loss in the escape process. An analysis of the energy distribution of photoemitted electrons yields information about the energies of occupied one electron states.

The binding energies in (1) and (2) represent the one electron energy levels of the core shell neglecting the relaxation shift. So XPS allows a direct observation of core terms. This fact immediately provides chemical specificity for the spectra [12]. In an altered chemical environment, the core levels exhibit a small shift due to the different contributions of the charge density of the valence electrons at the core orbit. Thus the chemical shift permits conclusions on the binding of atoms involved.

For XPS, the escape depth or penetration depths are usually very short ranging between 4-40Å and hence observation of photoemitted electrons emphasizes surface contributions and so one can obtain information about surface properties, adsorbed atoms and molecules on surfaces. In the case of adsorbed atoms and molecules, the binding energies of valence electrons can serve as a "chemical fingerprint" of the adsorbed species so that one can use the photoemission spectrum to follow chemical reactions on the surface [13]. When dealing with pure surfaces, the experiments are very sensitive to surface cleanliness and contamination. Thus reliable work requires ultrahigh vacuum and in situ prepared surfaces [14].

2.2 THEORY OF PHOTOEMISSION - THE THREE STEP MODEL.

The theory of photoemission is quite complicated and highly involved. A description is needed of both the equilibrium and excited electronic structure of a material and its interaction with the ion array with the driving electromagnetic fields, whose form is modified by the interaction. Both problems must be solved in the vicinity of the surface through which all system properties change dramatically.

Various attempts are made to incorporate all known phenomena in the theory of photoemission.

Photoemission is a many body problem. In real solid the electrons are involved in several types of interactions like electron-electron, electron- impurity, electron-phonon interaction. All these involve inelastic processes and are very important in photoemission. A microscopic formulation of photoemission process that includes inelastic scattering is developed by C.Caroli et al [15].

The significance of angular anisotropy in photoemission, and the influence of band structure in the photoemission processes is also studied [16].

In this thesis the interpretation of photoemission spectra is based on the three step model developed by Berglund and Spicer [17].

In this model photoemission is envisaged as three independent steps:- photoabsorption, propagation of excited electrons to the surface, and their escape into the vacuum.

The energy distribution curve (EDC) of the photoemitted electrons $I(E,\omega)$ is thus a sum of the primary distribution of electrons that have not suffered an inelastic collision and a background of secondary electrons which have suffered energy losses due to collisions.

$$I(E,\omega) = I_p(E,\omega) + I_s(E,\omega) \qquad (3)$$

In line with the three step model, the primary distribution is a product of three functions, the distribution of photoemitted electrons $P(E,\omega)$ the transmission function $T(E)$, and an escape function $D(E)$.

$$I_p(E,\omega) = P(E,\omega) \times T(E) \times D(E) \qquad (4)$$

To determine the energy distribution of photoemitted electrons, we start by calculating the probability of electron escape based on the following assumptions.

a) the distribution in direction of excited electrons is isotropic,

b) probability of inelastic scattering can be described in terms of a mean free path which is a function only of the electron energy.

c) In order to escape over the surface barrier, the electron must have a component of its total crystal momentum P perpendicular to the surface which is greater than some critical value P_c.

Choosing the surface of the photoemitter to be the plane $x=0$ with x increasing into the photoemitter, and if θ is the angle between the direction of electron momentum upon excitation, and the normal to the photoemitting surface , then the electron must move a distance $x/\cos\theta$ to reach the surface.

The probability of electron escaping without loss of energy following excitation to energy E is

$$P_{esc}(E,x) = \frac{1}{2}\int_0^{\cos^{-1}(P_c/P)} e^{-x/\lambda\cos\theta}\,\sin\theta\,d\theta \quad \text{if } P \geq P_c$$

$$= 0 \qquad P < P_c \qquad (5)$$

λ is the mean free path for inelastic scattering.

Under the assumption that the inelastic scattering probability can be characterized by an isotropic mean free path $\lambda(E)$ that depend only on the energy E, the transmission function T(E) is given interms of $\lambda_e(E)$ and the attenuation length of the photon $\lambda_{ph}(E)$.

$$T(E) = \frac{\lambda_e(E)/\lambda_{ph}(E)}{1 + \lambda_e(E)/\lambda_{ph}(E)} \qquad (6)$$

According to assumption (C) the escape from the solid is possible only for those electrons with a kinetic energy sufficient to surmount the potential barrier $E_F + \phi$. Assuming the photoelectrons to be plane waves with $E = \frac{k^2\hbar^2}{2m^*}$ this condition defines an escape cone with an opening angle relative to the surface normal.

$$\cos\theta = \left(\frac{\phi + E_F}{E}\right)^{1/2} \qquad (7)$$

For an isotropic distribution of electrons inside the solid, the fraction D(E) which escapes is given by

$$D(E) = \frac{1}{2}\left[1 - \left(\frac{E_F + \phi}{E}\right)^{1/2}\right] \quad , E > E_F + \phi$$

$$= 0 \quad , E < E_F + \phi \qquad (8)$$

D(E) like T(E) is a smooth function of E beyond the low energy cut off, and while both factors may distort the energy distribution of photoexcited electrons, they are not in themselves expected to give rise to structures in $I_p(E,\omega)$.

The primary physical feature characterizing the surface photoeffect discribed by $P(E,\omega)$ is the existence of a vector potential. The quantum mechanical interaction of an electromagnetic field of vector potential A with an electron is given by

$$Hint = (\vec{A}.\vec{P} + \vec{P}.\vec{A}) \qquad (9)$$

Where P is the momentum operator of electron and terms of higher order in A are neglected. If this interaction appears as a small perturbation in a quantum mechanical system, the electron transition rate from an initial state|i> to a final state|f> is governed by the matrix element $M_{fi} = \langle f|Hint|i\rangle$. The photoelectron current observed through an analyzer set at the energy E and band width dE and accepting a solid angle d is given by

$$\frac{d^2J}{dE\,d\Omega} = 2eV\left(\frac{e}{2mc}\right)^2\left(\frac{\eta}{2\pi\hbar^2}\right)^2\sum_{fi}|M_{fi}|^2\,\delta\left(E-\hbar\omega-E_i\right) \qquad (10)$$

Where v is the observed electron velocity and - function insures energy conservation. The current is expressed as a sum over all occupied initial states. Thus the observed photoelectron current is determined essentially by the initial density of states |i> contributing as energy conservation permits with an intensity given by the square of the matrix element M_{fi}.

This means that the observed spectrum will reflect the initial state density provided sufficient number of final states is available and the matrix element may be regarded constant.

Intensity of the emission current and so the spectral shape is determined by the coupling strength due to the operator in the matrix element.

In XPS $\hbar\omega \approx 1.5$ keV) core levels become observable. Final states are free electron like and the matrix element is not affected by the surface conditions. Density of free electron final states is regular and slowly varying. Then the spectra are expected to change gradually representing the initial density of states. Thus under constant matrix approximation $P(E,\omega)$ reduces to the energy distribution of joint density of states (EDJDOS).

$$P(E,\omega) \sim \sum_{if} d^3\vec{k}\,|M_{fi}|^2\,\delta\left[E_f(k) - E_i(k) - \hbar\omega\right]\delta\left[E_f(k) - E\right] \qquad (11)$$

It follows that photoelectron spectrum is essentially a distorted replica of EDDOS in the framework of the three step model.

Despite the number of assumptions made however, the three step model has been quite successful in explaining photoemission spectra. The step model totally neglects surface effects and uses stationary one electron eigenfunctions in calculating transition matrix elements that involve highly excited final states. But these can be neglected while dealing with XPS.

2.3. BINDING ENERGY OF ELECTRONS : RELAXATION AND CHEMICAL SHIFT.

Binding energy of an electron is defined as the work required to remove the electron from its orbital to infinity with no kinetic energy. This ionization process leaves the system in an excited state and the binding energy is essentially equal to the difference in the total energy immediately after and before the ionization.

In the first approximation, the removal of an electron does not change the field inside the atom and one may assume that the orbitals of the other electrons remain unchanged during the process.

This is a single electron picture, but when considering N electron system, the removal of an electron by photoemission would leave (N-1) electron system. If N is very large the effect would be negligible, and the single electron picture could be employed, However if N is small, the removal of a single electron would force the other electrons to adjust to the new field leading to a relaxation to a lower energy. This extra energy is picked by the emitted electron and it appears at a higher final state energy.

In a polarizable medium the hole created by the photoemission process

acts as a local positive charge and attracts electrons that tend to screen it. The screening lowers the total energy and the difference in energy is again carried away by the photoemitted electron. This is common in adsorbed atoms or molecules on surfaces.

As a result of this rearrangement of atomic orbitals, the total energy is lowered by the relaxation energy ΔE_R, Hence one would measure

$$E_B = E_B^F - \Delta E_R \qquad (12)$$

Where E^BF - is the binding energy for the case of "frozen" orbitals, corresponding to the wave function values of the unperturbed system

The exact value of the binding energy measured for a given element depends on the chemical enviornment of that element. As a result core XPS lines show binding energy shifts. The binding energy shift is the binding energy difference [18].

$$\Delta E_B = E^{alloy} - E^{pure\ metal} \qquad (13)$$

Where E^{alloy} and $E^{pure\ metal}$ are the binding energies of core electrons related to an atom in an alloy and in the corresponding pure metal. The physical origin of this shift is related to the change transfered on forming a chemical bond between two disimilar atoms and the altered screening condition of the positive nuclear charge. This shift can be used to identify the chemical environment of an element by comparison with the binding energies of a set of reference compounds involving the same element.

Various methods are used in the calculation of binding energy shifts

theoretically [14].

The binding energy E_b^i of the level i is the difference in total energy E of the system in its ground state and the state with one electron missing in the orbital i

$$E_B^i = < E, q_i \ 0 \ n-1 > - < E, q_i = n > \qquad (14)$$

Calculation of the chemical shift E_B involves the calculation of 4 total energies, a ground-state and a hole state calculation for each system. This method uses the Hartree-Fock method of independent electron approximation, where the electron is assumed to move in a potential determined by the nuclei and the average field of all other electrons. Wave functions are expressed as Slater determinants and no correlation between electrons of different spin is considered.

The other method treats relaxation energies as perturbations on binding energies derived from ground state properties alone.

In the case of alloys, several factors contribute to the shift of the XPS electron binding energies (ΔE_B^F for an atom in a solid [19].

These are difference in valance electron density $\frac{\Delta q}{r}$ crystal field potential (ΔV) work function, ($\Delta \phi$) and relaxation energy (ΔE_R) . This is expressed as

$$\Delta E_B^F = \Delta q/r - \Delta V - \Delta E_R - \Delta \phi \qquad (15)$$

When considering metals and alloys, There seems to be a difference in core level binding energies between surface and bulk atoms. This difference is due to the fact that surface atoms experience a potential different from the bulk due to the lower coordination number [19].

2.4. SECONDARY ELECTRONS:- ENERGY RESOLUTION

Ideally there arises only a single peak due to electron ejection in photoemission. This corresponds to the removal of a single electron which yields a single final electronic state. However, photoemission is a many electron event, and the removal of an electron causes the other electrons to adjust to the new environment, and they can no longer be in the ground state. These new states are accessible to final state electrons, giving rise to assymmetric peak shapes, various peak widths, as well as peak splitting.

The asymmetries in the XPS corelines are due to the creation of electron hole pairs at the Fermi level during the photoemission process.

The width of core levels (Γ) is determined by (a) resolution of the photoelectron spectrometer (Γ_{sp}). The energy resolution of analyzers is usually defined as the ratio $\Delta E/E_o$. Where ΔE is the full width at half maximum (FWHM) of the energy distribution after the analysis of a monochromatic beam, and E_o is the energy at which the analyzer is tuned, (pass energy). In calculations it is often easier to determine the base resolution ΔE_b and for wall designed analyzer, $\Delta E = \Delta E_{b/2}$ [20]. (b) presence of satellites that are not resolved and (c) the intrinsic life time width of core holes.

Satellite broadening can be brought about by the influence of phonons whose contribution to the line width is proportional to the square root of E_R and the ratio of the longitudinal optical phonon energy $\hbar\omega_{LO}$ to the energy equivalent of the temperature T, 2KT [14] and is expressed as

$$\Gamma_{phonon} = 2.35 \left(\hbar\omega_{LO} E_R \coth \frac{\hbar\omega_{LO}}{2kT} \right)^{1/2} \qquad (16)$$

(16)

Where E^R is the relaxation energy

The intrinsic width of a line is determined by the life time of the hole left behind the photoemission process. Γ and τ are related through Heisenberg's uncertainity relation

$$\Gamma_{int} = \frac{\hbar}{\tau} \qquad (17)$$

The width of the core line determined by all the three factors is thus expressed as

$$\Gamma = \sqrt{\Gamma_{int}^2 + \Gamma_{ph}^2 + \Gamma_{sp}^2} \qquad (18)$$

As a result of many electron processes, several peak splittings appear in the spectra. As a result of coupling of electron spin and angular momentum, spin-orbital splitting occurs, and whenever an interaction takes place between the unpaired electrons formed by photoelectron ejection and any unpaired electron already existing in the atom in any of its incomplete shells, multiplet splitting arises.

Apart from splittings, asymmetries, peak widths, and satellite structures are observed. The sudden removal of an electron from one of the inner shells of an atom, causes a change in the effective charge experienced by the electrons in the outer shell which may lead to the simultaneous removal of one of these electrons which if excited to a

discrete state gives rise to shake up satellite and if it goes into continuum we have a shake off satellite.

Finally the occurence of inelastic scattering events, -electron-electron, electron-impurity and plasmon excitations, give rise to secondary electrons.

A proper interpretation of XPS spectra is possible if the effects mentioned above are properly understood, and one should be aware of this things to avoid misinterpretation.

2.5. QUANTITATIVE DETERMINATIONS BY XPS.

XPS is widely used for quantitative determinations of elemental composition of surfaces. For the determinations of composition profiles to greater depth XPS is combined with inert-ion bombardment of the surface and the erosion of the surface layer would proceed layer by layer. This technique involves the recording of several XPS spectra after every ion bombardment.

Recently a new technique is proposed [21] in which information on the depth composition is extracted from a single XPS spectrum. This method relies on the fact that due to elastic and inelastic electron scattering the energy distribution of the emitted photon excited core electrons depend strongly on their depth of origin. In this method a quantity is defined which is a ratio of XPS peak area to the increase in the background signal associated with the peak. This quantity is a strong function of the depth composition for inhomogeneous samples.

In this work we shall follow the former method. The counting rate detected in photoelectron peak from an element in a thick homogeneous sample covered by a contaminating adsorbed layer is given by [22].

$$I = A n f \sigma \phi y T \lambda C \qquad (19)$$

Where

A - sample area from which photoelectrons are detected

n - concentration of atoms per cm^3.

f - photon flux in photon per cm^2

σ - cross section per atom for photoionization of the particular level

ϕ - angular correction factor

y - fraction of photoelectric transitions from the given level that result in an ion in the ground state and a photoelectron of appropriate energy

T - inherent effeciency of detection by the spectrometer of electrons originating from the sample.

λ - mean free path of photoelectrons in the sample medium

C - fractional efficiency of emergence through a contaminating adsorbed layer.

And for a given homogeneous solid

$$n = \frac{I}{A f \sigma \phi T \lambda C y} = \frac{I}{S} \qquad (20)$$

where $S = A f \sigma \phi T \lambda C y$

Thus for two elements in solid

$$\frac{n_1}{n_2} = \frac{I_1 S_2}{I_2 S_1} \qquad (21)$$

In applying this relation, we are interested in ratios of concentrations and hence factors that are kept constant in the experimental procedure cancel out.

The factors that are kept constant are

A = area of the sample, f = photon flux in photon/cm^2

Y, ϕ, C, are also kept constant.

Thus the ratio of concentrations are dependent on σ, λ, T, and I. Let's consider each of these separately.

a) Photoionization Cross Section σ

An exact knowledge of the subshell photoionization cross section is a prerequisite for the quantitative analysis of the surface chemical composition by XPS.

The partial cross section depend on the angle θ between the incoming x-ray beam and the outgoing electrons according,

$$\sigma_\theta = \sigma_o \left[1 + \beta/2 \left(\frac{3}{2} \sin\theta - 1 \right) \right] \qquad (22)$$

σ_o = is the total atomic cross-section

The parameter β varies from -1 to +2 depending on the angular momentum of the atomic orbitals and photoelectron kinetic energy. For energies in excess of 100eV it levels off at the value β =2 (s -shell) and β =1.5 (p shell). The correction is not more than 10% for θ =90^o.

b) Electron Inelastic Mean Free Path, λ

Analysis of experimental factors shows that the IMFP has a minimum value for energies around 100eV and that at higher energies it varies roughly as the square root of the electron energy.

Thus if we neglect the dependence on sample material, we have [23]

$$\lambda(E) \sim E^{\frac{1}{2}} \tag{23}$$

c) Transmission Function of Electron Analyzer, T.

T takes the energy dependence of the analyzer transmission into account.

For a commonly employed analyzer with preretardation and constant pass energy,

$$T(E) \sim (E)^{-1} \tag{24}$$

Thus the ratio of concentrations of two elements in a given sample is

$$\frac{n_1}{n_2} = \frac{I_1 \sigma_2 \lambda_2 T_2}{I_2 \sigma_1 \lambda_1 T_1} \tag{25}$$

Where the subscripts 1 and 2 stand for two different elements.

The intensity of a given line for a given element is related to the area under the spectra a corresponding to the appropriate peak, and the instrumental conditions. Specifically

$$I \sim aS$$

and (26)

$$I \sim 1/N$$

where S - is the digital scale

N - is the number of sweeps.

thus Eq (25) can be written as

$$\frac{n_1}{n_2} = \frac{a_1 S_1 \sigma_2 \lambda_2 T_2 N_2}{a_2 S_2 \sigma_1 \lambda_1 T_1 N_1} \qquad (27)$$

Using the explicit dependence of T and λ on the kinetic energy of photoemitted electrons from Eq (23) and Eq (24) we have

$$\frac{n_1}{n_2} = \frac{S_1 a_1 \sqrt{E_1}\, \sigma_2 N_2}{S_2 a_2 \sqrt{E_2}\, \sigma_1 N_1} \qquad (28)$$

In this approach the following factors could contribute to the variability of the values of n_1/n_2.

a) Emitted intensity of a particular photoionization line is reduced by a factor [24].

$$\lambda(E) = Exp\left[-\langle d \rangle / \lambda'(E) \right] \qquad (29)$$

Owing to the attenuation of photoelectrons within the sample and by

any adsorbed gas layer $\lambda(E)$ and $\lambda'(E)$ represent attenuation lengths for electrons in the sample and overlayer respectively, while <d> is an estimate of the average distance which an electrons will travel through the adsorbed gas layer before escaping into vacuum. We have neglected this term in the ratio n_1/n_2 which could cause an error if the contamination is high.

There can be inaccuracy in integrating the photoelectron peaks (uncertainity in choosing the base line).

2.6. ION SPUTTERING

Ion bomardement sputtering is widely used in combination with surface analysis to determine elemental composition of solids as a function of depth (composition profiling).

The surface composition of an alloy undergoing sputtering will be significantly different from its bulk composition if the sputter yield of constituents are not equal. The species with the highest sputter yield will be initially sputtered preferentially and this causes the near surface region to be enriched in the constituents with a lower sputter yield. Since the concentration of the material sputtered from the surface must be equal to the concentration of the bulk material, in the steady state the surface concentrations of the constituent elements must be proportional to their bulk concentrations divided by their effective sputter yields [25].

Apart from creating differences in concentration on surfaces, ion bombardment creates severe microroughness which can influence depth profiling measurements in several ways. Depth resolution and sensitivity of instruments are influenced by topography.

Further ion bombardment of a solid surface can cause motion of sample

constituents in several ways. An atom in the solid can suffer a collision with the incoming ion and can be driven deeper into the solid (recoil implantation or knock on process). Diffusion processes (both bulk and surface) is greatly enhanced by ion bombardment. This expedites segregation of constituents.

In the case of oxides, unless the partial pressures of all oxygen containing molecules are very low there is the possibility that, an ion bombardment induced reduction of the oxygen concentration in the altered layer will be obscured by re- oxidation of the gas phase species, and further more the sticking coefficient can be dramatically increased by ion bombardment.

To determine the bulk composition of an ion sputtered sample from a measurement of surface concentration of altered layer requires a knowledge of the effective sputter yield of the various components in a multicomponent solid.

Several factors are considered to be responsible for sputter yield. Atoms of lower mass are considered to have a higher sputter yield in an alloy. Sputter yield also depends on the binding energies (heat of vaporization). The component with a lower binding energy will have a higher sputter yield.

Usually the relative sputtering yields of components in a multi component system is given by the sputtering yields of the pure elemental constituents.

For a perpendicular angle of incidence, the sputter yield of a pure element is shown to be given by [26]

$$Y = \frac{0.042\ \alpha \left(M_2/M_1\right) S_n(E)}{U_s} \qquad (30)$$

Where U_s = Surface binding energy

(Sublimation energy)

$S_n(E)$ = Nuclear stopping cross section

$\alpha (M_2/M_1)$ = energy independent function of mass ratio between target mass M_2 and ion mass M_1.

$$S_n(E) = 4\pi Z_1 Z_2 e^2 a_{12} \left[\frac{M_1}{(M_1+M_2)}\right] S_n(\epsilon)$$

and

$$a_{12} = 0.8853\, a_0 \left(Z_1^{2/3} + Z_2^{2/3}\right)^{-1/2}$$

$S_n(\epsilon)$ is the reduced nuclear stopping cross section for the Thomes Fermi interaction.

$$\epsilon = \frac{M_2 E / M_1 + M_2}{Z_1 Z_2 e^2 / a_{12}}$$

a_0 = bohr radius

Z_1 and Z_2 are atomic numbers.

$S_n(\epsilon)$ is the reduced nuclear stopping cross section and the values are given for thomas-Fermi interaction.

The equation above only gives the dependence of the sputtering yield on the energy and mass at a perpendicular angle of incidence. It is also shown that [27] the sputtering yield coefficient is proportional to Sec θ_o where θ_o is the angle of incidence of the bombarding particle. As increases the sputtering coefficient is observed to increase not so rapidly as Sec θ_o and at $\theta_o > \frac{\pi}{3}$. The sputtering coefficient reaches the maximum and it starts to decrease after this.

Once the sputter yield is known, we need to know the amount of material which must be removed from the virgin surface before steady state condition is reached. Since the rate of ion etching at a particular point on the surface profile depends on the corresponding angle of incidence (θ). The surface erosion generally takes place at different rates at different points on a rough surface.

Assuming that the sputter rate is a function only of the beam specimen geometry, the erosion at a given point (x,y) is described by [28].

$$\frac{\partial r}{\partial t} = -\frac{\Phi}{N} S(\theta) \cos\theta \qquad (31)$$

Where $\frac{\partial r}{\partial t}$ is the erosion rate along the direction.

Normal to the surface at (x,y), Φ is the ion flux (ions $m^{-2}s^{-1}$) assumed constant over the eroded surface N is the surface atomic density, $S(\theta)$ is the sputtering yield from the surface. The figure below shows the sputtering geometry.

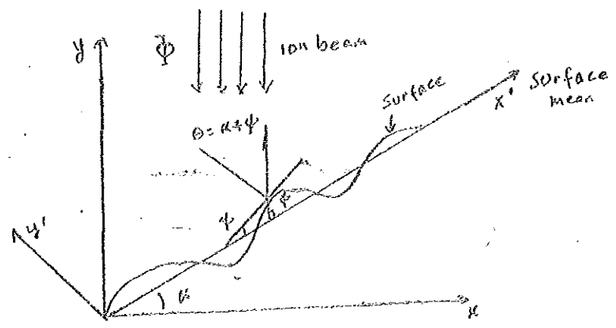

Sputtring Geometry for a two-dimensional irregularly-rough surface with the ion beam incident on any point on the surface at an angle to the surface normal at that point.

CHAPTER 3

EXPERIMENT

MG $Fe_{40}Ni_{40}Si_4B_{16}$ was prepared by the melt spinning method (using one wheel only). From the ribbon of 10mm wide and 10μm thick, there were cut two samples. One was measured on the "top side" and the other on the "wheel-side".

prior to inserting into the preparation chamber of the spectrometer ESCA 3 MARK II of Vacuum Generators, they were first washed in aceton and then in a mixture of pure benzine and ethyl alcohol in ultra sound frequency washer. Finally they were dried by fan in dried air and inserted into the spectrometer. We define this treatment of the sample as "as recieved". All other treatments were done "in situ" in UHV. Ion bombardement of samples was done with argon ions of energy 1.6KeV and ion current density of $10\mu A cm^{2}$ in three steps, that is, 5,15 and 30 minutes respectively. The final treatment consisted of pure heating of the sample in UHV (in situ!) to $580^{o}C$.

Photoelectron spectra were obtained upon excitation by $Al_{K\alpha}$ line (photon energy =1486.6eV). The X-ray lamp conditions were defined by 8kV acceleration voltage of electrons, and 20mA current of electrons. The hemispherical analyzer of 10cm radius was set to 100eV pass energy and the slit width was 4mm. The spectrometer was caliberated to the Au 4f7/2 line of binding energy 84eV. Binding energies were determined with an accuracy of $\pm$0.15eV.

After each treatment photoelectron spectra were recorded under two detection angles (15^{o} and 55^{o})measured from the sample surface normal.

CHAPTER 4

RESULTS AND DISCUSSION

In the discussion that follows reference is made to the spectra in appendix A and tables in appendix B. In appendix A, the wide scan spectra, the valence band spectra and the spectra of individual elements are shown for the two detection angles on the wheel-side and top-side of the sample. The wheel-side refers to the sample side in contact with the copper wheel and the top-side refers to the one open to the air, during the preparation of the sample.

The intensity is given in arbitrary units where the intensity of each spectrum is compared to the intensity of the as recieved sample and is stated as multiples of the latter as indicated on the left side of the figures. The numbers on the right side corner indicate sample treatments where the numbers 1 to 5 refer to the spectra of (1) the as recieved sample (2) to the 5 minutes sputtered sample (3) to the 15 minutes sputtered sample (4) 30 minutes sputtered and (5) to the sample heated to 580^{o}C respectively. In appedix B we have tables of the results of concentration calculations for both angles and both sides of the sample and for each treatment.

4.1 QUALITATIVE INTERPRETATION

4-1.1 The Wide Scan Spectra.

The wide scan spectra serve as a preliminary qualitative identification of elements present within the surface, usually one can quickly judge the

cleanliness of the surface or in other words to determine the contaminants present.

Both the wheel-side and the top-side of the sample surfaces are covered with the contaminants. They are contaminited with C and O and to some extent with N, which appears only on the as recived sample. The C_{1s} and O_{1s} and N_{1s} peaks are observable. The peaks due to the matrix elements in the sample are not resolved, however after 5min sputtering these are observable. After 30minutes sputtering the C_{1s} and O_{1s} peake are weak and the N_{1s} peak disappears. The Fe_{2p} and Ni_{2p} peaks are sharp having high intensity. Finally when the sample is heated, carbon and oxygen are once more adsorbed and the intensity of these peaks increases while there is a decrease in the intensity of the other peaks. Apart from the peaks due to the photoexited electrons, Auger peaks of Ni, Fe, and O are observed in the spectra recorded after sputtering (fig 8 a-k). The spectra of individual elements are discussed in the next section.

4-1.2 The Core Level Spectra.

The main source of information in core electron spectra is the leading photoelectron peak. The core line spectrum of an element is a unique property, a "finger print" of the element which can be used for qualitative and quantitative chemical analysis [2].

Generally core XPS lines show bindining energy shifts which depend on the chemical environment of the atom. The core electron binding energy shifts with respect to the pure alloy constituent of most intense core lines show a relatively small binding energy shift (0.5eV). This indicates that only a small charge transfer occurs on alloying.

The shifts in the core level binding energy (chemical shift) are also due to alterations in the electron density of the valence shell, eg. a more

highly oxidizes species gives rise to a higher binding energy while a more reduced species shows the opposite effect. [25]

Further, since surface atoms experience a potential different from the bulk due to the lower coordination number, there is expected a somewhat different core level binding energy shift for the surface atoms as compared to the bulk atoms. Comparison of the core level binding energies of both sides of the sample for the two detection angles seems to be in aggreement with this fact (table 1 a-d), allowance being made for the uncertainity in measurement ($\pm$0.15eV). eg. Fe2P has binding energies 707.1 and 706.7 eV for two different angles. Generally the binding energies of all the elements are slightly lowered after 30 minutes sputtering. The assignment of peaks and chemical shifts of individual elements are stated in the discussion that follows.

BORON : In the XPS spectra two states of boron are observed. B I (187.8eV) and B II (192.4eV). (Fig 2 a-d). The third peak which was observed in the spectra of FeBSi [30] is not observed in our case.

The binding energy of B I peak is equal to its value for single substance and the peak intensities are higher after sputtering than B II peaks. The B II peaks have higher binding energy than the value of their single substance and is close to the value of its compounds. The B II peak disappears on prolonged sputtering indicating that it is more on the surface than in the bulk and reappears on crystallization. While this is true on the top side the same peak shows an increase in intensity after 5 minutes sputtering on the wheel side and as in the top-side, disappears on prolonged sputtering. Further on the wheel side, the B II peak shows a splitting of 1.1eV in both the as recieved sample and after 5 minutes

sputtering. The B I peak intensity is weaker for 55° and is stronger for 15° in the recieved sample.

In the study of Iron Borides [31] the bond between Fe and B is found to be greater in Fe_2B than FeB, in the former the Fe -Fe and Fe-B interaction is found to be predominant. For MG's most models assume that the local bonding model remains the same as in crystalline materials. Further Fe -B glassy compounds show similar trends in their electronic structures to the crystalline iron borides. There is enough evidence that the bonding and close range atomic order in iron-boron glasses is similar to crystalline Fe_2B and that the d states are modified by the presence of boron. Iron borides have also been shown to be typical interstitial compounds with boron occupying interstitial positions in a distorted iron lattice.

In the same work [31] it is shown that the XPS B_{1s} binding energy for iron borides is found to be 188eV, It is therefore reasonable to consider the B I peak to be due to the bonding of iron and boron.

For interstitial solid solution the atoms of added component must be small in diameter if they are to occupy interstitial positions [32] Since the diameter of boron is small, it is reasonable to consider that B I is in the interstitial regions.

Boron compounds usually resemble those of other nonmetals notably silicon in their properties and reactions. Despite the $2s^2 2p$ electronic structure of boron it is always trivalent and never monovalent [33], and its strongest affinities, that is its most strong links are with F, N, and O. The most common compound boron forms with oxygen is B_2O_3. In the study of the chemical bonding and electronic structure of B_2O_3 [34] the B_{1s} peak has binding energy 193.4eV and O_{1s} peak 533.2eV.

Hence the B II peak in our case with binding energy 192.4eV corresponds to the B_{1s} peak in the chemical compound B_2O_3 for two reasons. First, the

peak disappears on sputtering on the top side, with the decrease in the oxygen concentration on the surface. This same peak increases after 5 minutes sputtering on the wheel side which is in agreement with the increase in the oxygen concentration (table 3 a-d). Second, this peak shows an increase in intensity when the sample is heated, again in agreement with the increase in oxygen concentration on heating.

In the XPS study of FeBSi alloys [30] the B II peak was considered to correspond to the bonding state newly created between interstitial-like B_{2p} and Fe_{3d} which in our case is not true.

The splitting observed in B II peaks (fig 2, cand d) is observed only on the wheel side, which could be the result of the preparation technique (effect of the wheel), or a different chemical form of boron.

Boron also forms compounds with Ni in the form Ni_2B and NiB_2 and with silicon in the form SiB_3 and SiB_6. Boron has a peculiar behavior in its binary compounds with metals. It is in some way an electropositive element and its metallic compounds are not usually ionized [35]. The peaks due to these compounds of boron are not observed in the XPS spectra.

SILICON : Two states of silcon are observed, Si I (99.0eV) and Si II (102.2eV). (fig 3, a-d)

The Si I peak has a binding energy close to the value of its single substance, and Si II peaks have higher binding energy than the value of their single substance and is close to the value of their compounds. After sputtering the Si I peak increases while the Si II peak decreases on the top side but shows an increase on the wheel side after 5 minutes sputtering. But on further sputtering this peak also disappears on both sides. The intensity of this peak again increases on heating. The same argument as in boron is also applicable to silicon. The Si II peak is due to the four

valent oxide of silicon and the small diameter of silicon makes it an interstitial element and the silicon Si I peak is due to silicon atoms in the interstitial sites and have a strong bonding with Fe 3d to stabilize the amorphous phase[30].

IRON AND NICKEL : The Fe_{2p} and Ni_{2p} peaks in the as recieved sample surfaces appear as weak ill defined peaks. Two additional peaks are observed on the higher binding energy side of Fe_{2p} peaks in the as recieved spectra of the top side and the as recieved and 5 minutes sputtered spectra of the wheel side. These peaks have binding energies of 711.5eV and 724eV. The peak due to $Fe_{2p3/2}$ in the oxide Fe_2O_3 is found to be at the energy of 724eV [29] and the $Fe_{2p1/2}$ peak in Fe_2O_3 is found to be at the energy of 711.5eV, [29]. Hence these two peaks correspond to the Fe_{2p} peaks in Fe_2O_3. This confirms the existence of a separate iron oxide phase on the surface [36]. This oxide forms disappear on sputtering and they do not show up when the sample is heated. The existance of this peak after 5 minutes sputtering on the wheel side is in agreement with the increase in oxygen concentration on the wheel side after 5 minutes sputtering. There is no evidence to indicate the existence of any oxide form of nickel.

The difference in binding energy between the two Fe_{2p} peaks for the two detection angles 55^{o} and 15^{o} are 13.1eV and 13.6eV respectively and for Ni_{2p} peaks these differences are 17.1eV and 17.4eV. This indicates that the spin orbital splitting is lower on the surface (table 1, a-d).

Study of the 2p X-ray photoelectron spectra of the 3d group transition metal compounds has shown satellites due to simultaneous excitation of 3d electrons. These satellites (shake up) in transition metal compounds are due to larger overlap of 3d and conduction band wave functions. [37]

These satellite structures are observed both on the top and wheel side

spectra of Fe_{2p} and Ni_{2p} peaks. The ΔE for the $Fe_{2p1/2}$ satellite is 13e V and ΔE for the $Fe_{2p3/2}$ satellite is about 5eV. The satellites of Ni_{2p} are observed at ΔE=7.3eV and ΔE=5.5eV.

The transition metal 3d bands often show (exhibit) two peaks due to multiplet splitting [29]. This splitting is not observed in our spectra but we instead have the broadening of the peaks (fig 3, a-d and fig 5, a-d). The Fe_{3s} peaks show a shift toward higher binding energy on the surface (fig 3, a & c) which is a result of the oxidation of Fe.

CONTAMINANTS, O,C &Ar. There is a shift towards lower binding energy of C_{1s} peaks on sputtering and the O_{1s} peak is shifted toward higher binding energy when the sample is heated. Heating does not produce iron oxide but the oxides of boron and silicon show an increase in peak intensity when the sample is heated. These elements have a strong affinity for oxygen and the shift in O_{1s} peak on heating can only be due to the strong chemical compound it creates with Si and B.

Carbon also forms compounds with boron in the form B_4C and $B_{12}C_3$. The binding energy of C_{1s} is higher in the as recieved and heated samples. The shift could be due to the chemical compound carbon forms with boron or oxygen. But the peaks due to these compounds are not resolved in the spectra, and nothing could be said about the chemical forms of carbon.

Sputtering introduces Ar into the surface which almost disappears on heating.

4-1.3. The Valence Band Spectra.

Band structure calculations in general make important contributions to the understanding of electron spectroscopy data. However, no electronic structure calculations of the structurally disordered alloys have been

performed so far. Hence comparison of experimental data with theoretical results is restricted to band structure calculations for ordered alloys.

Various studies on the electronic structure around the Fermi level of crystalline and amorphous samples on different MG's are performed by photoelectron spectroscopy [18]. For MG $Fe_{82}B_{12}Si_6$ the ultraviolet photoelectron spectra from amorphous and crystalline samples are distinctly different in the energy range 0-3eV below the Fermi level [38].

The main band just under the Fermi edge arises mainly from the 3d electrons of the transition metals and the peak of the main band is located about 1.3eV under the Fermi level in the XPS spectra, in our case. This is true even after the sample was heated to 580°C. No significant difference is observed between the amorphous and crysalline phase in the valence band and the position of the peak with respect to the Fermi level. Comparison of the valence band spectra from amorphous and crystalline phases indicates that the gross features of the electronic structure are the same. In the valence band spectra of the as recieved samples of the wheel side the main peak is around 3.2eV for 55° and 2.5eV for 15° and for 55° on the top side it is at about 1.7eV. This shift in the main band is due to the contaminants present on the sample in its as recieved form.

Most of the peaks in the valance band spectra are not properly resolved. There are more peaks present in the spectra of the as recieved sample and heated sample due to the contaminants.

In Fe_2B, boron binding states occur at 4, 6.5 and 10.5eV [31]. We attribute the peaks at 6.5eV and 10.5eV to boron. By comparison with the data of Fe_2B, the 10.5eV peak is at the same energy as the B_{2s} peak of Fe_2B. This is due to the bonding state of metalloid s and p electron states with transition metal Fe s,p,d electron states. This is true because in transition metalloid alloys, the transition metal and metalloids form

covalent bonds by hybridization between energetically low lying metalloids and higher-lying p electrons states with transition metal s,p, and d electron states respectively [18].

Boron 2s - 2p contribution to the valence band within 5eV of the Fermi level is overwhelmed by the Fe_{3d} bands. The boron 2p peak is not resolved in the spectra due to the low photoionization cross section of B_{2p} at XPS energies. The Fe_{4s} and Ni_{4s} peaks are of very low intensity and structurless and they are unresolved.

An additional peak around 25eV is observed in every valence band spectra with the highest intensity in the as recieved and heated samples spectra. This is the O_{2s} peak in the chemical compound of oxygen. This is the peak due to the complicated chemical compounds oxygen forms with the matrix elements. A peak around 22eV is also observed on the wheel side as recieved sample spectra. Since no such peak exists on the top side, we attribute this peak to be due the preparation technique that is , it could be the influence of the copper wheel on the sample in the cooling process.

An important question is regarding the behavior of the density of states near the Fermi level related to the stability model of Nagel and Tauc [39]. As most XPS experiments have shown [18], the position of the Fermi level in the deep minimum of the density of states is not a necessary condition for the occurence of the glassy phase. Our result affirms this fact once more.

4-2. QUANITTATIVE INTERPRETATION

4-2.1 Outline of Concentration Calculations:

The concentration n for various elements in the sample surface is carried out using the formula

$$n = \frac{aS\sqrt{E}}{\sigma N}$$

N and S are found on each spectra. The area a under the peaks is obtained using a planimeter. The photoionization cross section are taken from the theoretically calculated values by Scofield [40]. The values of n used to calculate ratio of concentrations of the elements on the top side and wheel side for the two detection angles and each sample treatment are listed in table 3, a-d.

The concentrations of each element with respect to the concentration of Fe_{2p} is carried out using equation (28) for each sample treatment and for two detection angles and is listed in table 4, a&b. The percentage concentration of each element with respect to the concentration of Fe is calculated for each angle and treatment and is listed in table 5, a&b. Finally the ratio of percentage concentrations for the two angles is calculated and is listed in table 6.

Each of these results are ploted in Fig 9 a-j in appdix A.

4-2.2 Discussion of Concentration Tables.

The as recieved sample is highly contaminated on both sides with carbon and oxygen. The amounts of carbon for both angles on the top side are comparable, and there is roughly two times more oxygen on the top side surface (detection angle 55^{o}) than detection at 15^{o}. On the wheel side the surface carbon concentration is nearly twice for 55^{o} and oxygen concentration for 55^{o} is nearly five times that of the concentration at 15^{o}. The concentration of the other elements seems to be high on the surface than the bulk. But the effect of the adsorbed species in the process of transmission of photoelectrons through the sample is not

considered in the calculations, and this causes the discrepancy.

After 5 minutes the C and O concentrations show a sharp drop on the top side, and on the wheel side there is a sharp decrease in the carbon concentration but there is still more oxygen on the wheel side surface.

Its concentration at 15^{o} detection angle is doubled. The metastable conditions induced by sputtering trigger re-oxidation and diffusion processes [36], and the increases in oxygen concentration on sputtering could be a result of this effect. But this effect should not be limited on the wheel side only, similar effects should have been observed on the top side. So we are inclined to consider this increase in oxygen concentration to be a result of the preparation, i.e. there must be more oxygen in the bulk in the wheel side. The concentration of other elements also increases.

After 15 minutes sputtering, the oxygen concentration on both sides and the carbon concentration on the top side drops but, the concentration of carbon increases on the wheel side. This increase in carbon concentration is due to the fact that the sample was left for one night in UHV chamber which was continuously vacuated by diffussion pumps, and the 15 minutes sputtering and recording of the spectra were carried out the next day.

Neverthless after 30 minutes sputtering the concentrations of oxygen and carbon decrease significantly, but, even after such a prolonged sputtering, we could not obtain a clean surface. The concentration of these two elements is still significant, and even higher than the concentration of Ni and Si. This is probably due to the high concentration of O and C in the melt. This would mean that the sample is not pure enough, and the contaminants, carbon and oxygen are not only on the surface but are implanted in the matrix. The reoxidation induced by sputtering could also contribute to the continuous presence of oxygen.

It is observed that the concentration of Fe and B on the surfaces increases drastically after each sputtering while the concentrations of Si and Ni remain low in comparison to the concentrations of Fe and B.

In sputtering a multicomponent material is found in general that the surface compositin is changed due to preferential sputtering. Enrichment of the surface is found in the low sputter rate constituent provided both components have nearly the same recoil energy densities for the pure elements. In this case enrichment is mainly determined by the surface binding energies of the alloy constituents in the alloy [41].

In the MG under study the bulk concentrations of Ni and Fe are very high while there is a very low concentration of B and Si. But it is seen from the tables that the surface is more enriched by boron and iron (and of course C and O) and the concentrations of Ni and Si remain very low. Ni has the lowest surface concentration.

This is due to preferential sputtering where, Ni is sputtered off more leaving the surface enriched by the other components, or sputtering has enhanced the diffusion of boron to the surface or both.

On the final treatment (heating) the sample crystallizes, and once more the carbon and oxygen concentration increases and the concentration of all other elements decreases. Under Stable conditions, chemical potential is minimum and solubility is high. Hence the increase in O and C concentration.

In table 6 the ratio of percentage concentrations for two angles is given. This table shows the relative values of concentrations of the elements for the two detection angles. In the as recieved samples on both sides the surface is covered with carbon, and there is less oxygen on the surface. After 5 minutes sputtering the carbon concentration decreases on the top surface and the oxygen concentration on the top side surface

increases, while on the wheel side there is still more carbon on the surface, boron and silicon concentrations on the surface are higher on the wheel side than the top side. After 30 minutes sputtering the surface concentrations of nickel, iron and boron are larger on the wheel side surface than at 15^{o} detection, but on the top side carbon and oxygen concentrations are still higher on the surface and the nickel concentration is also higher on the surface than at 15^{o} detection. After 30 minutes sputtering the Ni and Fe concentrations on the wheel side surface is higher than that detected at 15^{o}, while on the top side the concentrations of C, O and Ni are higher on the surface than those detected at 15^{o}. when the sample is heated the wheel side surface concentration of C and O increases and is higher than 15^{o} concentration and so are the concentrations of Ni and B, while on the top side the surface concentration of C and O is higher than the concentrations at 15^{o}. The concentration of all the other elements is lower on the surface.

In the calculations of concentrations there are certain fundamental problems that make limitations on XPS [24]. Attenuation of X-rays in the solid is not considered. The cross sections tabulated by Scofield are good to about 10% accuracy at the best. Another difficult problem in treating data is connected with the handling of the background, where in principle the spectra are made up of large series of peaks which are due to secondary electrons in addition to the main peaks. The final spectrum is thus a convolution of all the separate photoelectron peaks and their secondary structures. Further in integreting the peaks areas we used a planimeter which is good to about 10% accuracy. Finally effects of the absorbed species in the process of electron transmission through the sample are not considered.

CONCLUSIONS

The Si I (99eV) peak and the B$\frac{1}{2}$ (188eV) peaks are due to the elements boron and silicon in the interstitial sites, which have a strong bonding with Fe3d electrons, while the B II (192.4eV) and SiII (102.2eV) peaks are due to the boron and silicon compounds with oxygen. In particular the B II peak corresponds to the B_{1s} peak in B_2O_3.

A separate oxide phase of iron exists on the surface but there is no evidence to show the existence of oxide forms of nickel.

Sputtering causes the enrichment of the sample surface with iron and boron. However the sample is highly contaminated by C and O and it is not possible to obtain a clean surface even after 30 minutes sputtering. There was probably higher content of O and C in the melt.

Crystallization of the sample by heating increases the concentration of C and O on the surface and only oxides of boron and silicon exist on the surface.

The valence band spectra show that the gross features of the electronic structure are the same in the sputtered amorphous samples and the crystalline samples around the Fermi level. The main peaks in the as recieved samples are depressed and shifted due to the contaminants.

There is a difference in the spectra of the wheel side and the top side. Additional peaks nonexistent on the top side are observed on the wheel side. The changes in the concentrations of the elements on the wheel side surface and the top side surface are quite different. The concentrations of the contaminants is higher at 15° detection angle than at 55° detection angle, on the wheel side while it is the opposite in the top side.

REFERENCES

1. Mrafko,P. "Metallic Glasses", Chechozlovak Journal of Physics, B.34: 1324, 1984.

2. Siegbhan,K. Principles and Applications of Electron Spectroscopy. In Interaction of Radiation with Condensed Matter, Vol I, Vienna: International Atomic Agency, 319 - 381, 1977.

3. Duwez,P. " A typical Example of Metastability: Metallic Glasses," Journal of Vacuum Science Technology,B I (2) 218-221, April - June, 1983.

4. Cohen and Turnbull. " Composition Requirements for Glass Formation in Metallic and Ionic Systems", Nature, 183: 131, 1961.

5. Beck,H. and Guntherodt, H.J. (eds.) "Glassy Metals I", Topics in Applied Physics. Vol 46. Berlin: Springer Verlag, 1981.

6. Fish, G.E. and Child, H.R. " Studies of Chemical Homogeneity and Magnetic Domain Walls in Fe Based Metallic Glasses Using Small Angle Neutron Scattering", Journal of Applied Physics, 52: 1880 - 1882, 1981.

7. Gaskell, P.H. Models for the Structure of Amorphous Metals. In Topics in Applied Physics, Vol 53, eds. H. Beck and H.J.Guntherodt. Berlin: Springer Verlag, 1983.

8. Kronmuller,H. " Micromagnetism and Microstructure of Amorphous Alloys",Journal of Applied Physics,52: 1859-1864,1981.

9. Takyoma, S. and Oi,T. " Effects of Processing Conditions on Magnetic Properties of Amorphous Alloys", Journal of Applied Physics, 50: 1595-1597, 1979.

10. Chien, C.L. et al. " Mossbauer Studies of Magnetic Ordering in Amorphous (Fe_xMn_{1-x}) $P_{16}B_6Al_3$ Under External Magnetic Fields", Journal of Applied Physics, 52: 1750 - 1752, 1981.

11. Durand, J. Magnetic Properties of Metallic Glasses. In Topics in Applied Physics, Vol.53, eds. H.Beck and H.J. Guntherodt. Berlin: Springer Verlag, 1983.

12. Feurbacher, B. and Fitton,B. Photoemission Spectroscopy In Topics in Current Physics. Vol. 4, ed. H. Ibach, Berlin : Springer Verlag, 1977.

13. Demuth,J. and Avouris, P. "Surface Spectroscopy", Physics Today, 62-68, Nov, 1983.

14. Cardona, M. and Ley,L. eds. "Photoemission in Solids I", Topics in Applied Physics. Berlin: Springer Verlag, 1978.

15. Caroli, C.et al."Inelastic Effects in Photoemission, Microscopic Formulation and Quantitative Discussion", Physical Review, B 8:4552-4569,Nov,1973.

16. Mahan,G.D."Theory of Photoemission in Simple Metals", Physical Review, B 2: 4334 - 4350, Dec.1970.

17. Berglung,C.N. and Spicer,W.E."Photoemission Studies of Copper and Silver: Theory", Physical Review,136:1030-1044,Nov,1964.

18. Oelhafen,P.Electron Spectroscopy on Metallic Glasses. In Topics in Applied Physics,Vol.53,eds.H.Beck and J.J Guntherodt,Berlin: Springer Verlag,1983.

19. Hedga,R.I.and Sinha,A.P."ESCA Study of Metals and Alloys", Applied Spectroscopy Reviews,19:1-103,1983.

20. Roy,D.and Carette,J.D. Design of Electron Spectrometers for Surface Analysis. In Topics in Current Physics,Vol.4, ed. H.Ibach,Berlin: Spriger Verlag,1977.

21. Tougaard,S.and Ignatiev,A."Concentration Depth Profiles by XPS: a New Approach",Surface Science,129:355-365,1983.

22. Wagner,C.D."Factors Affecting Quantitative Determination by X-Ray Photoelectron Spectroscopy",Analytical Chemistry, 49: 1282 - 1290, August,1977.

23. Seah,M.P.and Dench,W.A."Quantitative Electron Spectroscopy of Surfaces", Surface & Interface Analysis,1:2-11,1979.

24. Carlson,T.A."Basic Assumptions and Recent Developments in Quantitative XPS",Surface & Interface Analysis,4:125,1982.

25. Coburn,J.W."The Influence of Ion Sputtering on the Elemental Analysis of Solid Surfaces",Thin Solid Films,64:371,1979.

26. Sigmund,P. "Theory of Sputtering I. Sputtering Yield of Amorphous and Polycrystalline Targets", Physical Review 184: 383 - 416, August, 1969.

27. Firsov,C.B. On the Dependence of Target Sputtering Efficiency on the Angle of Incidence of Bombarding Particles. In Atomic Collision Phenomena in Solids. eds, D.W.Palmer et al, Amsterdam: North Holland Publishing Co, 1970.

28. Keenlyside,M. . Stott,F.H. and WOOD,G.C."Ion Sputtering in Surface Analysis of Practical Surfaces";Surface and Interface Analysis,5: 64-70, 1983.

29. Carver,J.C. ,Ichweltzer,G.K. and Carlson,T.A."Use of X-Ray Photoelectron Spectroscopy to The Study of Bonding in Cr, Mn,Fe and Co Compounds", Journal of Chemical Physics, 57: 973-982, 1972.

30. Taniwaki,M. et al. "XPS and Mossbauer Study on Amorphous FeBSi Alloys", Journal of Non-Crystalline Solids, 51&62: 397-402, 1984.

31. Joyner,D.J.etal. "Study of Iron Borides IV: Relation of Bonding Structure and Magnetic Behavior From Photoemission Assignments and Ab initio Calculations", Physical Review B,24: 3122-3137, 1981.

32. Tulloch, D.S. Physical Foundamentals of Material Science London : Butherworths, 1971.

33. Cotton, A. and Winkinson,G. Advanced Inorganic Chemistry. New York: Interscience Publishers, 1967.

34. Joyner, D.J. and Herculus,D.M. " Chemical Bonding and Electonic Structure of B_2O_3, H_3BO_3 and BN: An ESCA, Auger, SLS and SXS Study", Journal Of Chemical Physics. 72: 1095 -1108, 1980.

35. Sidgwick,N.V. Chemical Elements and Their Compounds. London: Oxford University Press, 1950.

36. Kauffer,M. and Lichtman,D. " XPS Studies of the Effect of Argon Ion Bombardment on Standard Reference Material 470: Glass K-411", Surface Science,139: 347-359, 1984.

37. Rosencwaig,A., Wertheim,G.K., and Guggenheim,H.J. "Origins of Satellites on Inner-Shell Photoelectron Spectra", Physical Review Letters,27: 479-481, 1971.

38. Kanski,J and Peto,G. Electron Spectroscopic Investigations of Amorphous and Crystalline $Fe_{82}B_{12}Si_6$", Solid State Communications,51: 747-750, 1984.

39. Nagel,S.R . and Tauc,J. " Nearly Free Electron Approach to The Theory of Metallic Glass Alloys", Physical Review Letters, 35: 380-383, 1975.

40. Scofield, J.H. Journal of Electron Spectroscopy,8:129, 1976.

41. Betz,G. "Alloy Sputtering ", Surface Science,92:283-309, 1980.

APPENDIX A

1. Valence Band Spectra
2. Spectra of Individual Elements
3. The Wide Scan Spectra
4. Graphs of Concentrations.

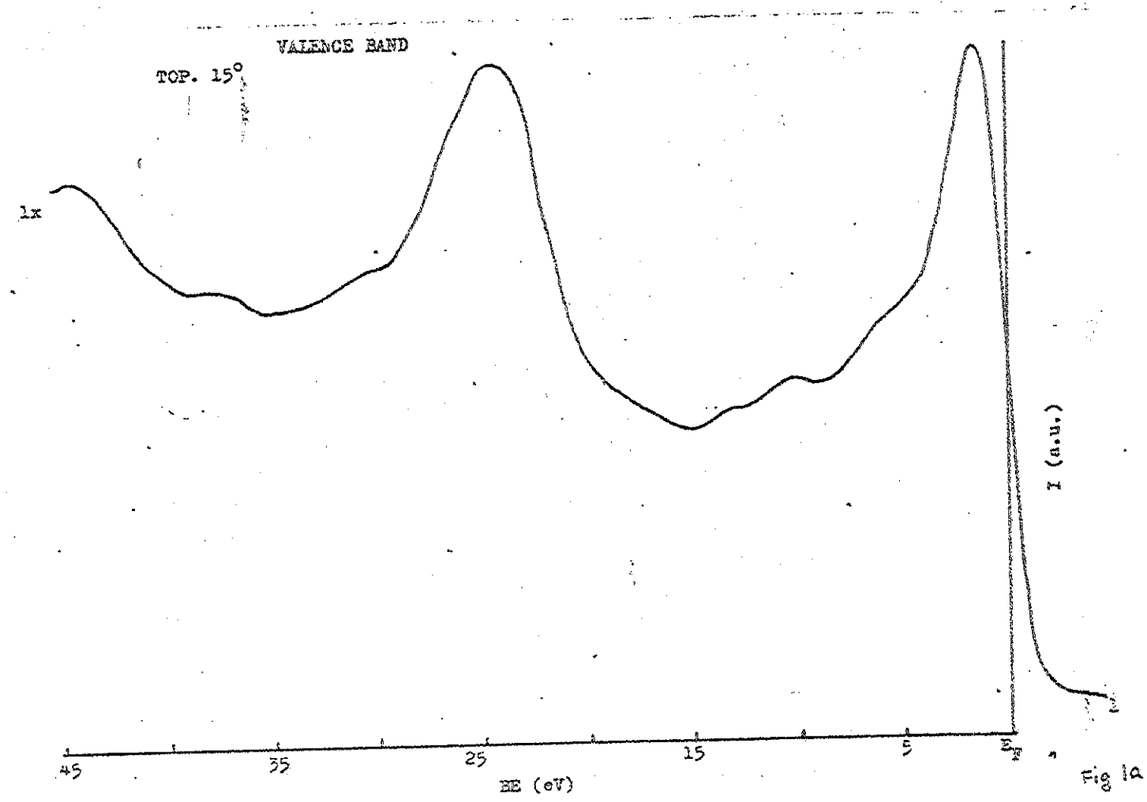

Fig 1a

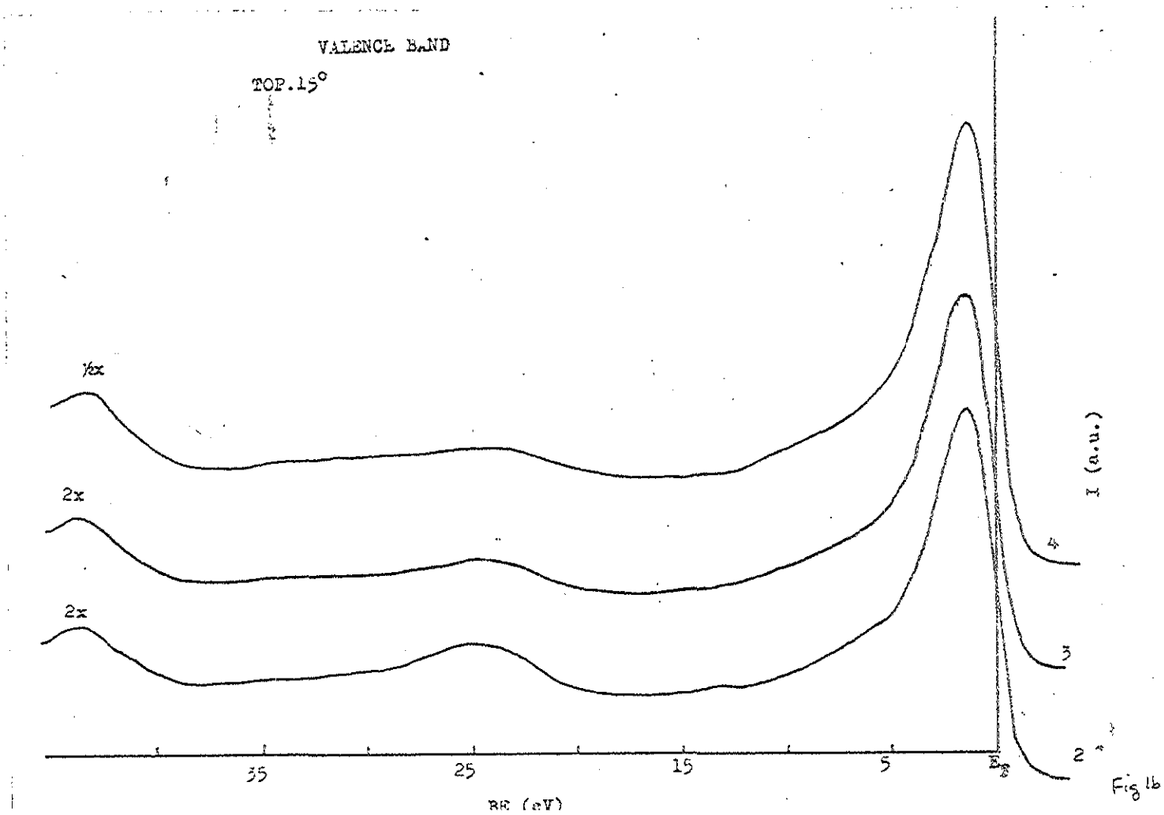

Fig 1b

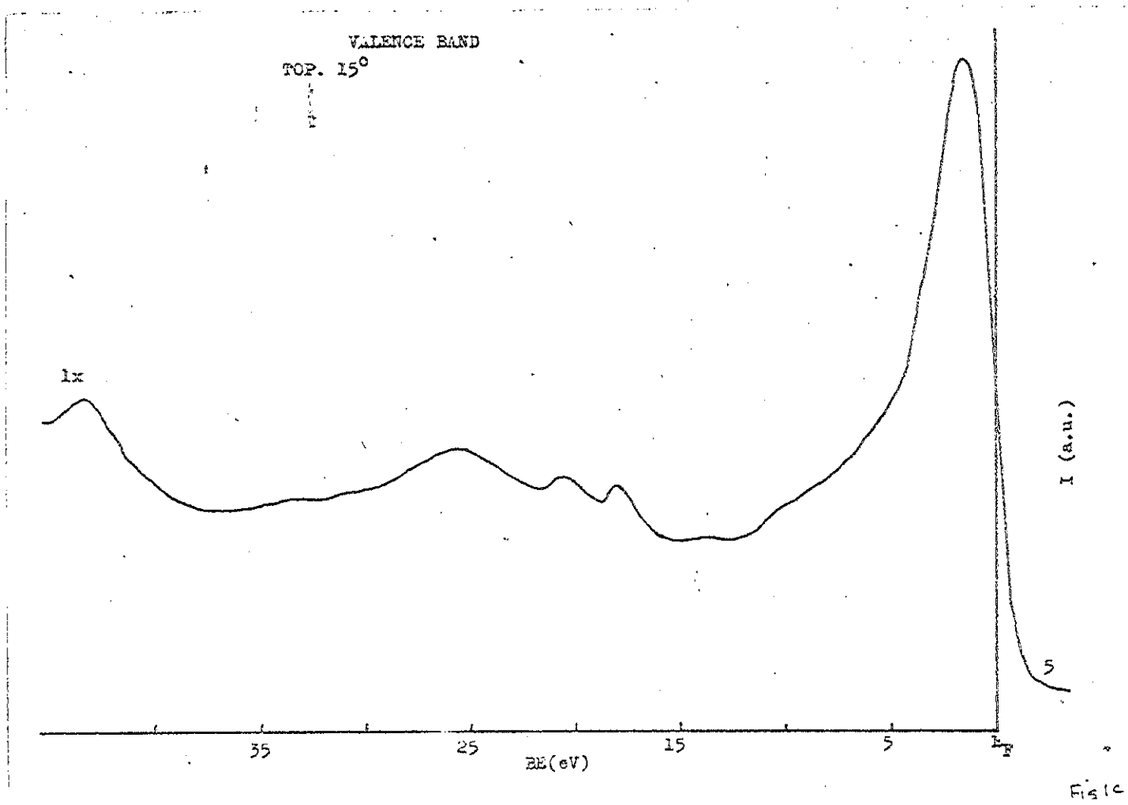

Fig 1c

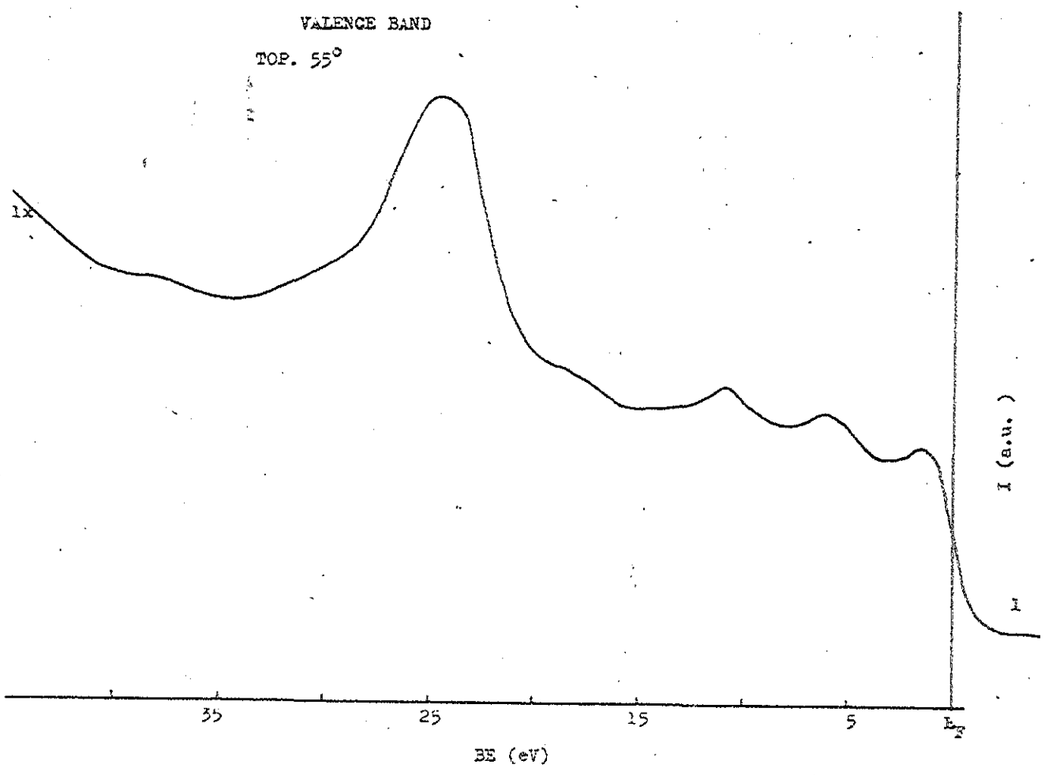

Fig 1d

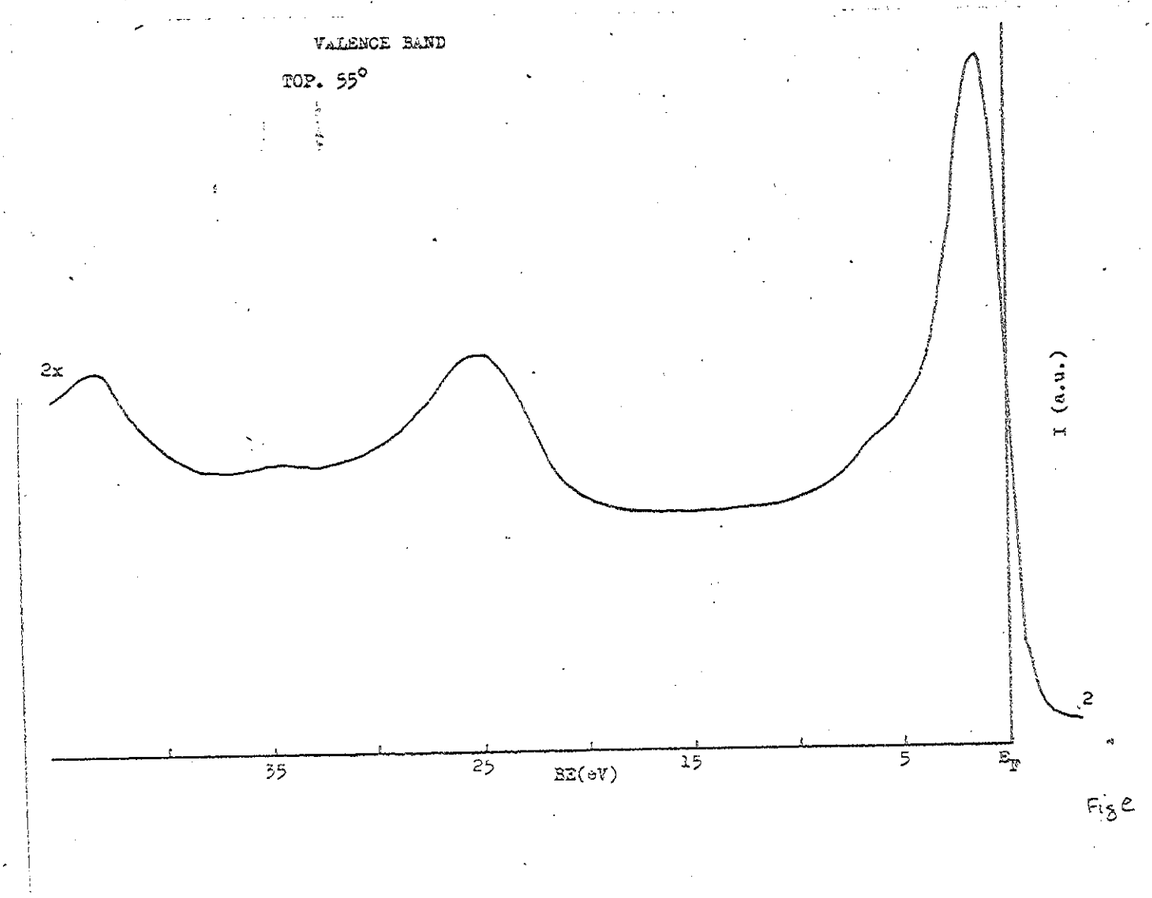

Fig e

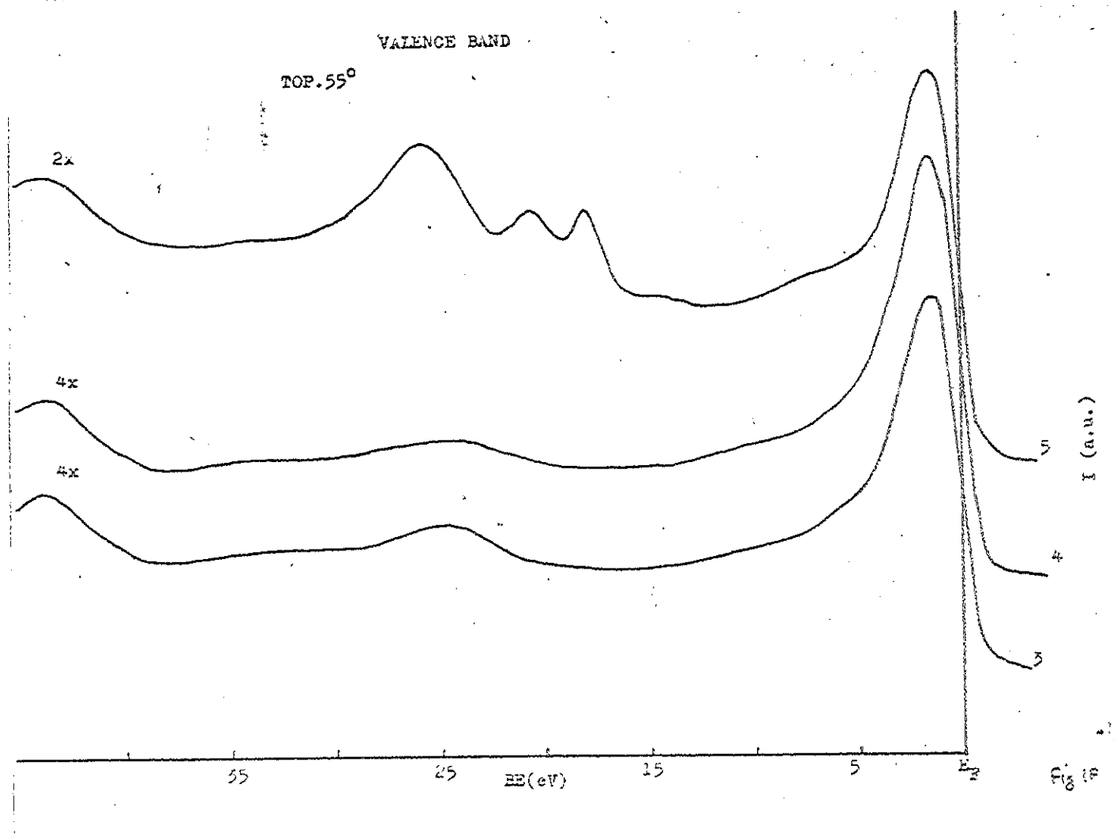

Fig 18

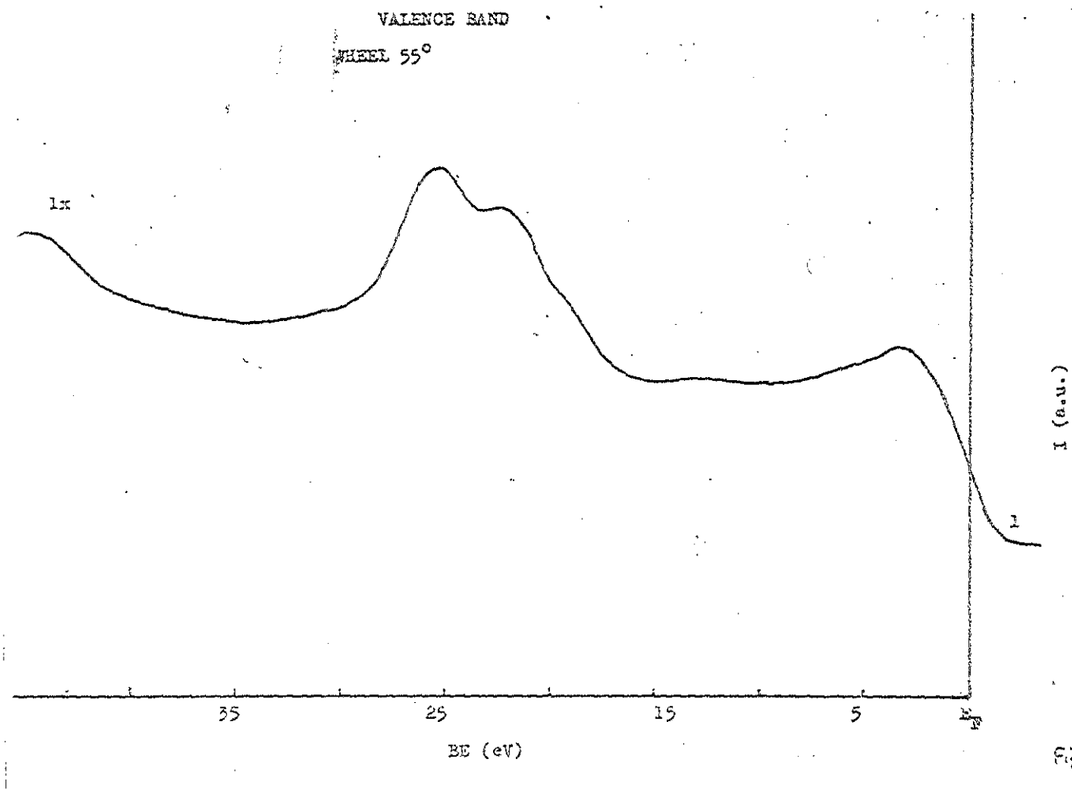

Fig 18

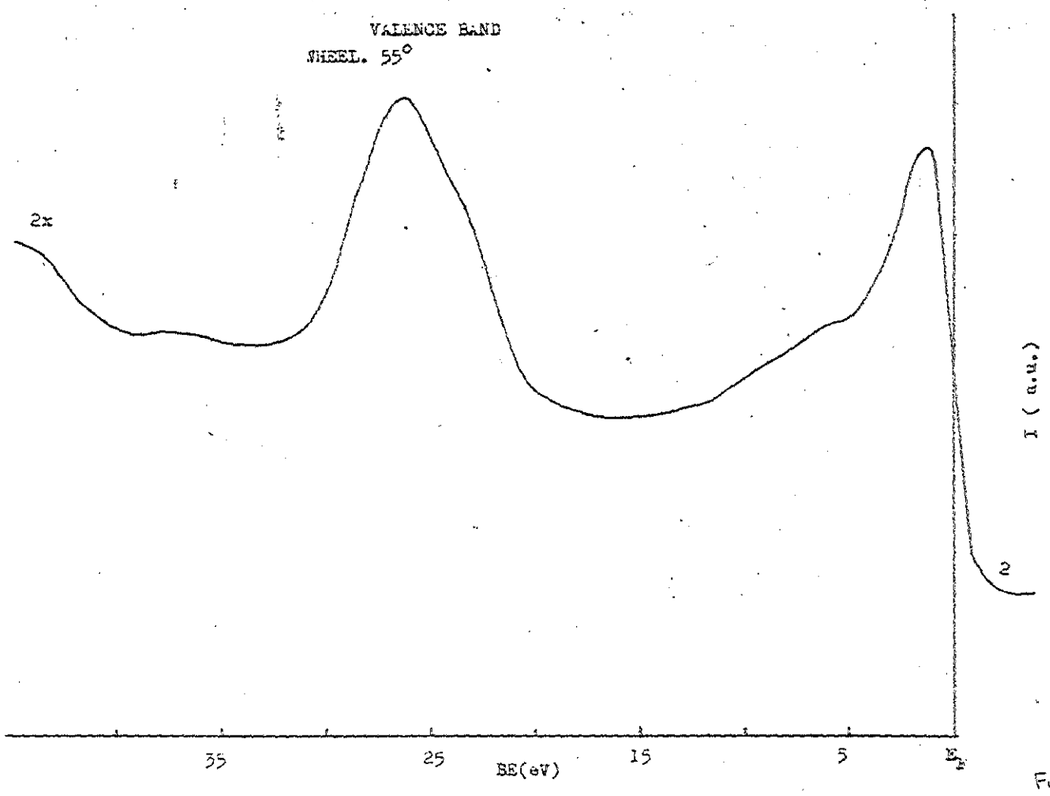

Fig 14

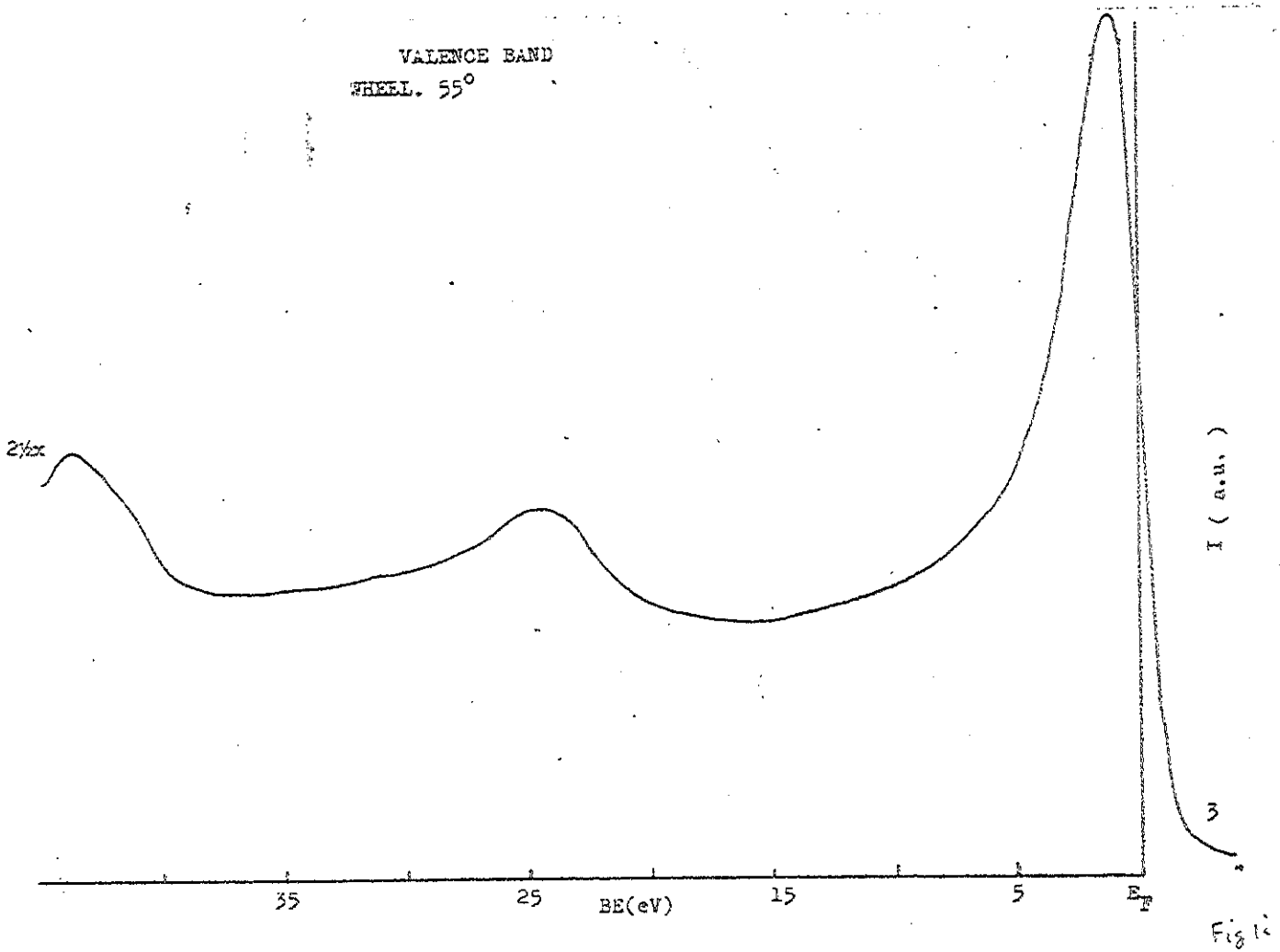

Fig 1:

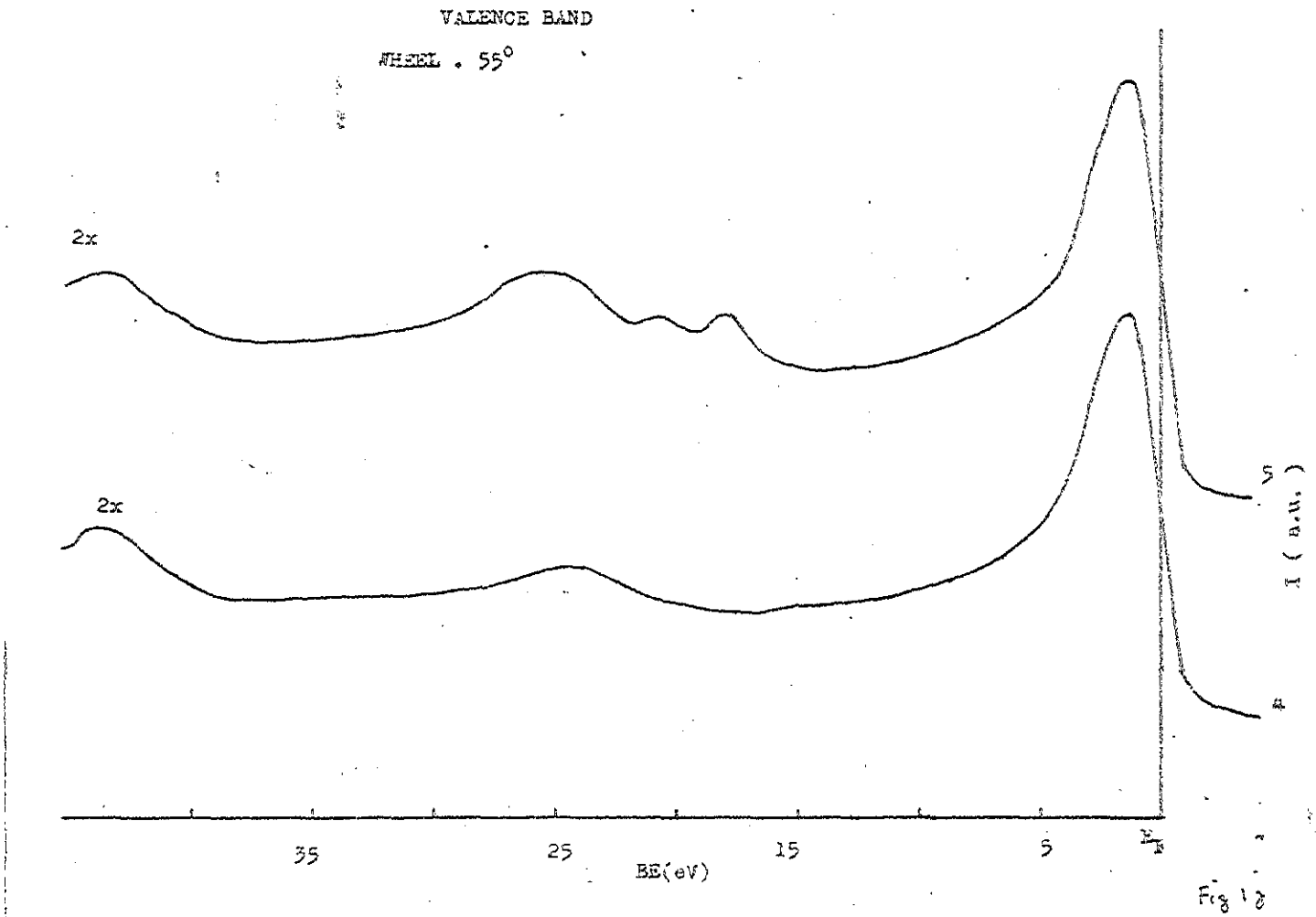

Fig 12

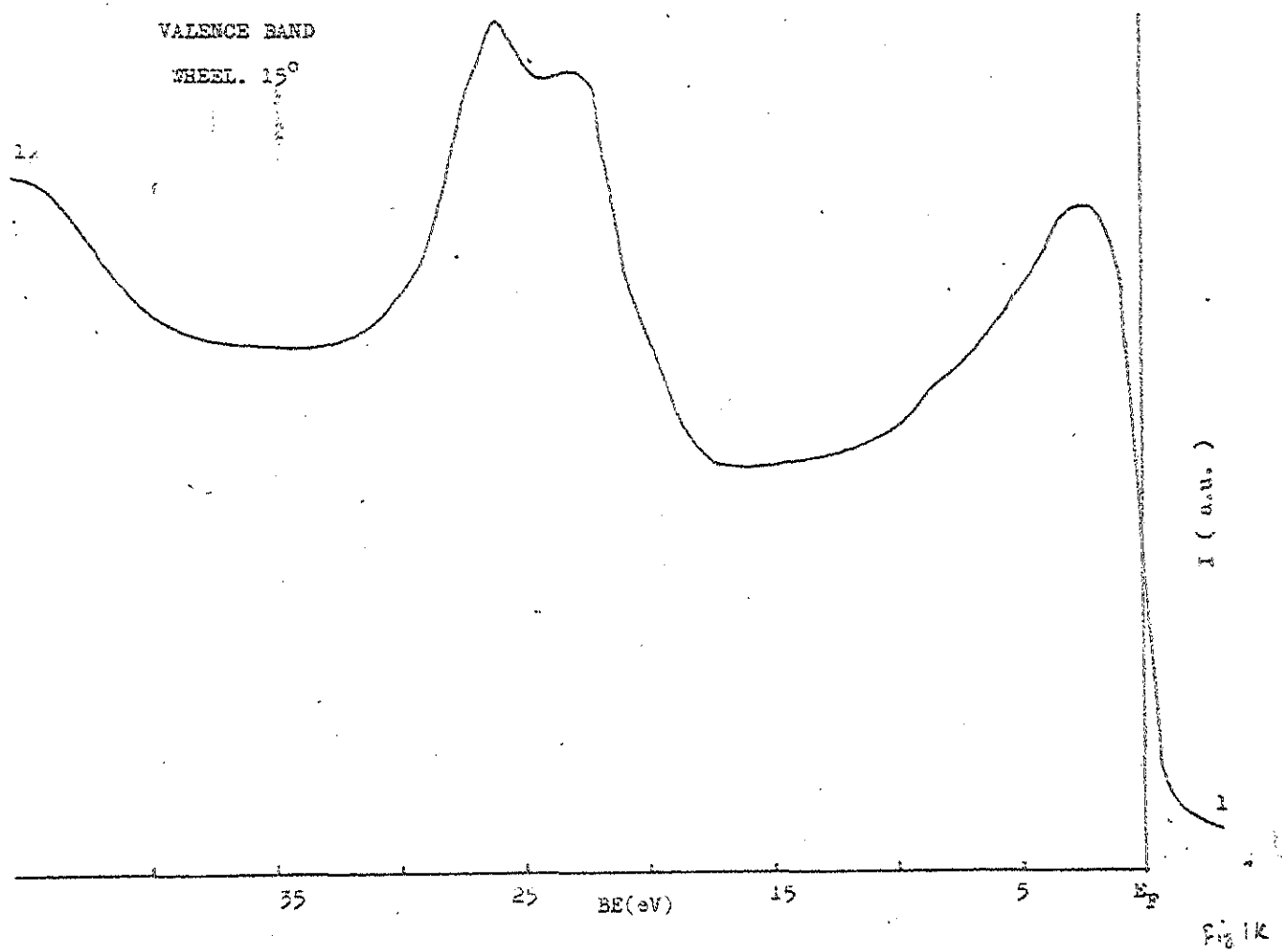
VALENCE BAND
THEEL. 15°
35
25
BE(eV)
15
5
E_F
I (a.u.)

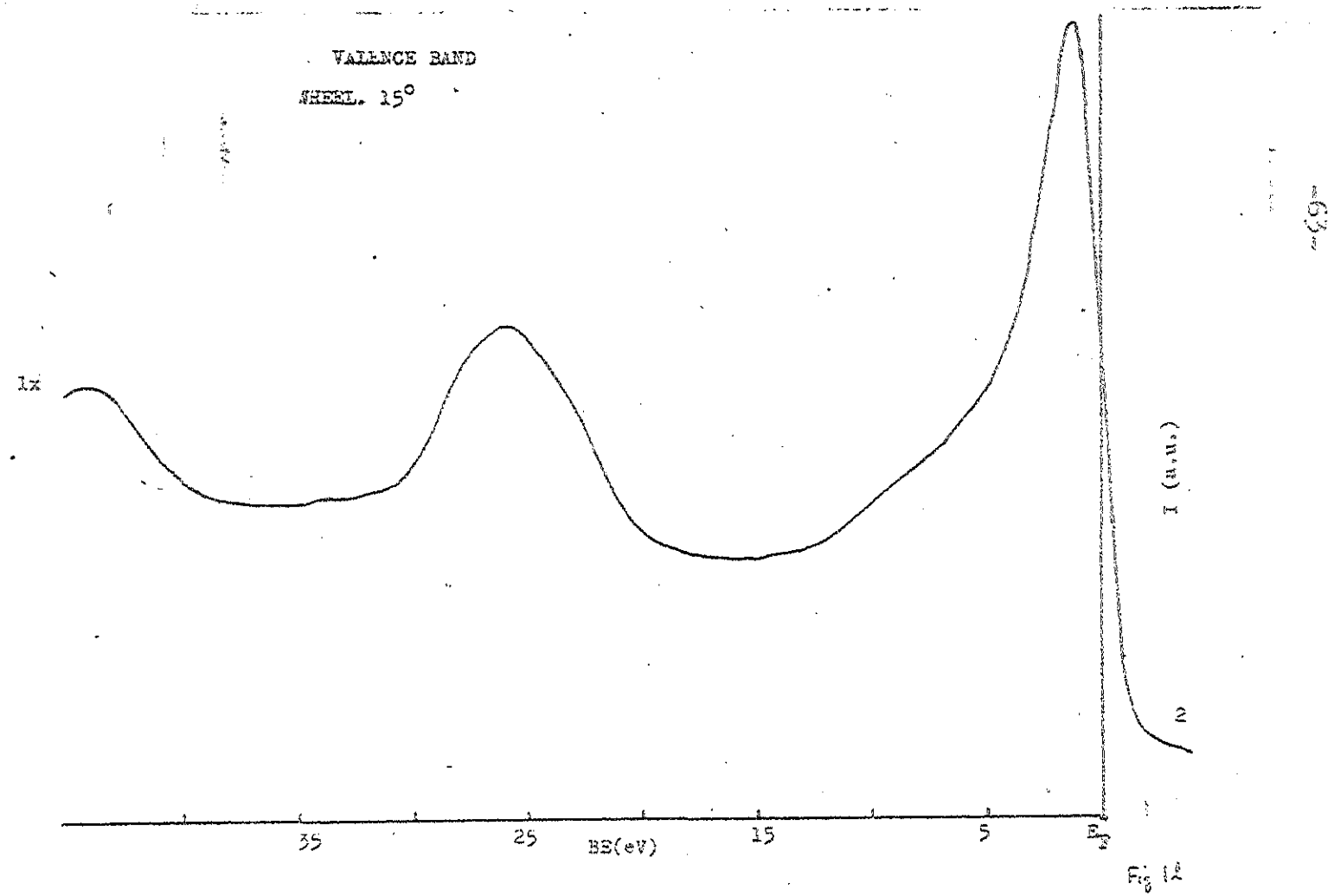

Fig 12

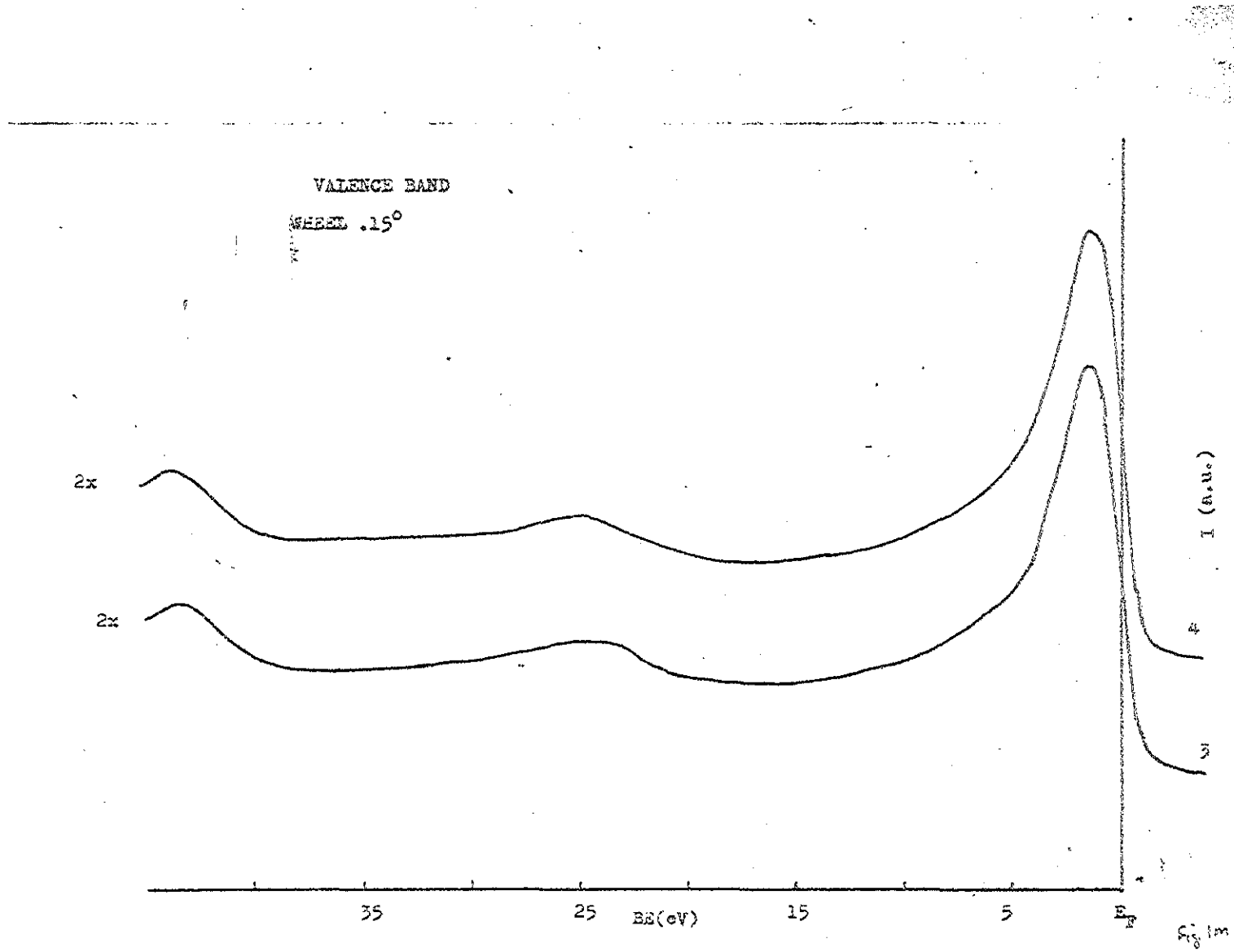
VALENCE BAND
WHEEL .15°
2x
2x
35
25
BE(eV)
15
5
E_F
I (a.u.)
ζ_0 Im

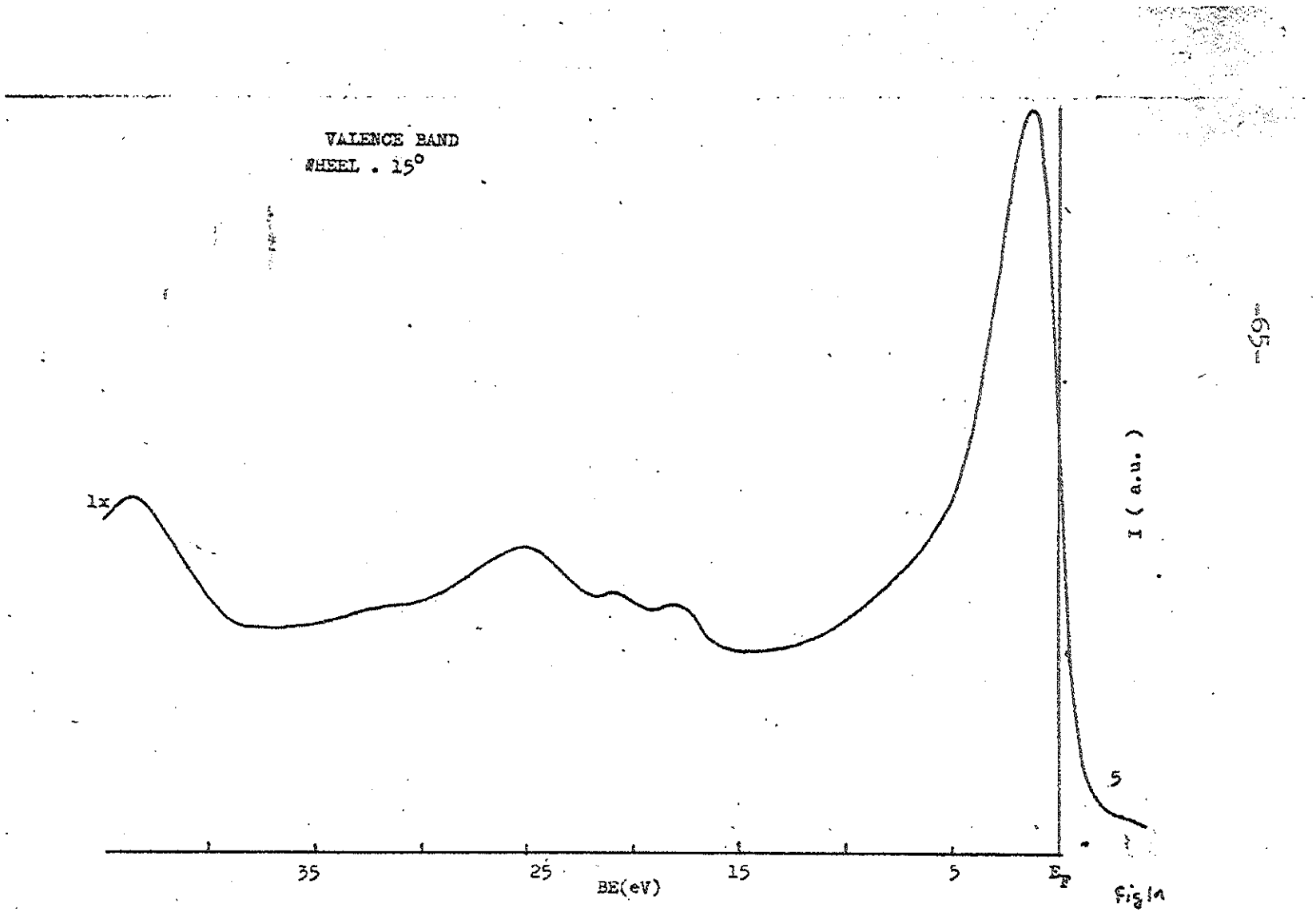

Fig 1a

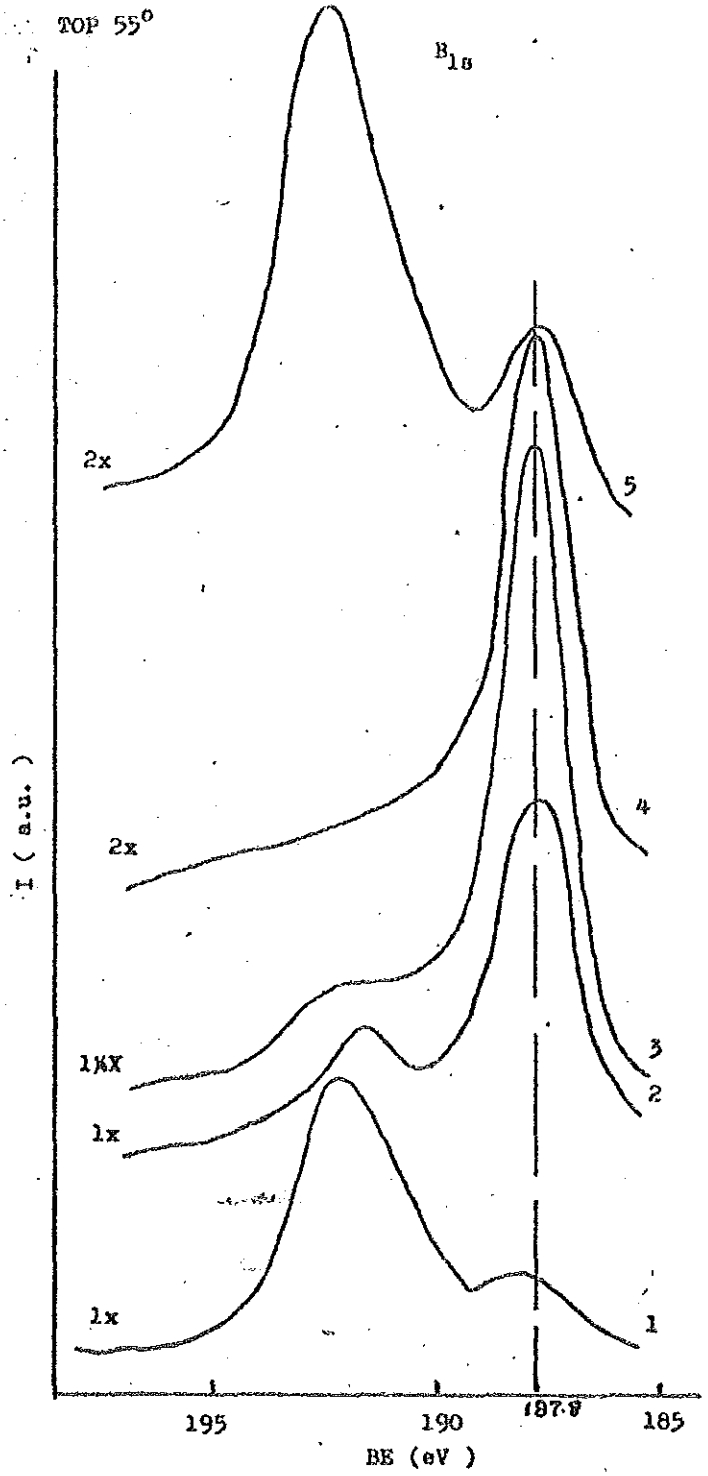

FIG. 2a.

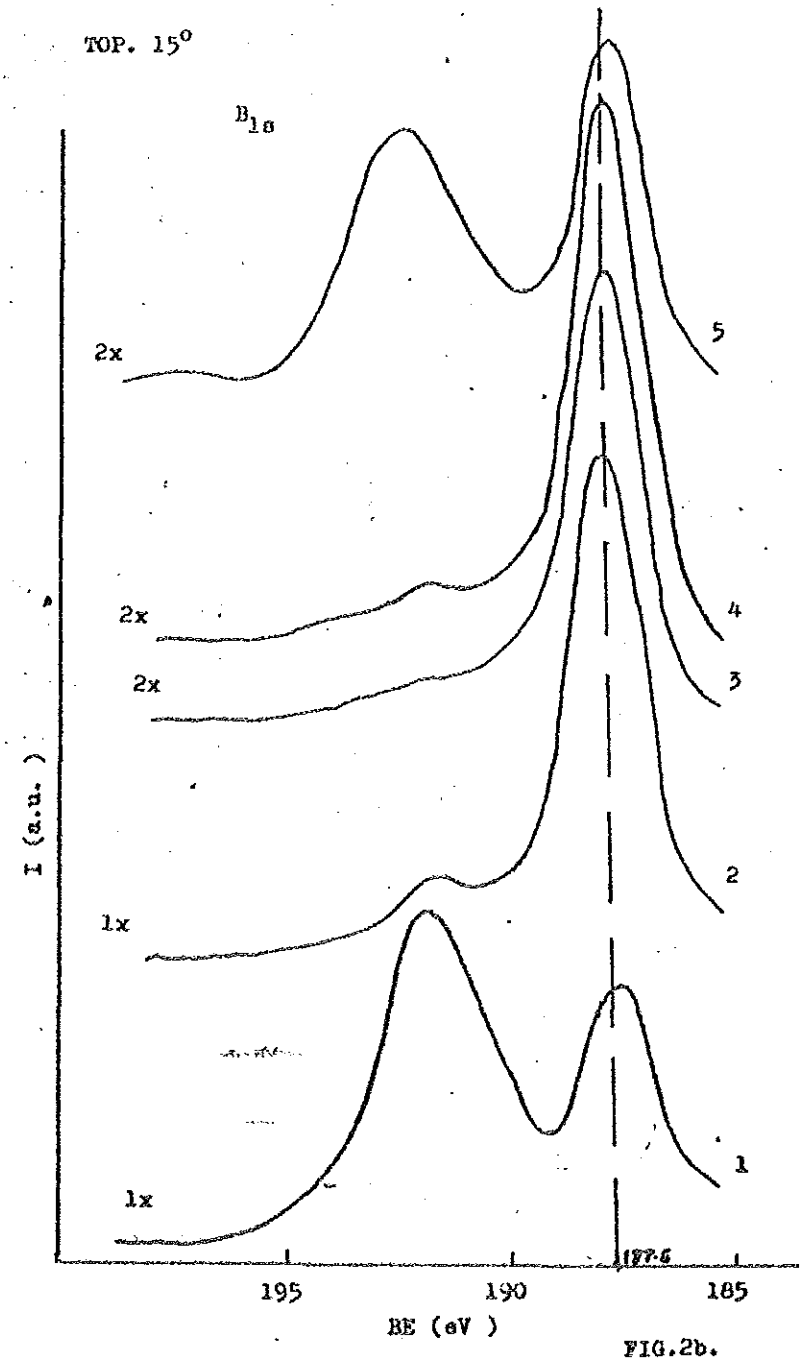

FIG.2b.

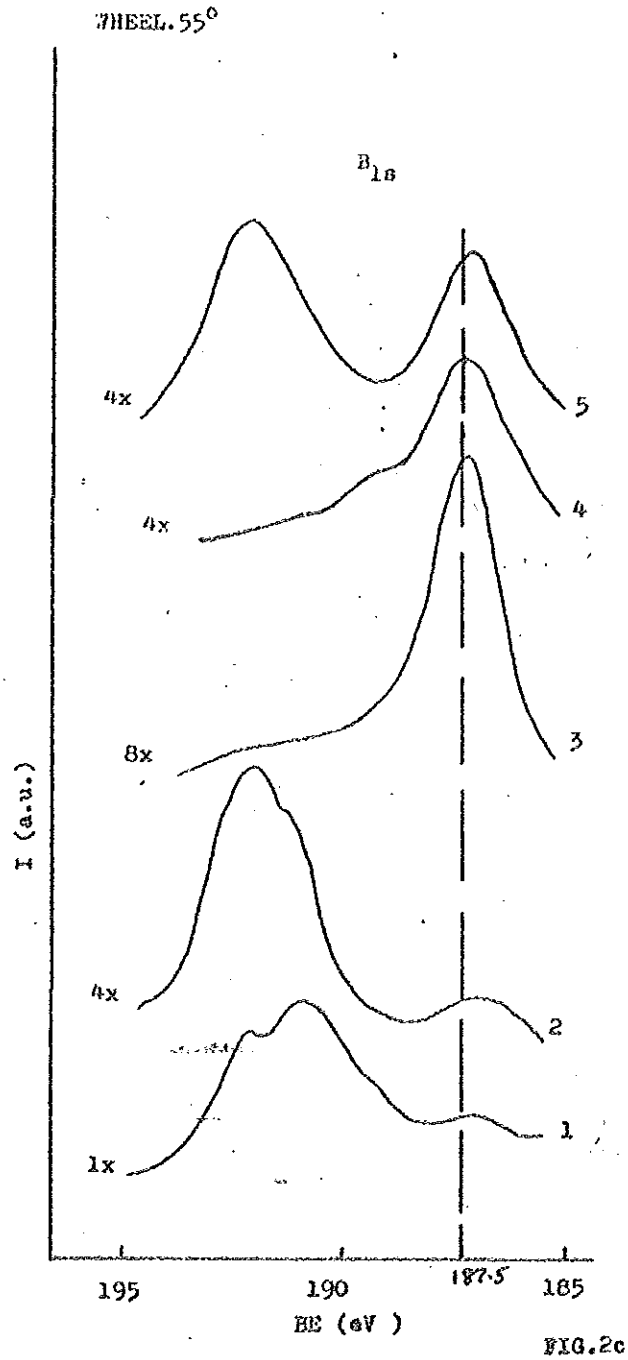

FIG.2c

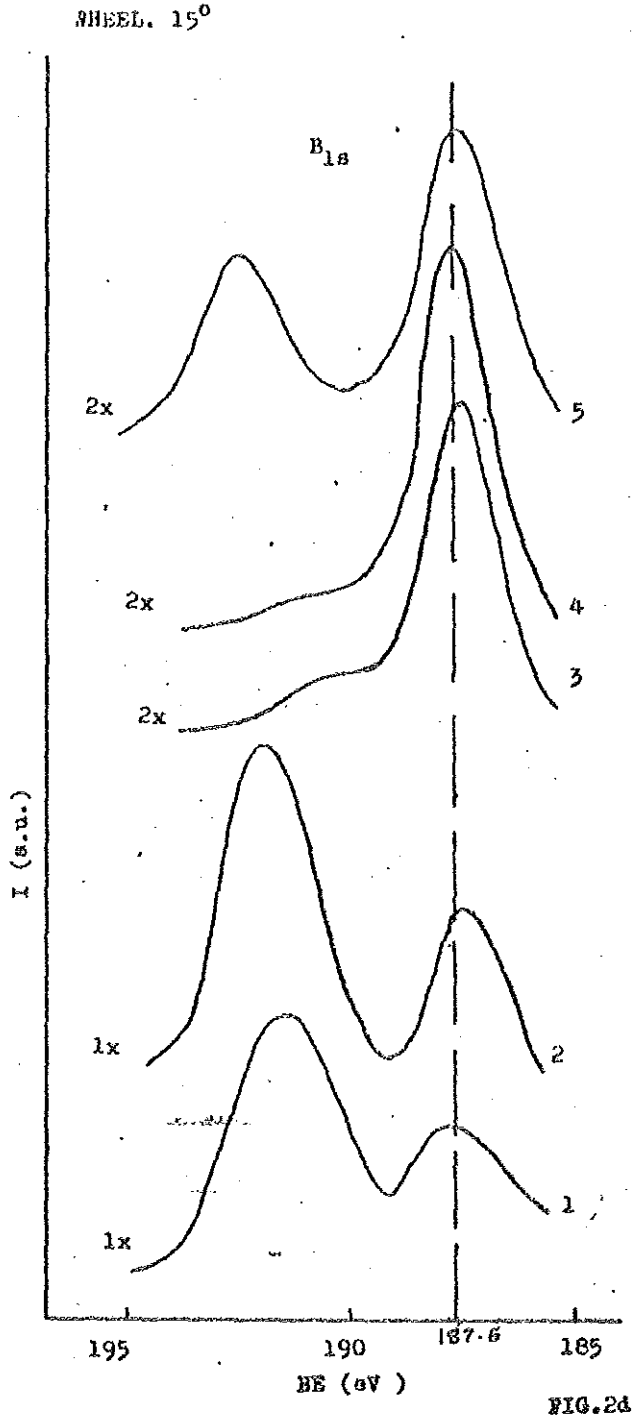

FIG.2d.

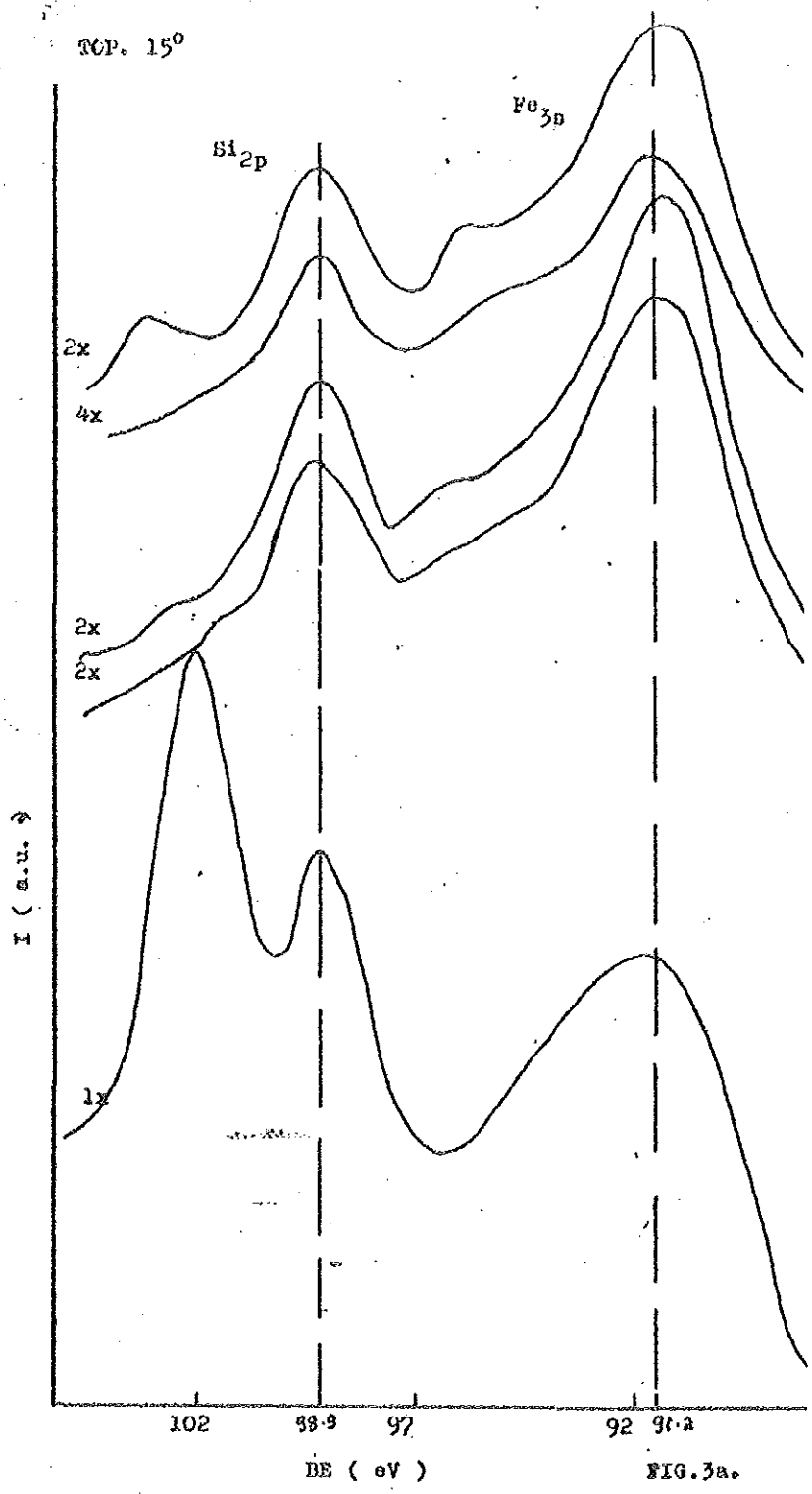

FIG.3a.

TOP. 55°

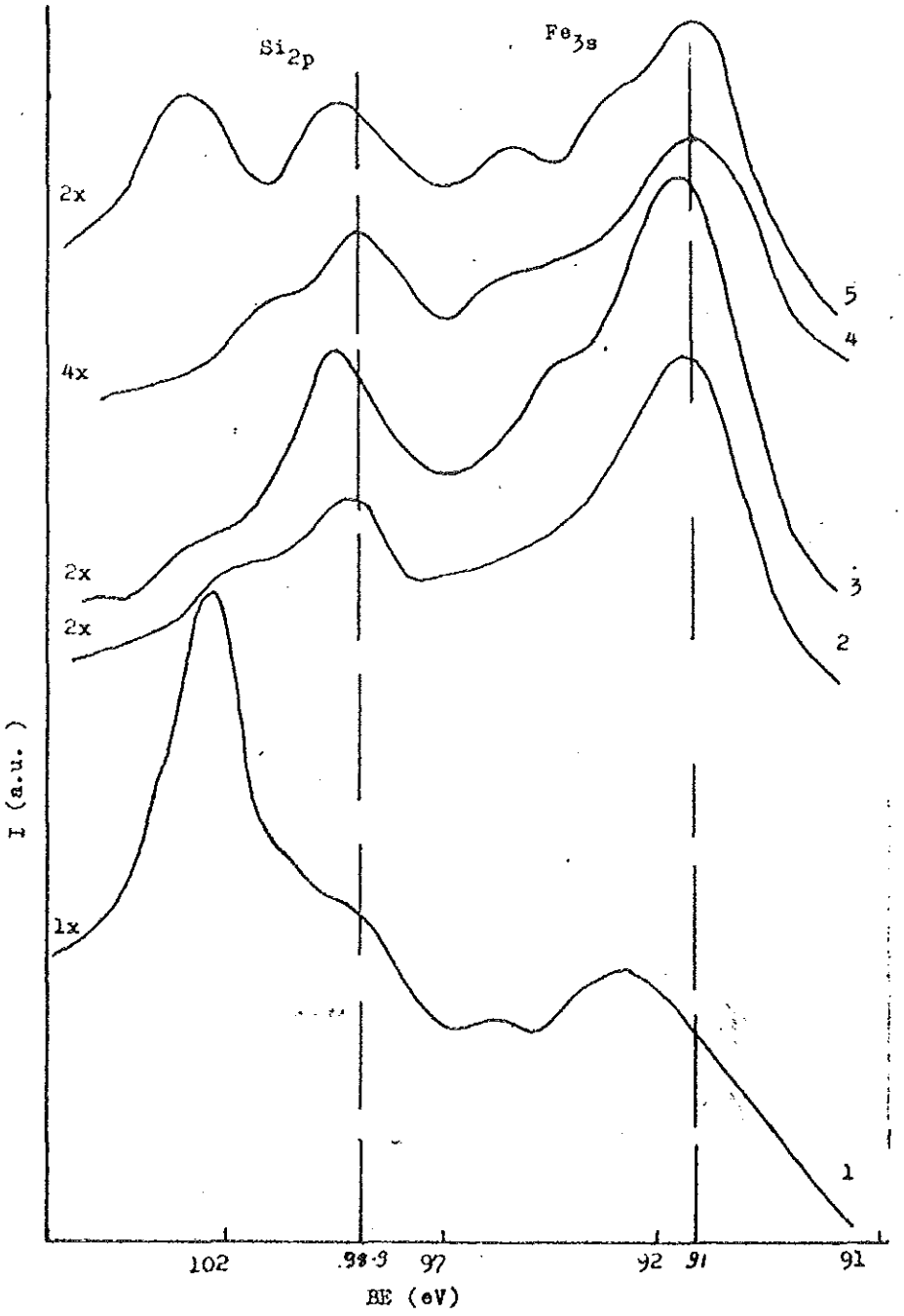

FIG.3b.

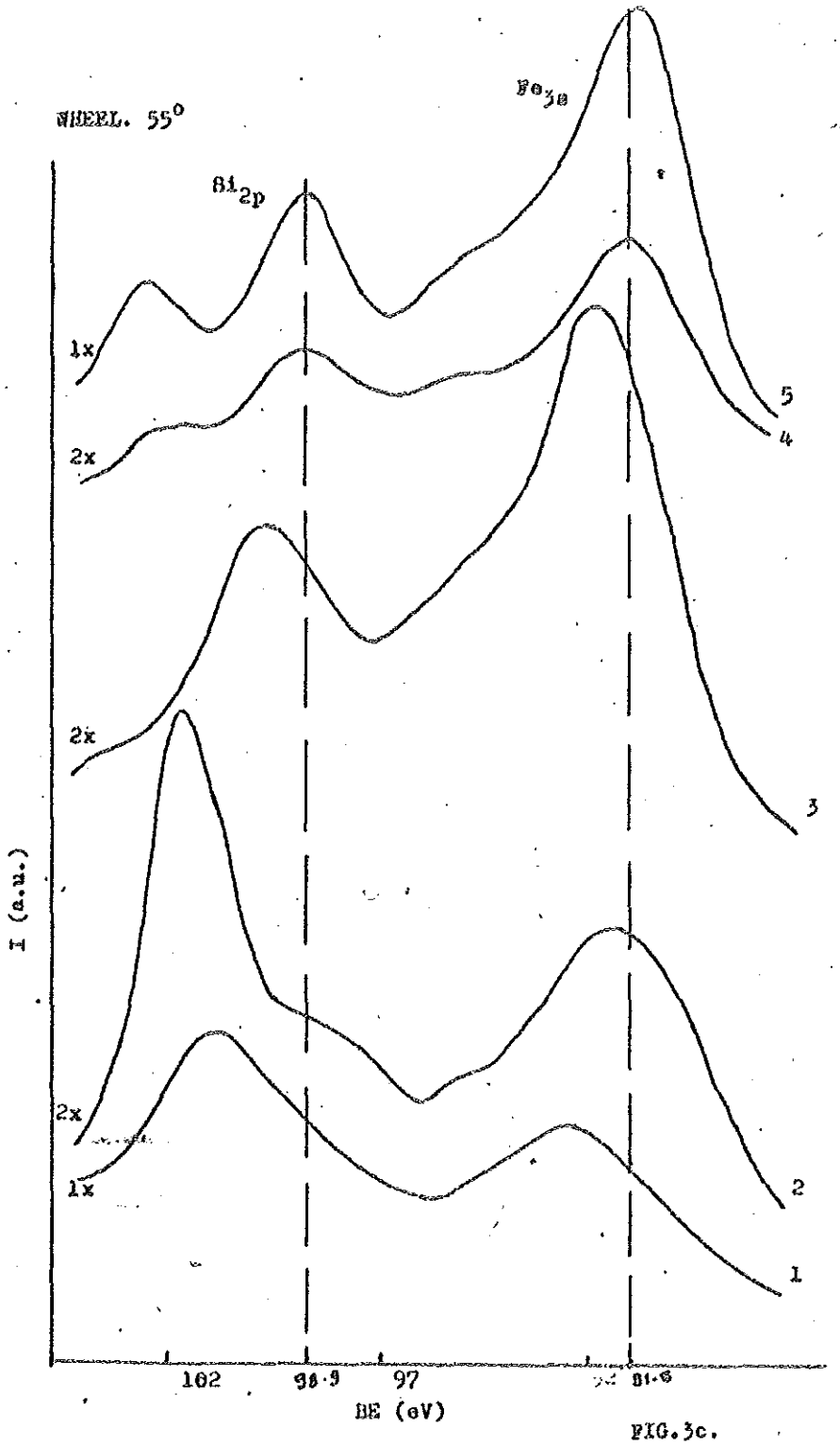

FIG.3c.

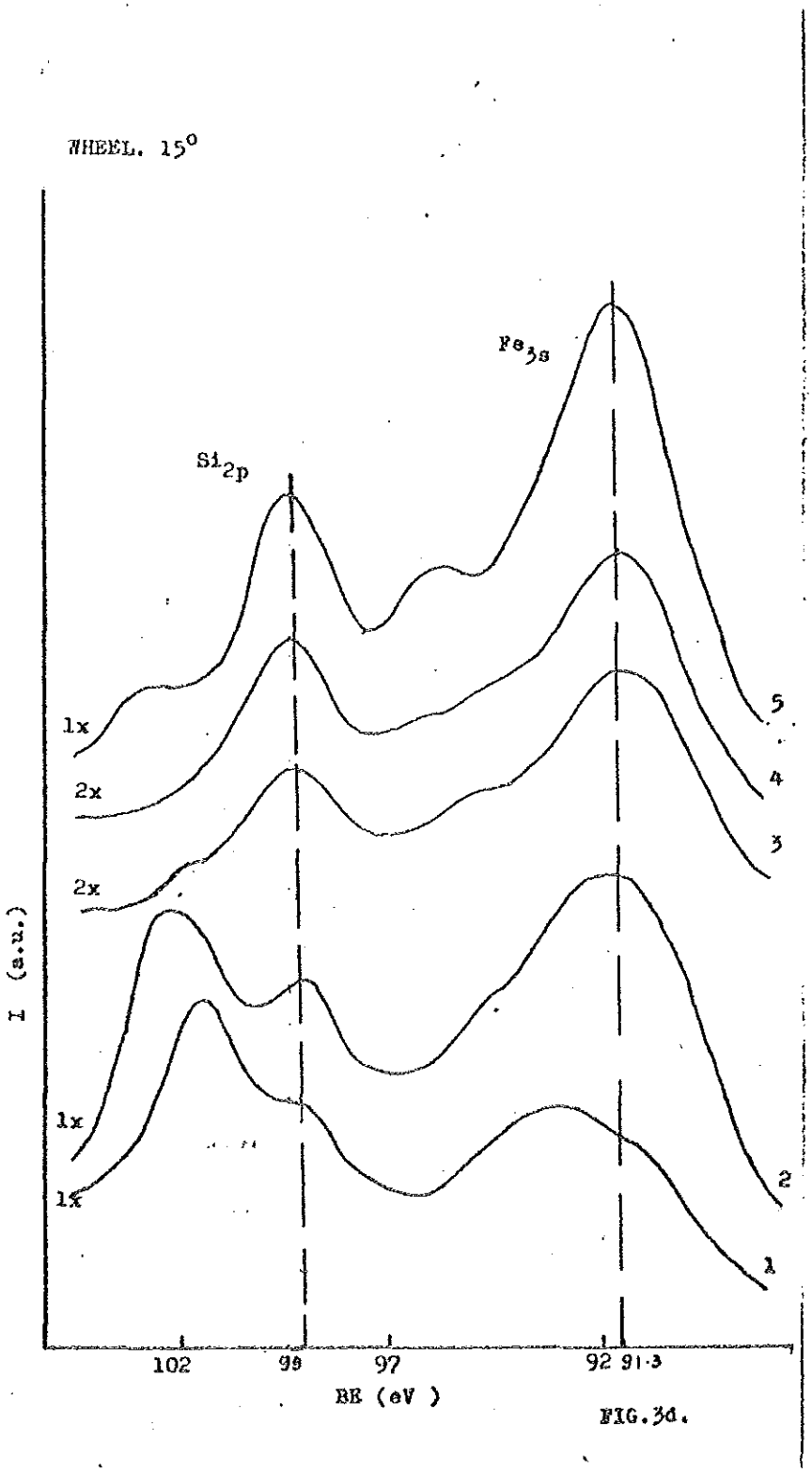

FIG.3d.

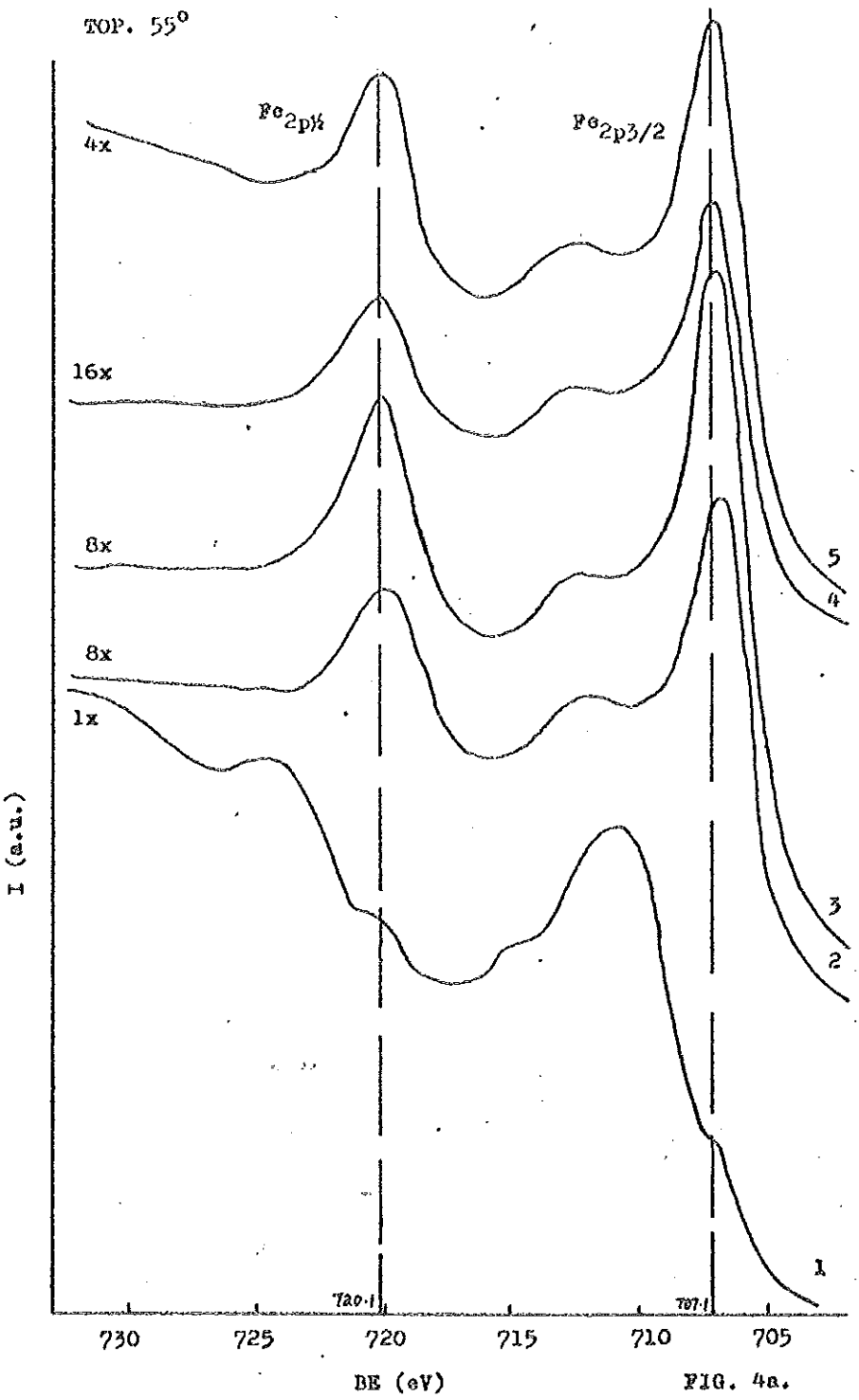
TOP. 55°
Fe2p½
Fe2p3/2
4x
16x
8x
8x
1x
5
4
3
2
1
I (a.u.)
720.1
707.1
730
725
720
715
710
705
BE (eV)

FIG. 4a.

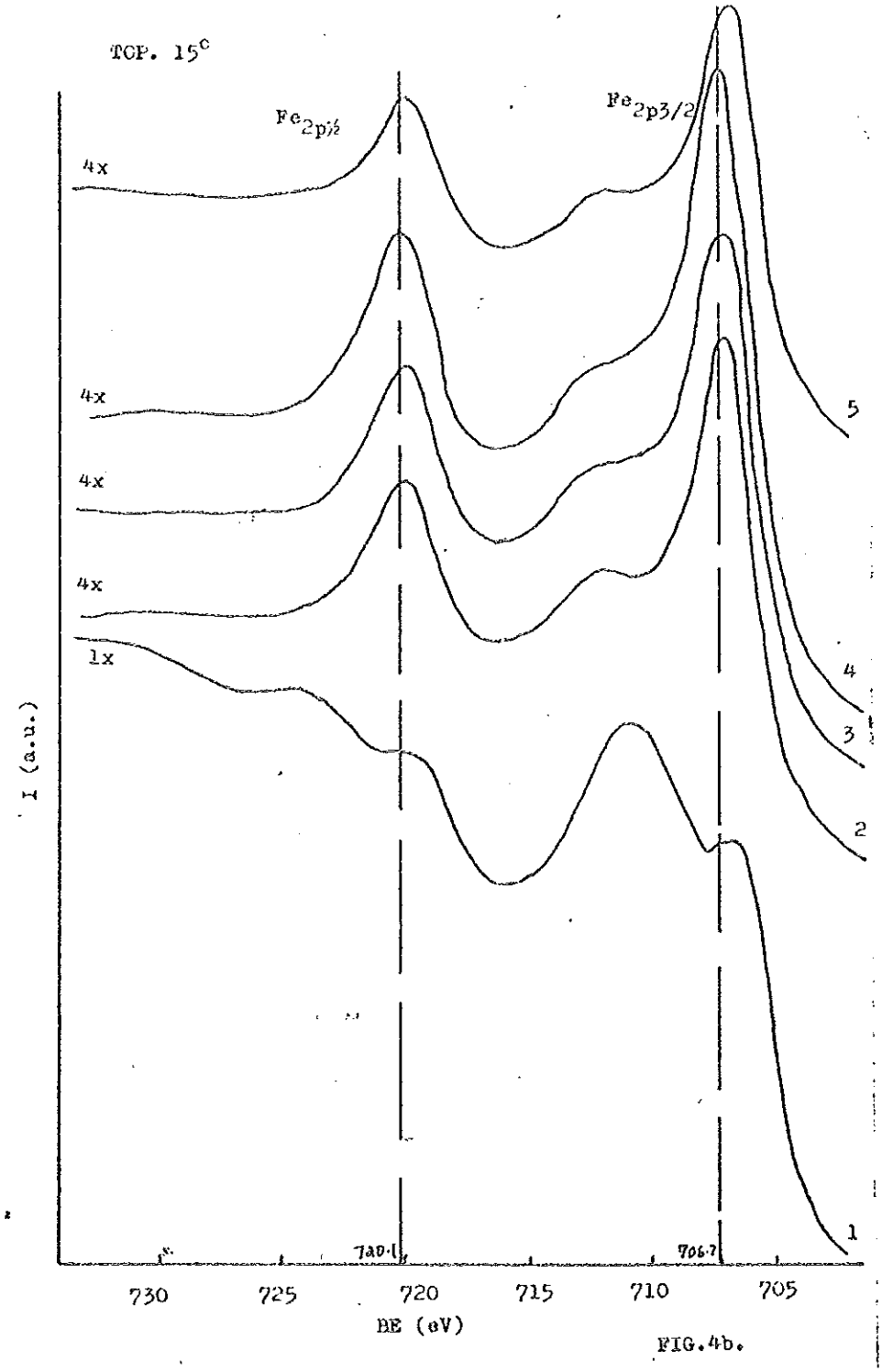
TCP. 15°
Fe2p½
Fe2p3/2
4x
4x
4x
4x
1x
5
4
3
2
1
I (a.u.)
720.1
706.7
730
725
720
715
710
705
BE (eV)

FIG.4b.

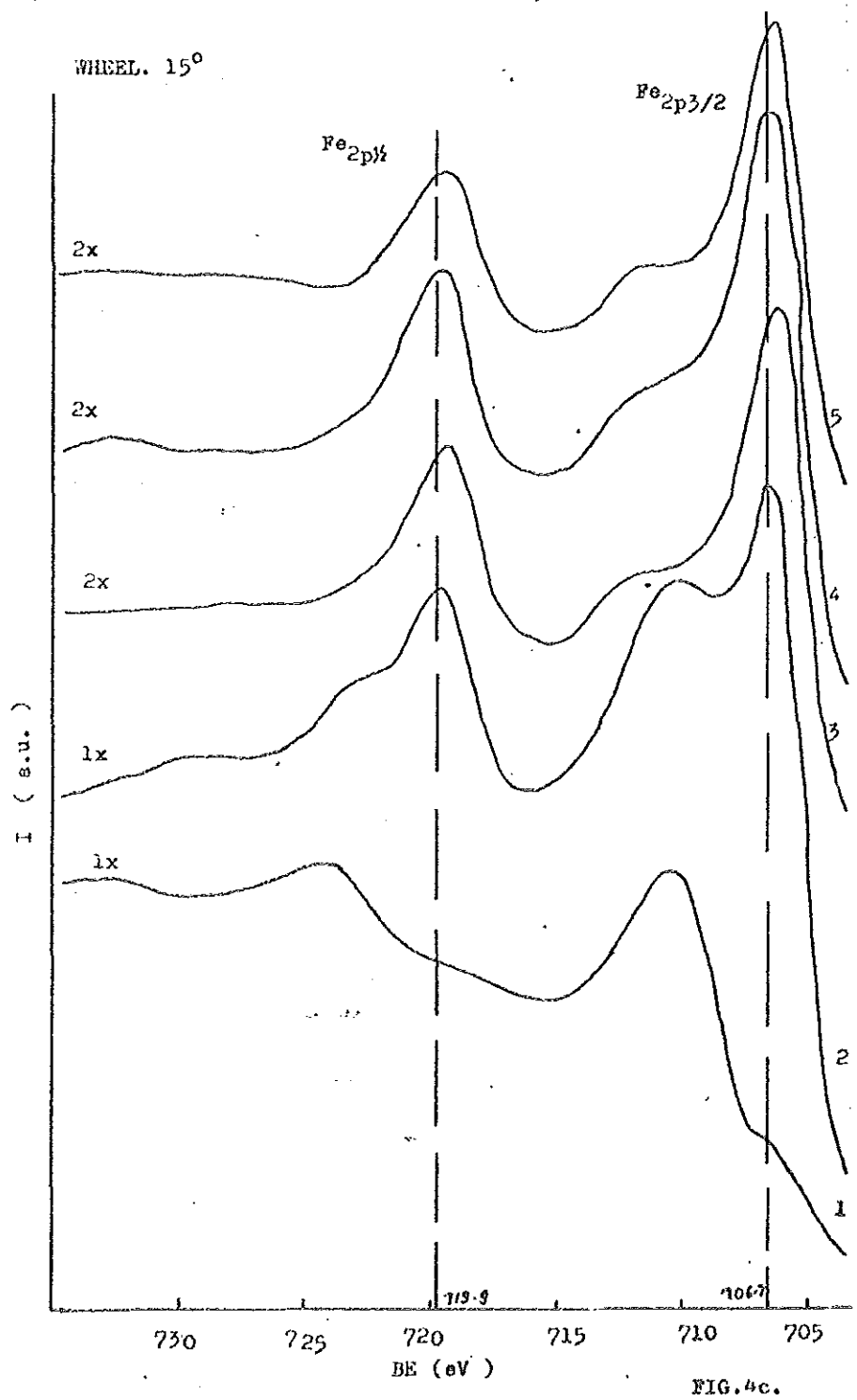
WHEEL. 15°
$Fe_{2p1/2}$
$Fe_{2p3/2}$
2x
2x
2x
1x
1x
5
4
3
2
1
I (a.u.)
719.9
706.7
730
725
720
715
710
705
BE (eV)

FIG.4c.

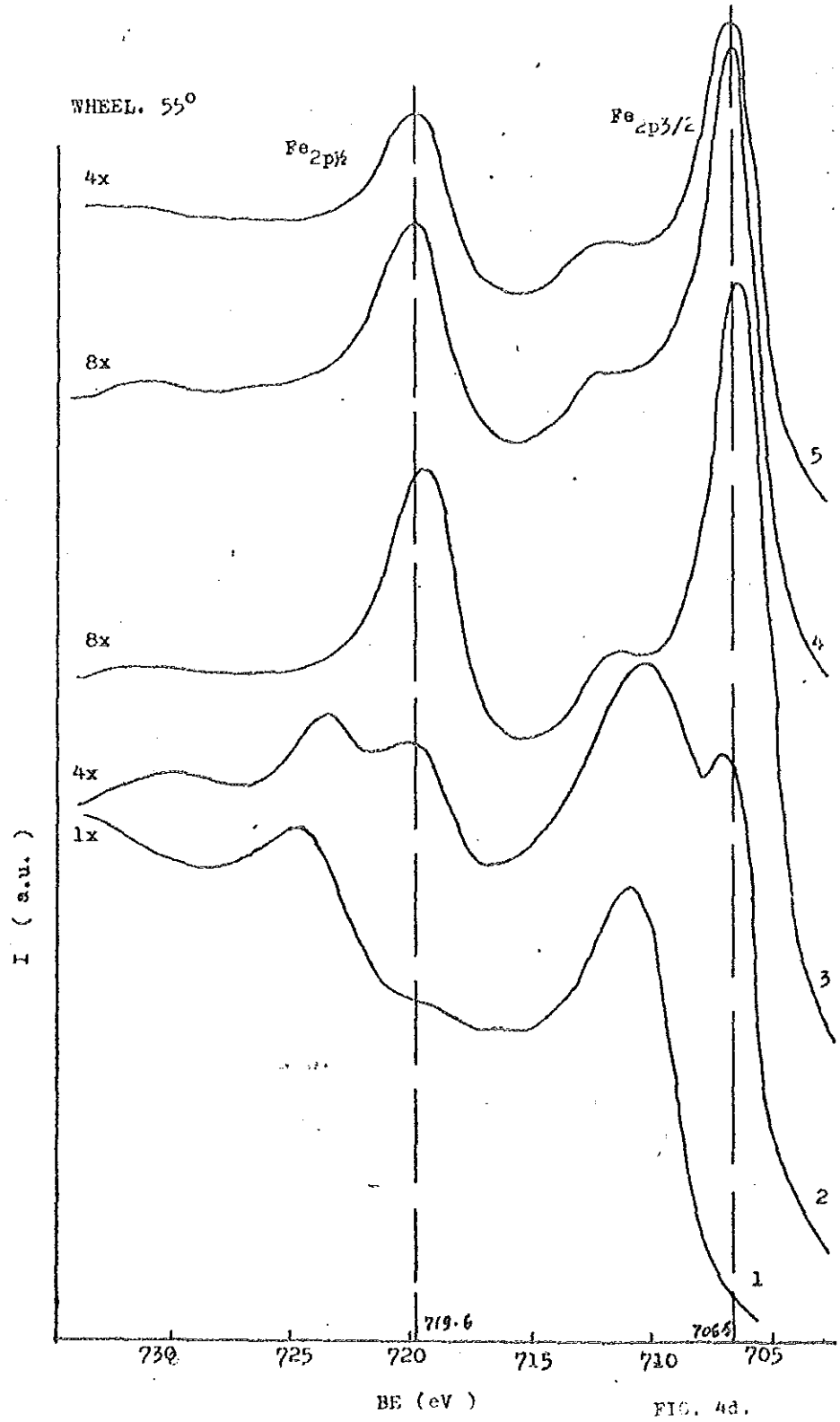
WHEEL. 55°
Fe 2p½
Fe 2p3/2
4x
8x
8x
4x
1x
5
4
3
2
1
I (a.u.)
719.6
706.5
730
725
720
715
710
705
BE (eV)

FIG. 4d.

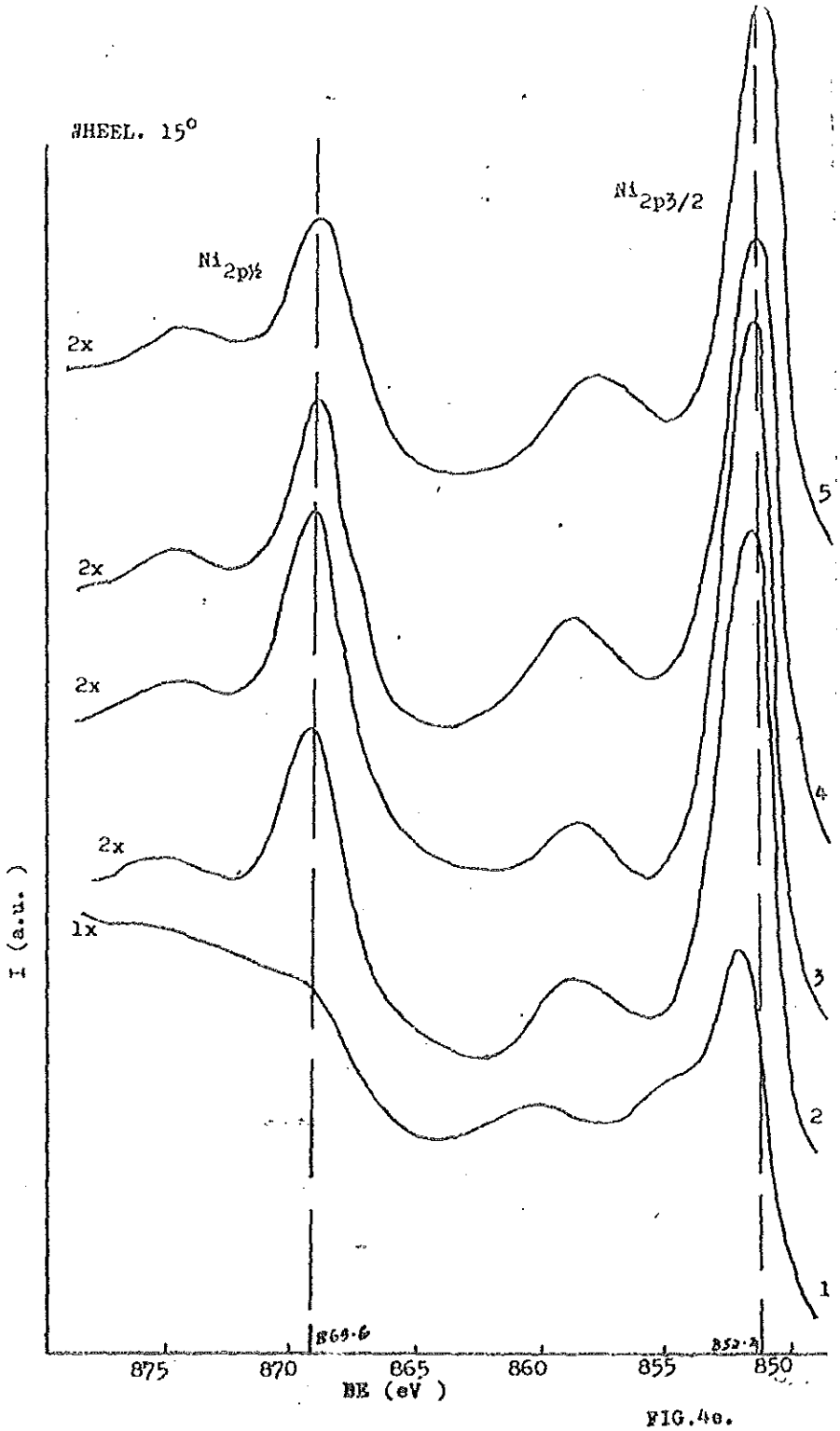
WHEEL. 15°
Ni 2p½
Ni 2p3/2
2x
2x
2x
2x
1x
5
4
3
2
1
I (a.u.)
869.6
852.3
875
870
865
860
855
850
BE (eV)

FIG.4e.

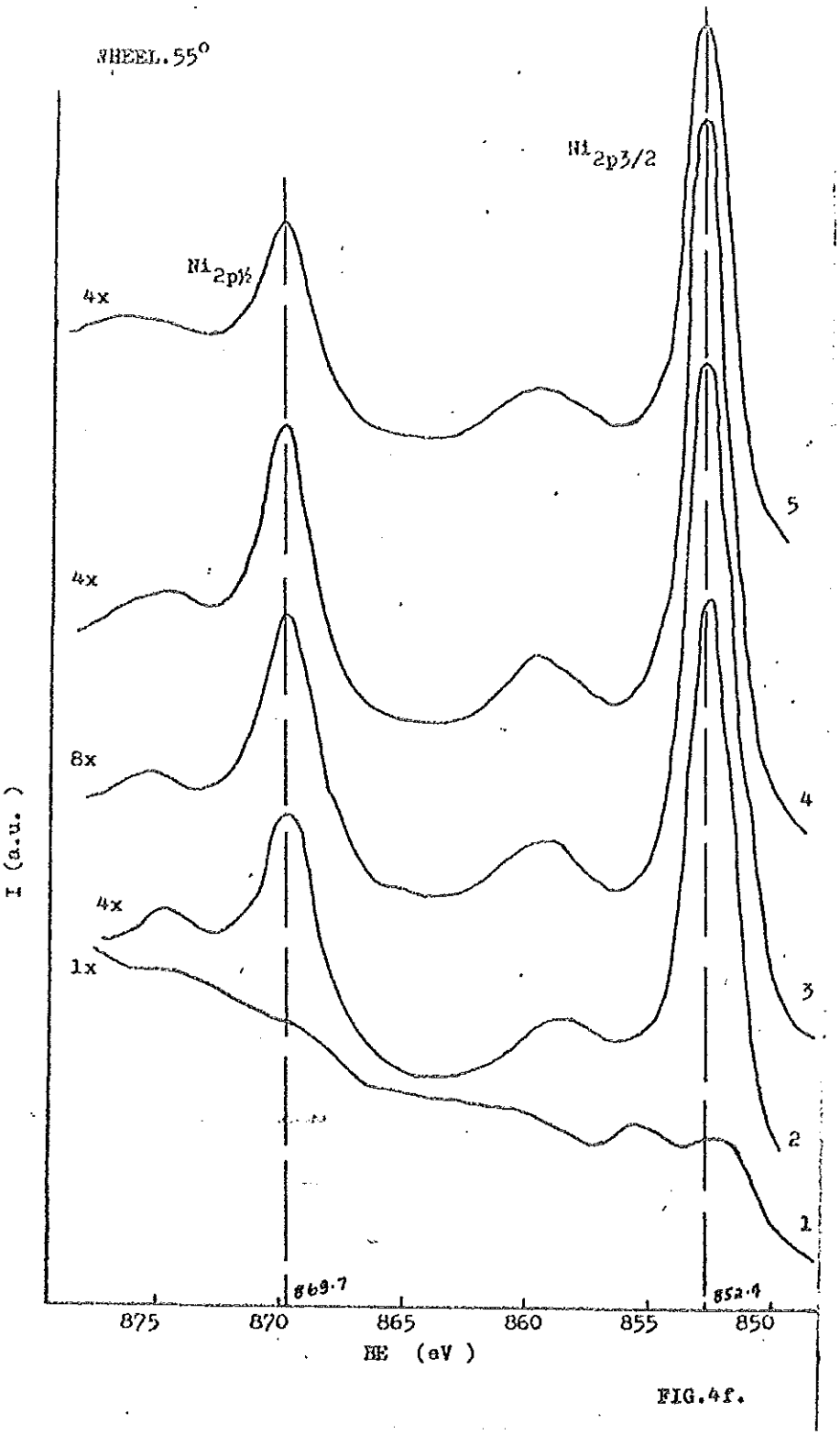
WHEEL. 55°
Ni 2p3/2
Ni 2p½
4x
4x
8x
4x
1x
5
4
3
2
1
I (a.u.)
869.7
852.4
875
870
865
860
855
850
BE (eV)

FIG.4f.

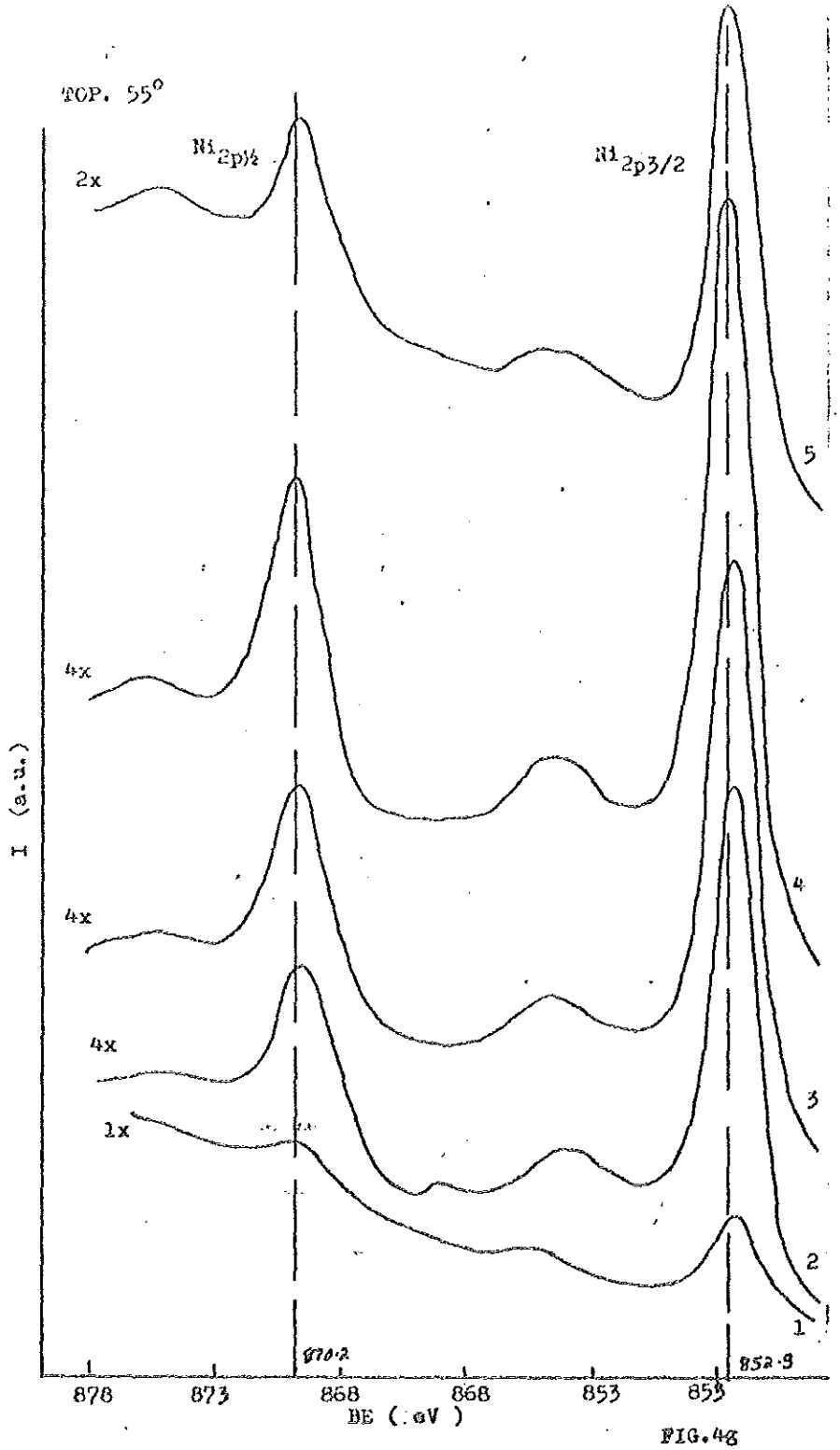
TOP. 55°
Ni 2p½
Ni 2p3/2
2x
4x
4x
4x
1x
5
4
3
2
1
I (a.u.)
870·2
852·9
878
873
868
863
858
BE (eV)

FIG.4g

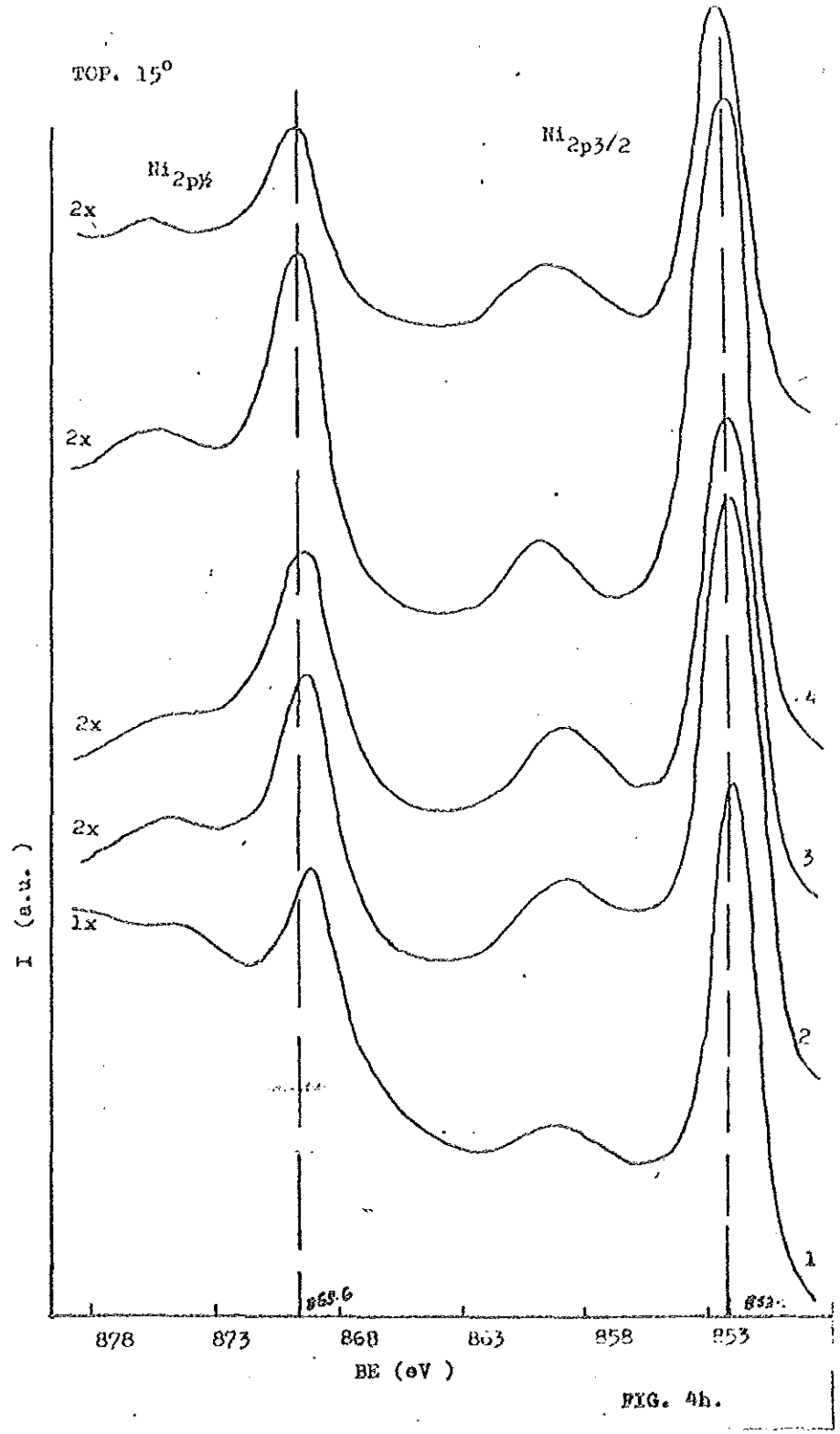
TOP. 15°
Ni 2p½
Ni 2p3/2
2x
2x
2x
2x
1x
I (a.u.)
1
2
3
4
868.6
852.
878
873
868
863
858
853
BE (eV)

FIG. 4b.

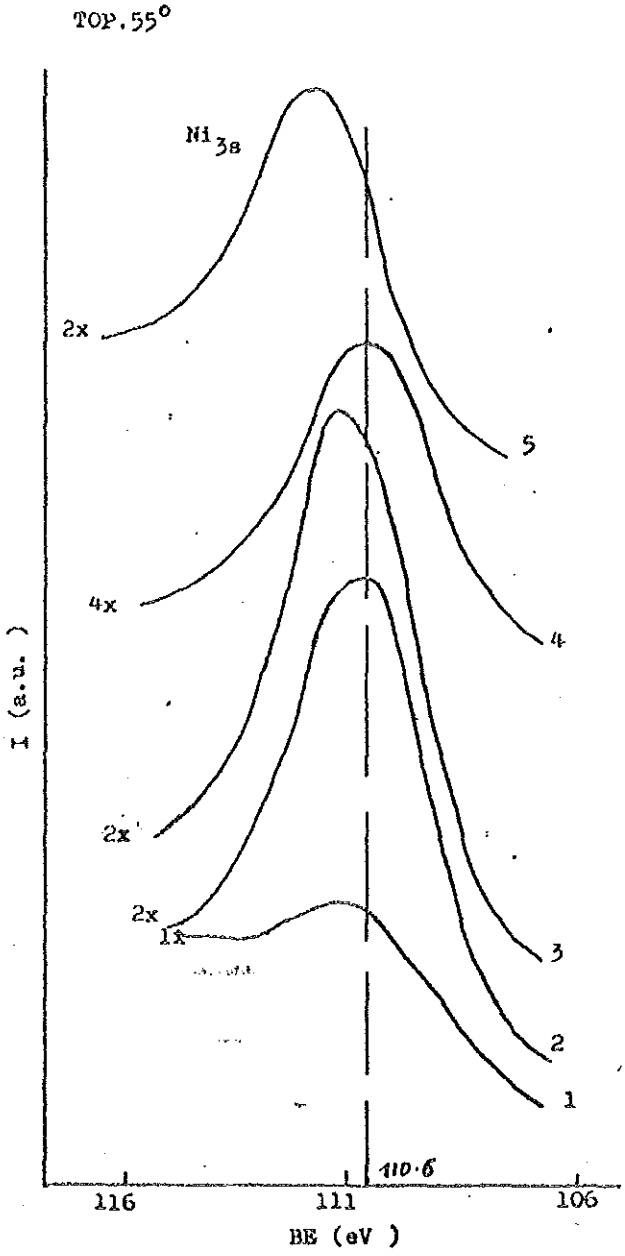

FIG.5a.

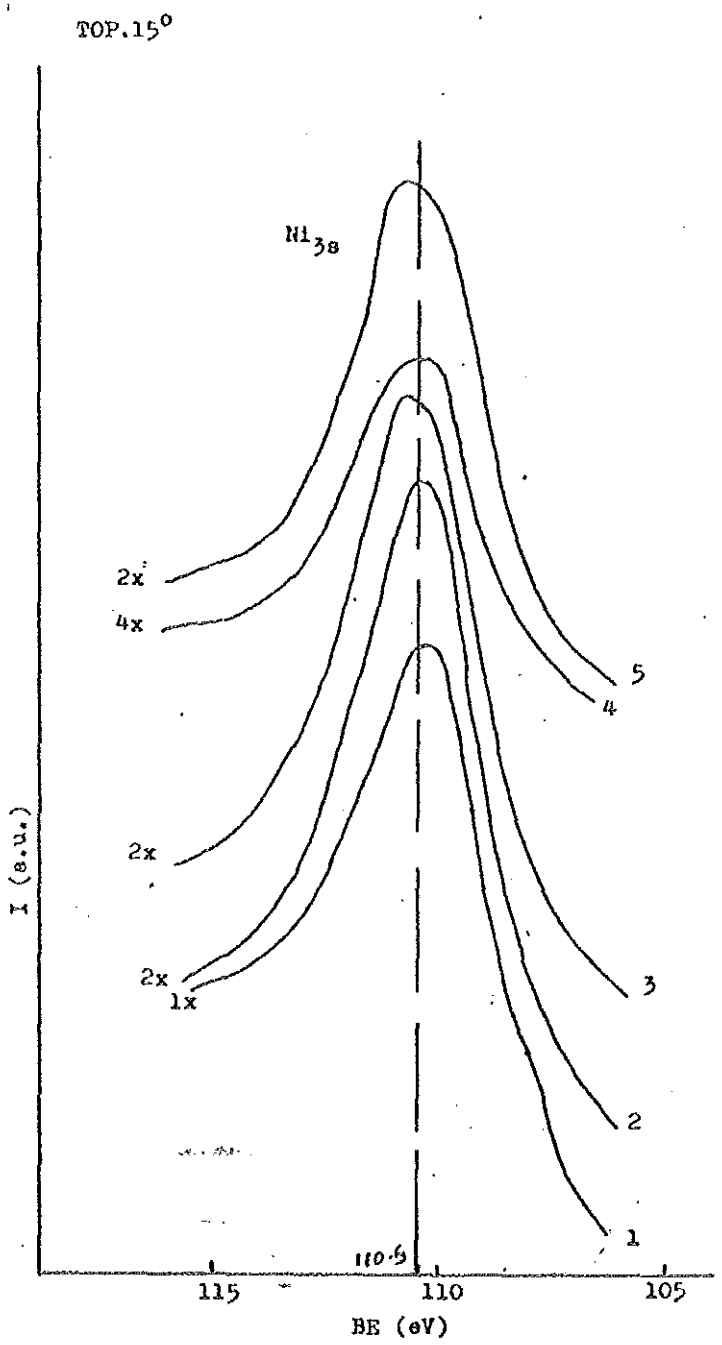

FIG.5b.

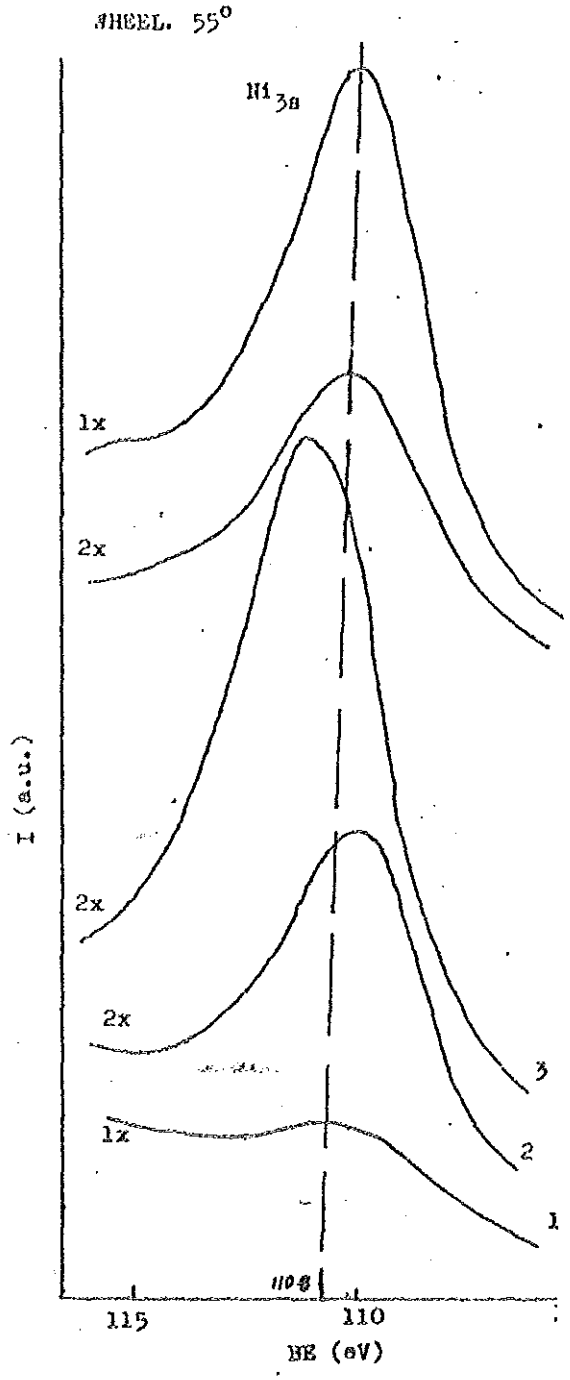

FIG

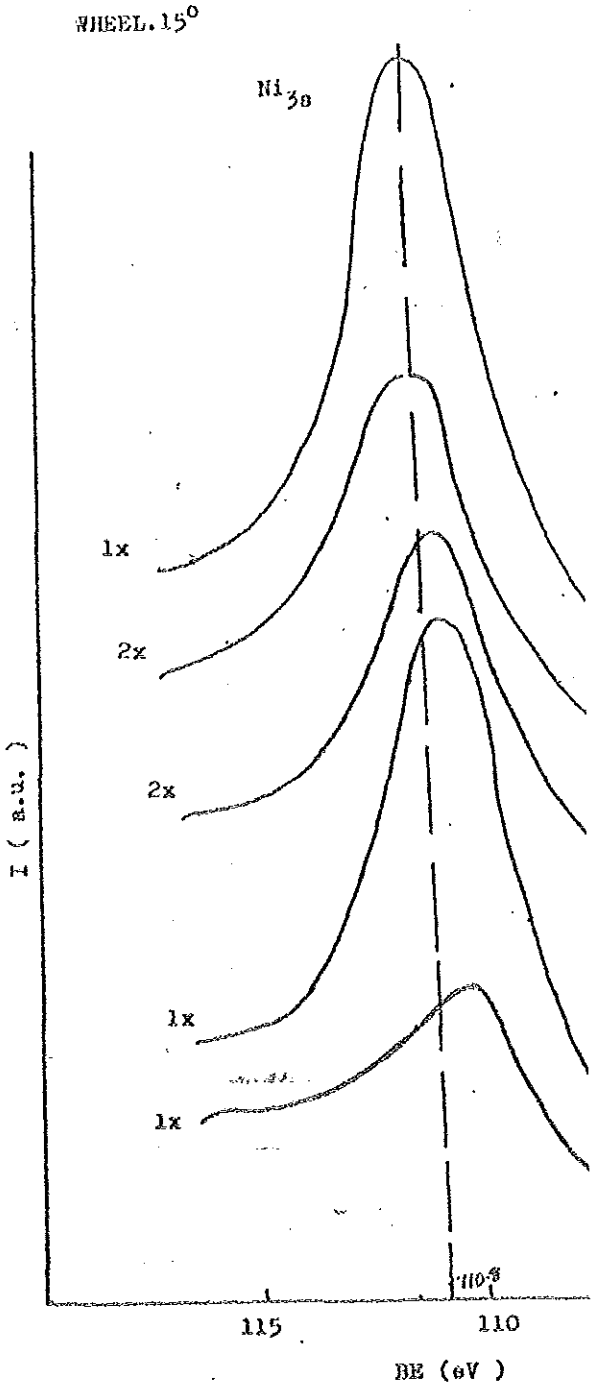
WHEEL. 15°
Ni 3s
1x
2x
2x
1x
1x
I (a.u.)
115
110
BE (eV)

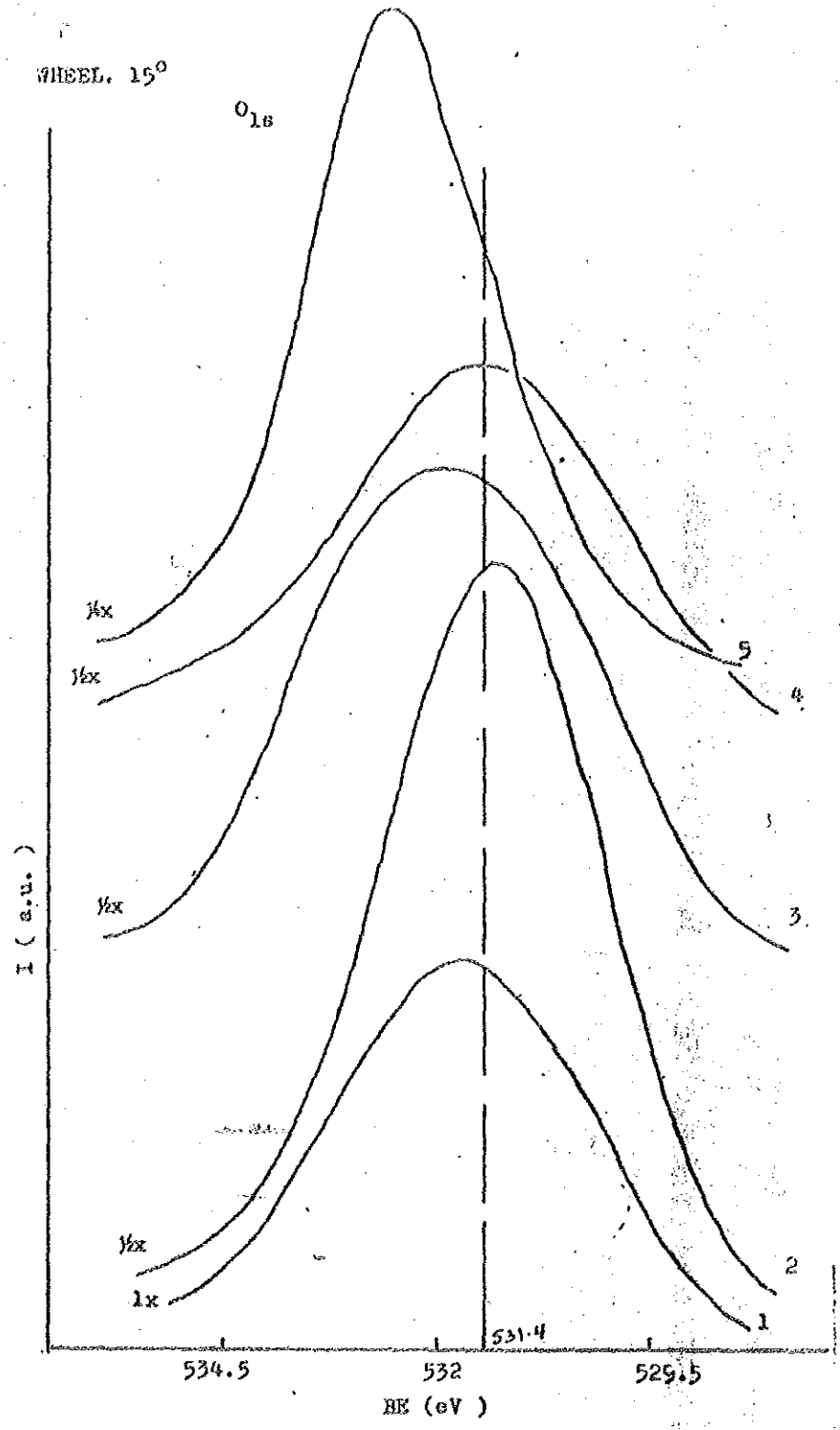

FIG.6a.

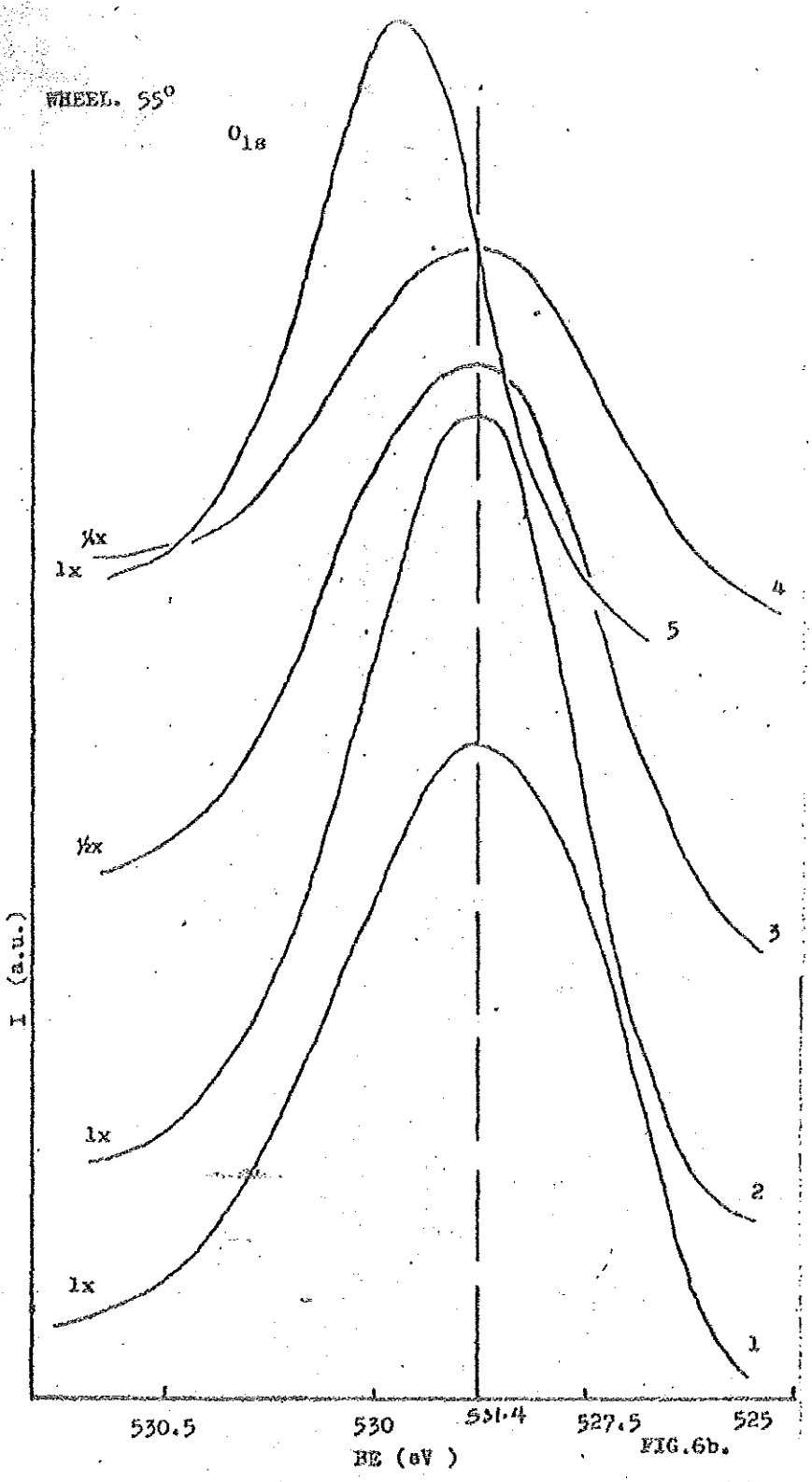
WHEEL. 55°
O_{1s}
½x
1x
½x
1x
1x
1
2
3
4
5
I (a.u.)
530.5
530
531.4
527.5
525
BE (eV)

FIG.6b.

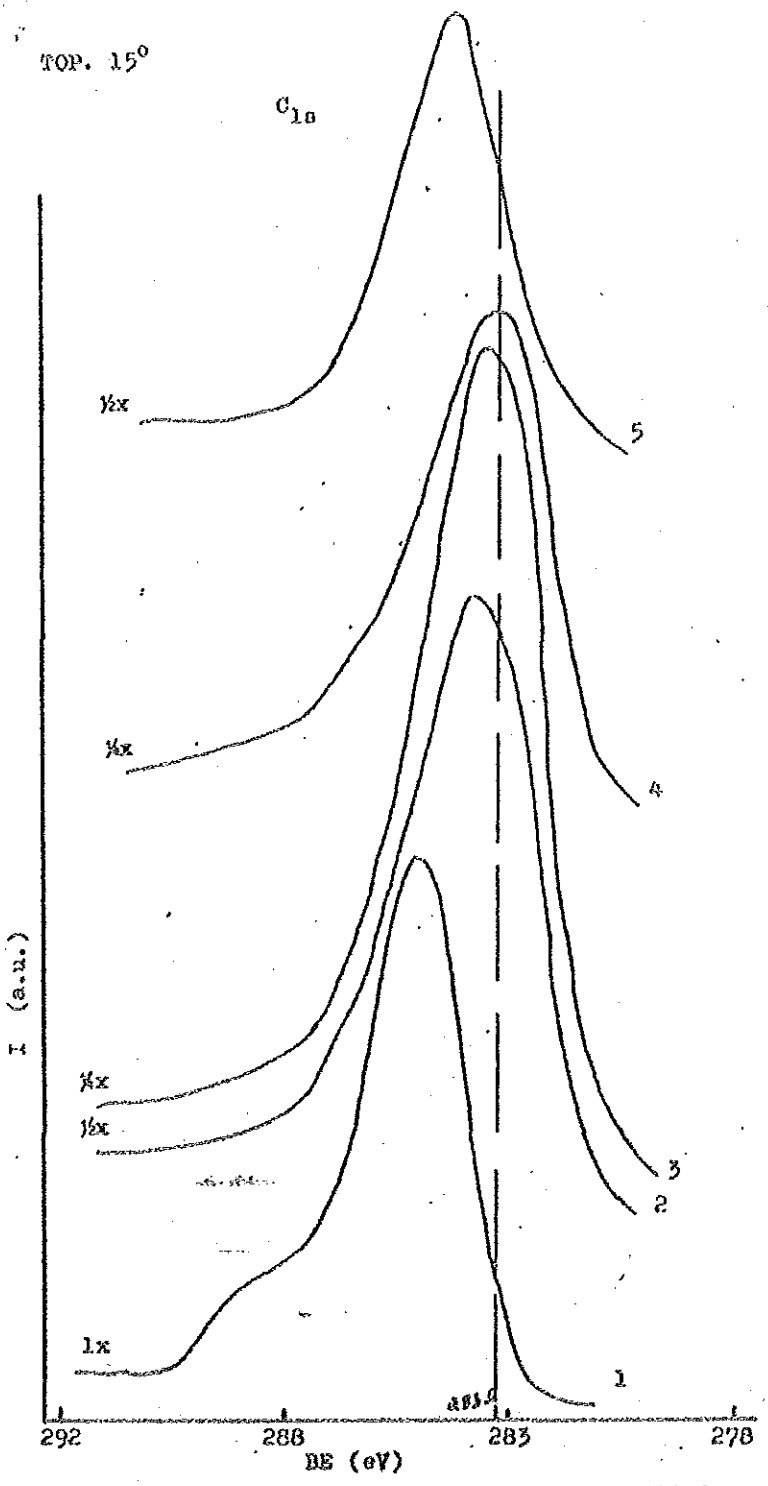

FIG.6c.

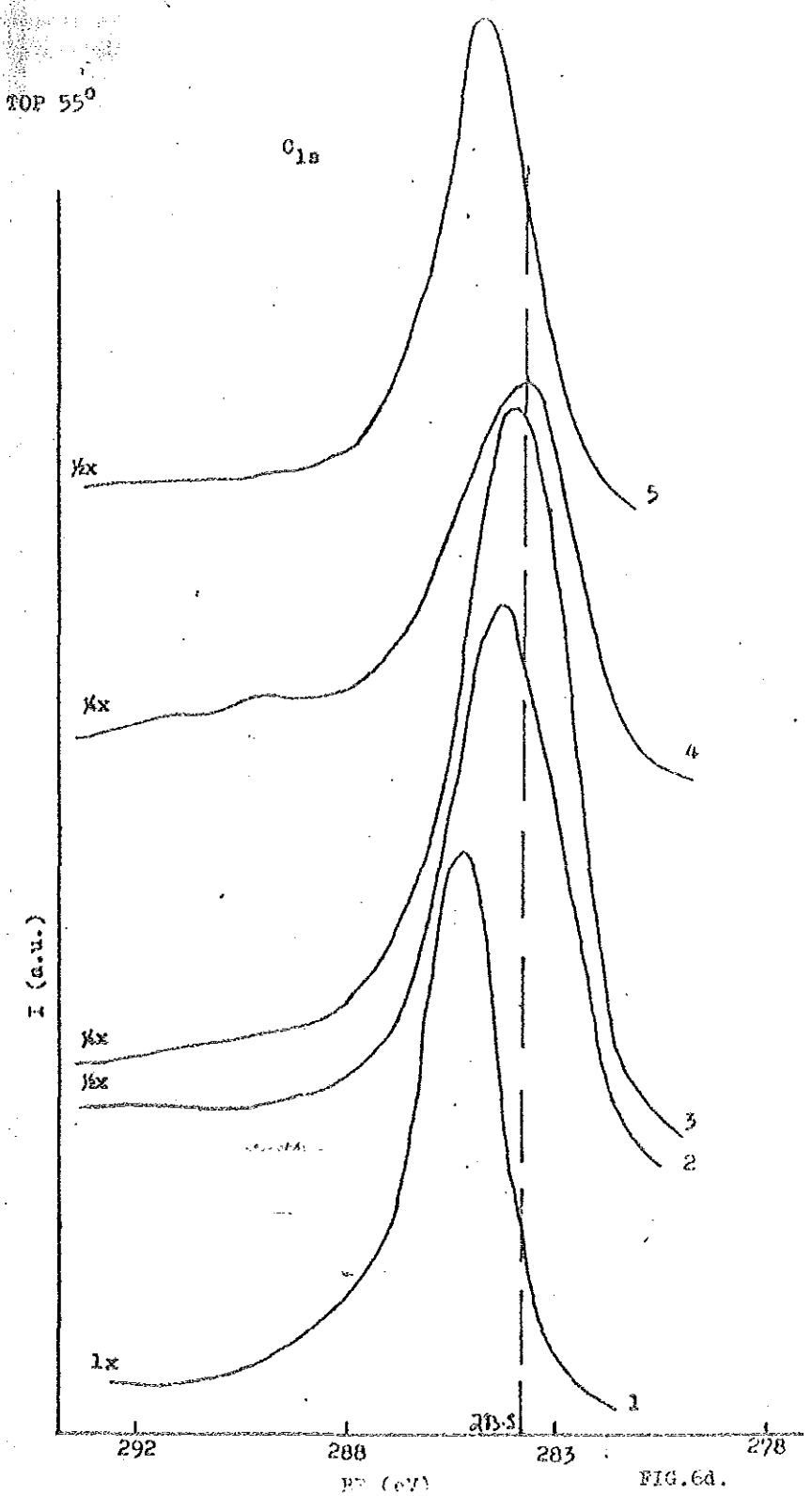

FIG.6d.

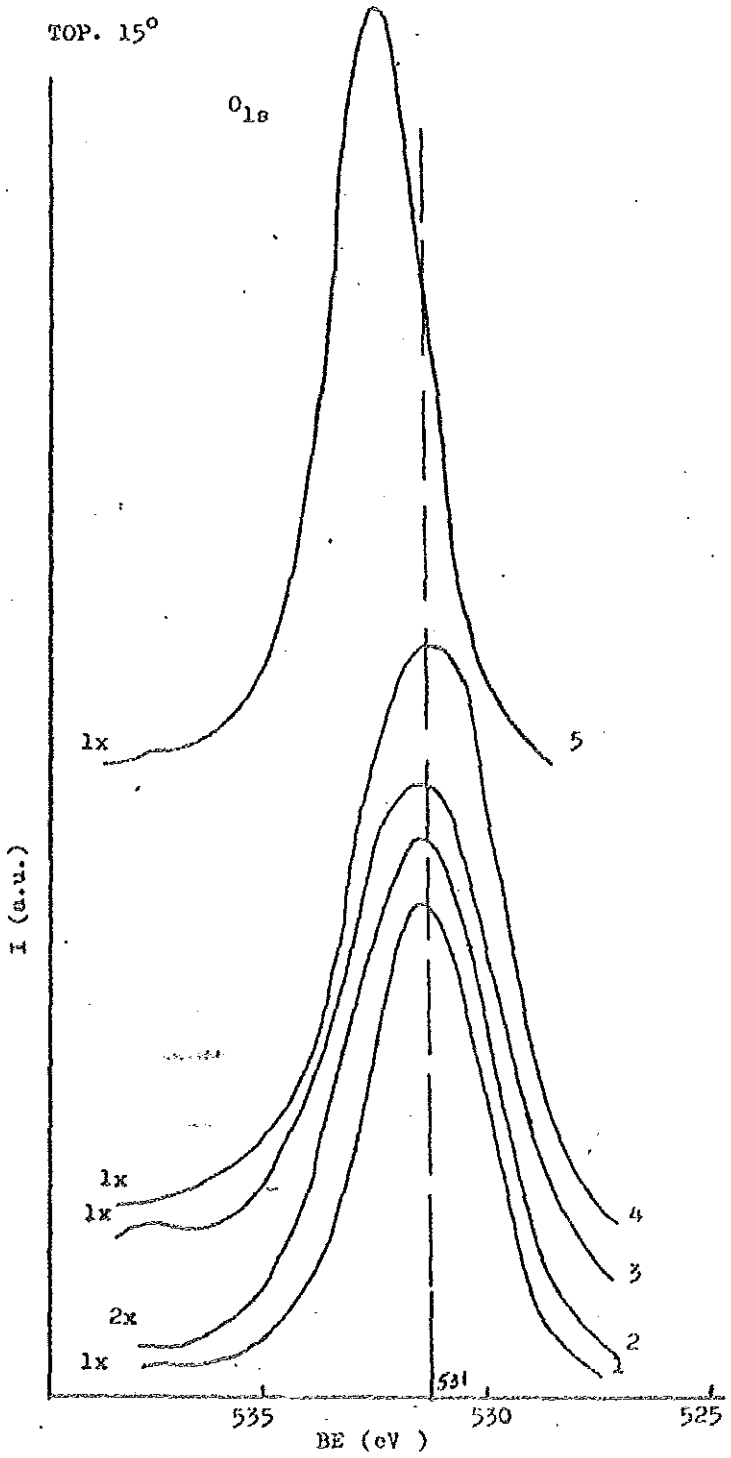

FIG. 6e

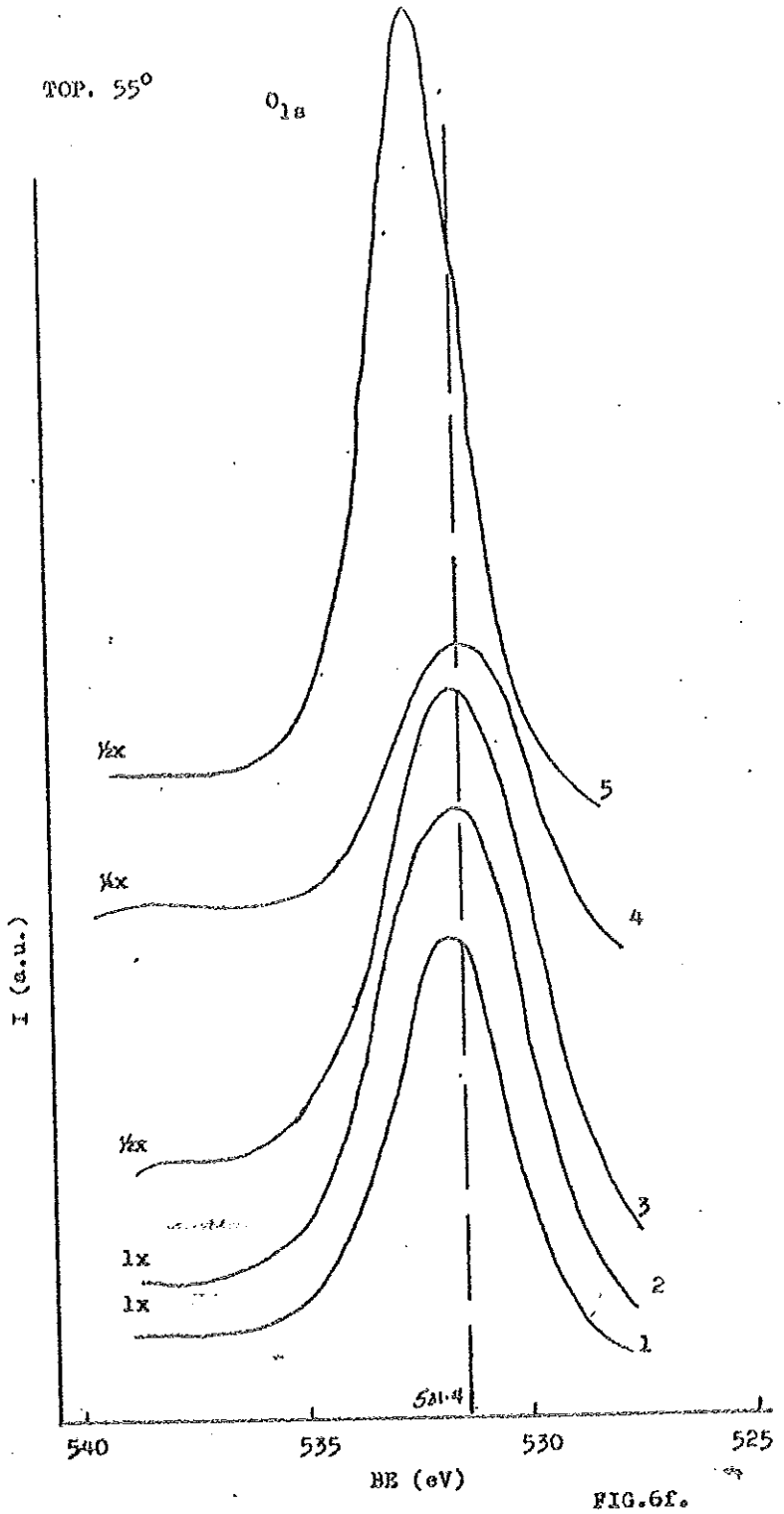

FIG.6f.

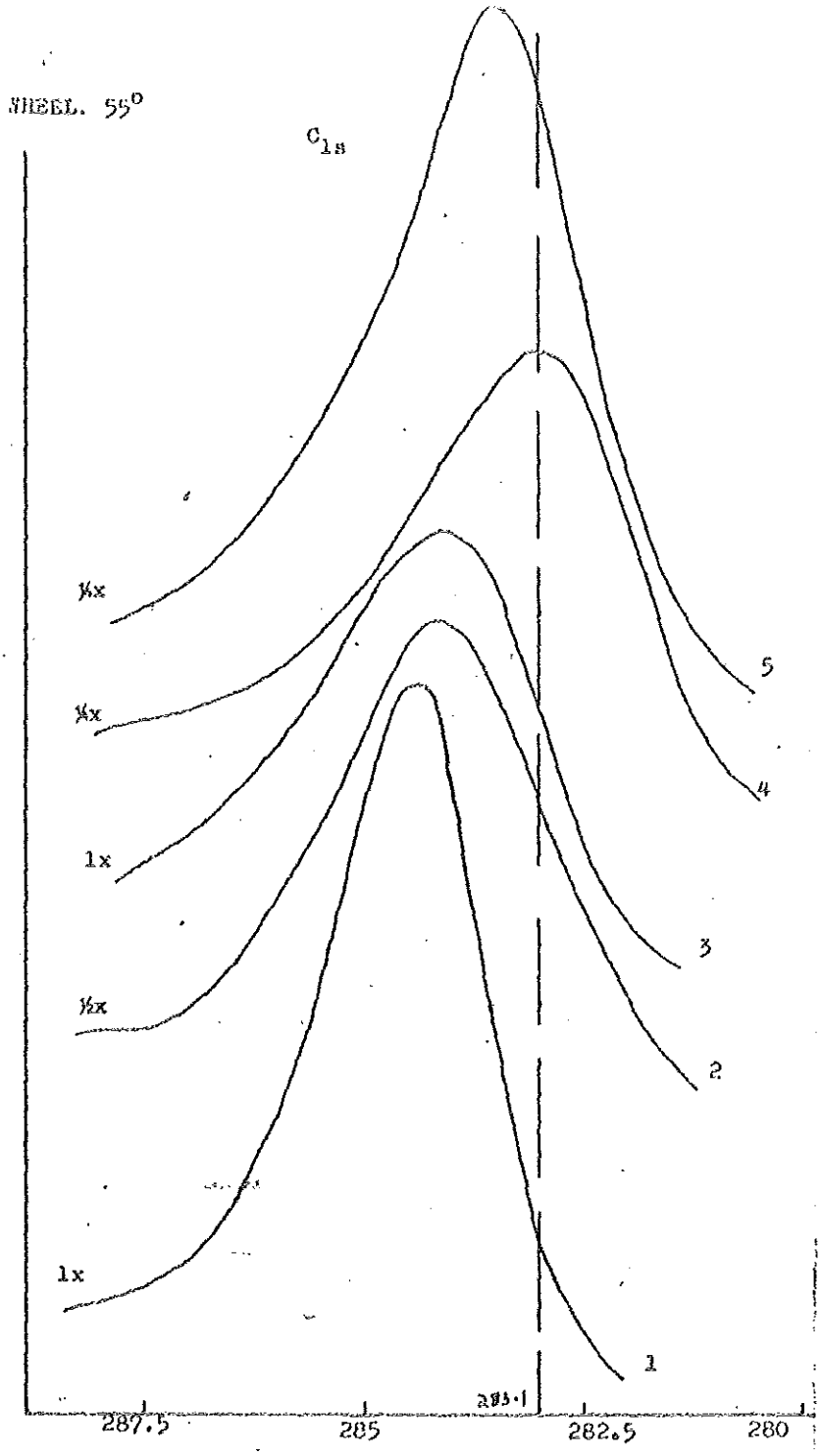

FIG.6g

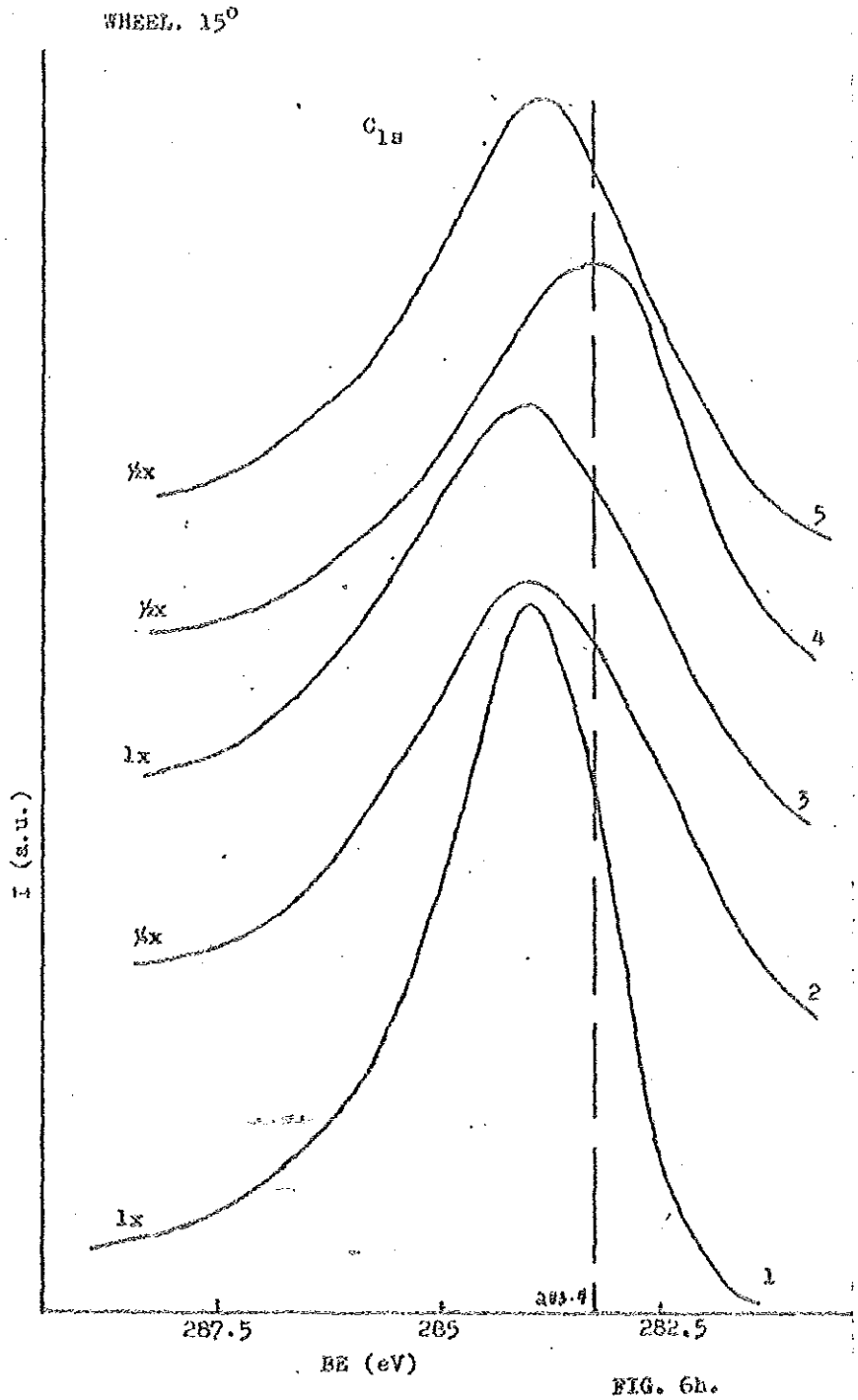

FIG. 6b.

TOP. 15°

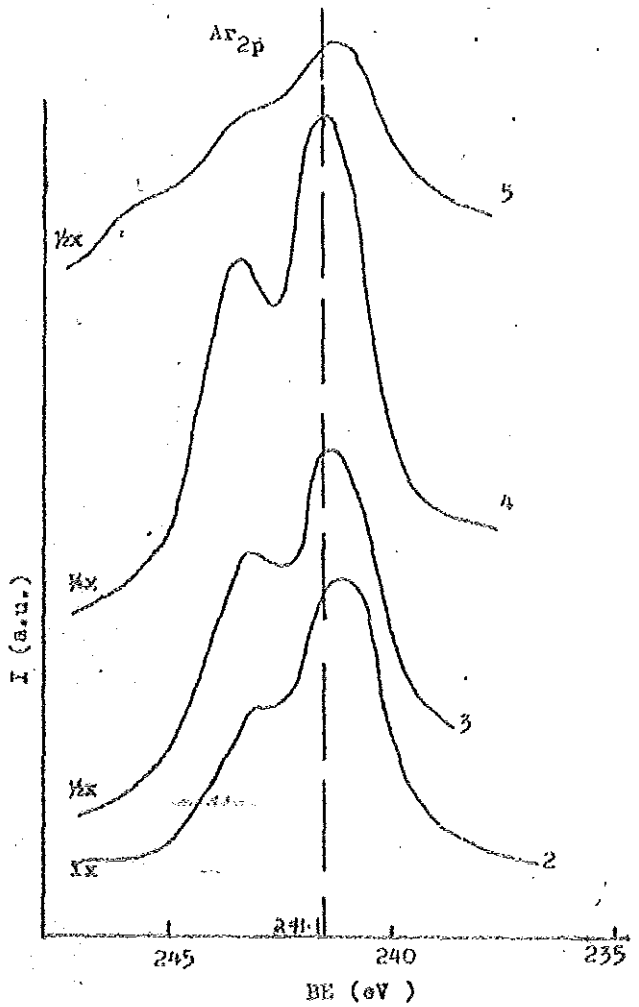

FIG.7a.

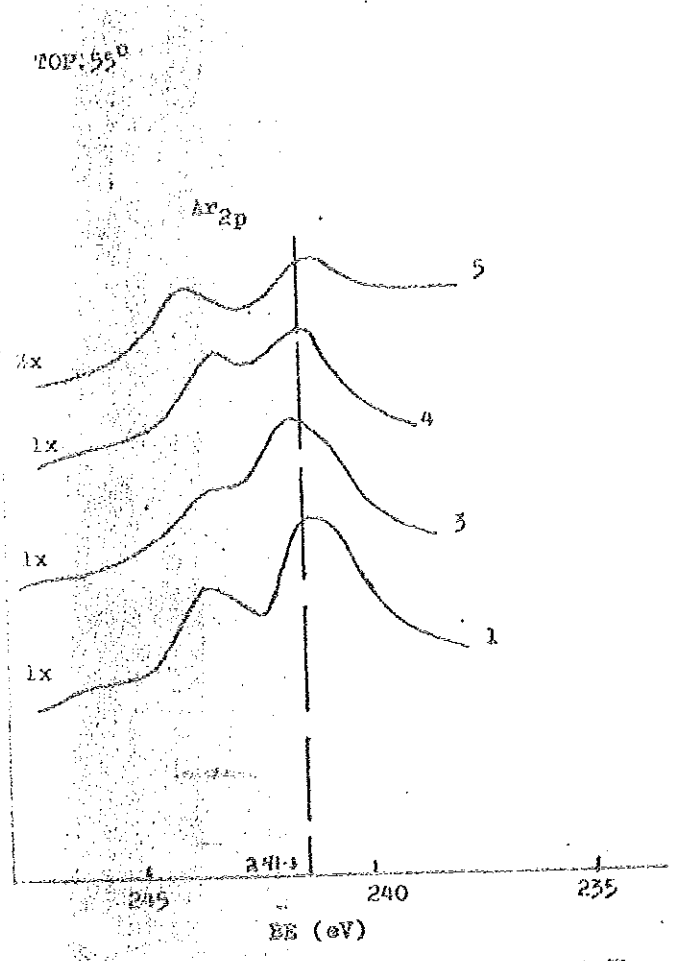

FIG. 7b.

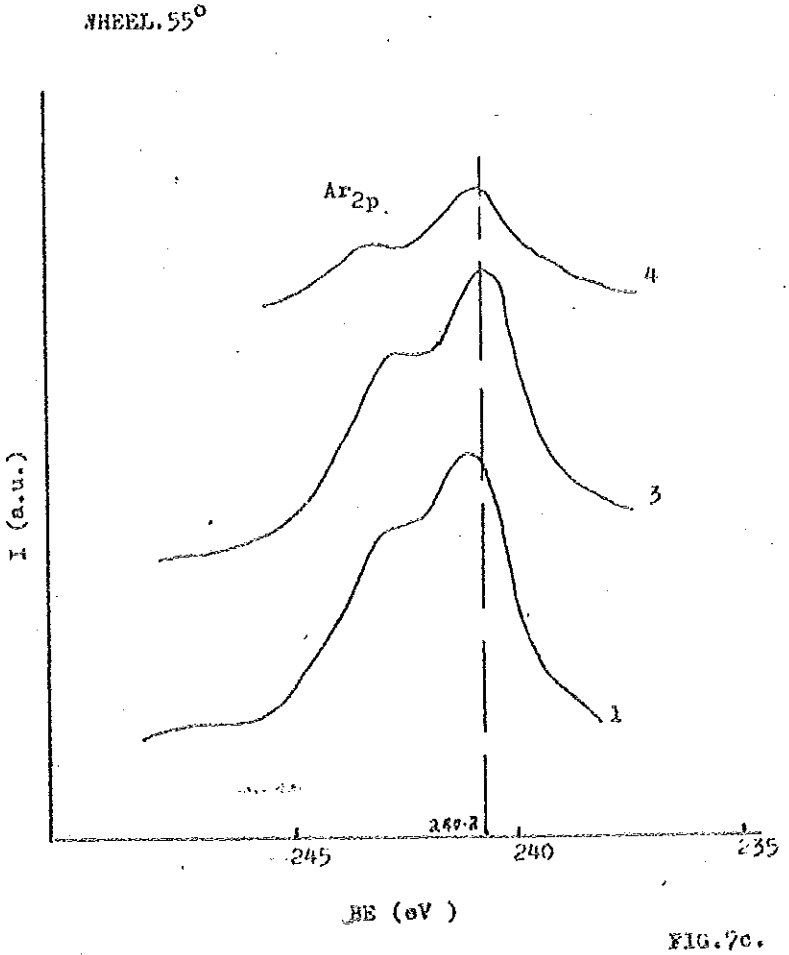

FIG. 7c.

WHEEL 15°

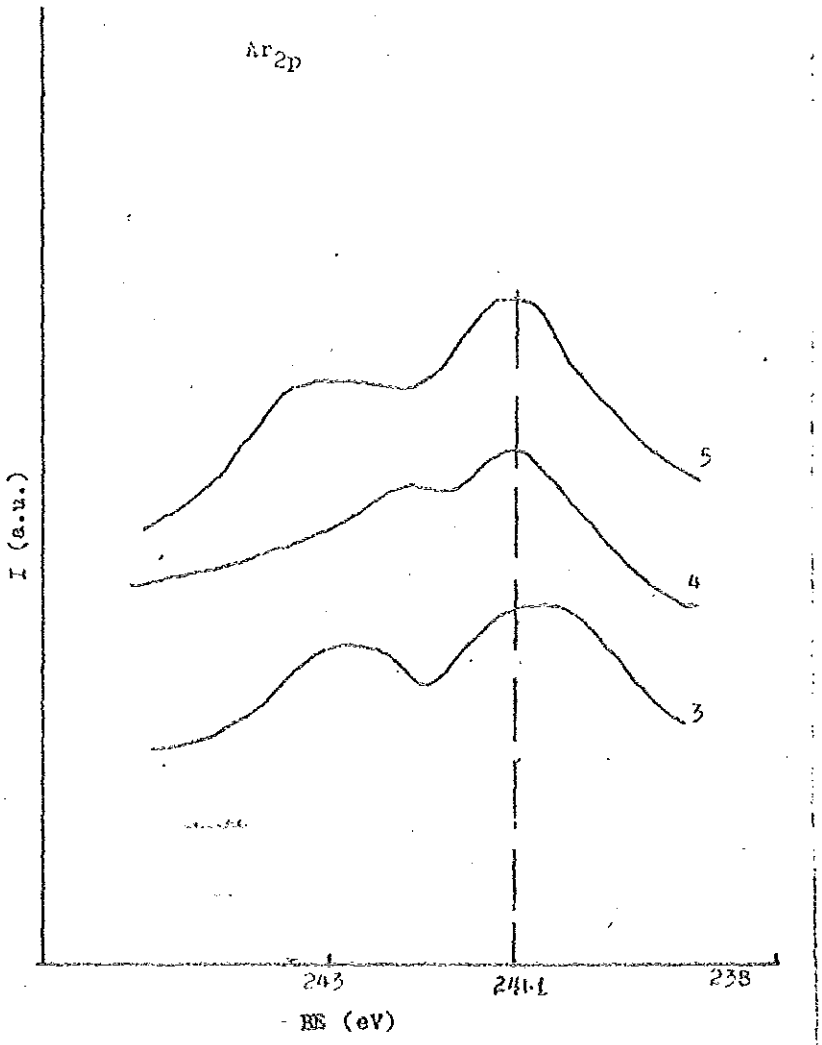

FIG.7d.

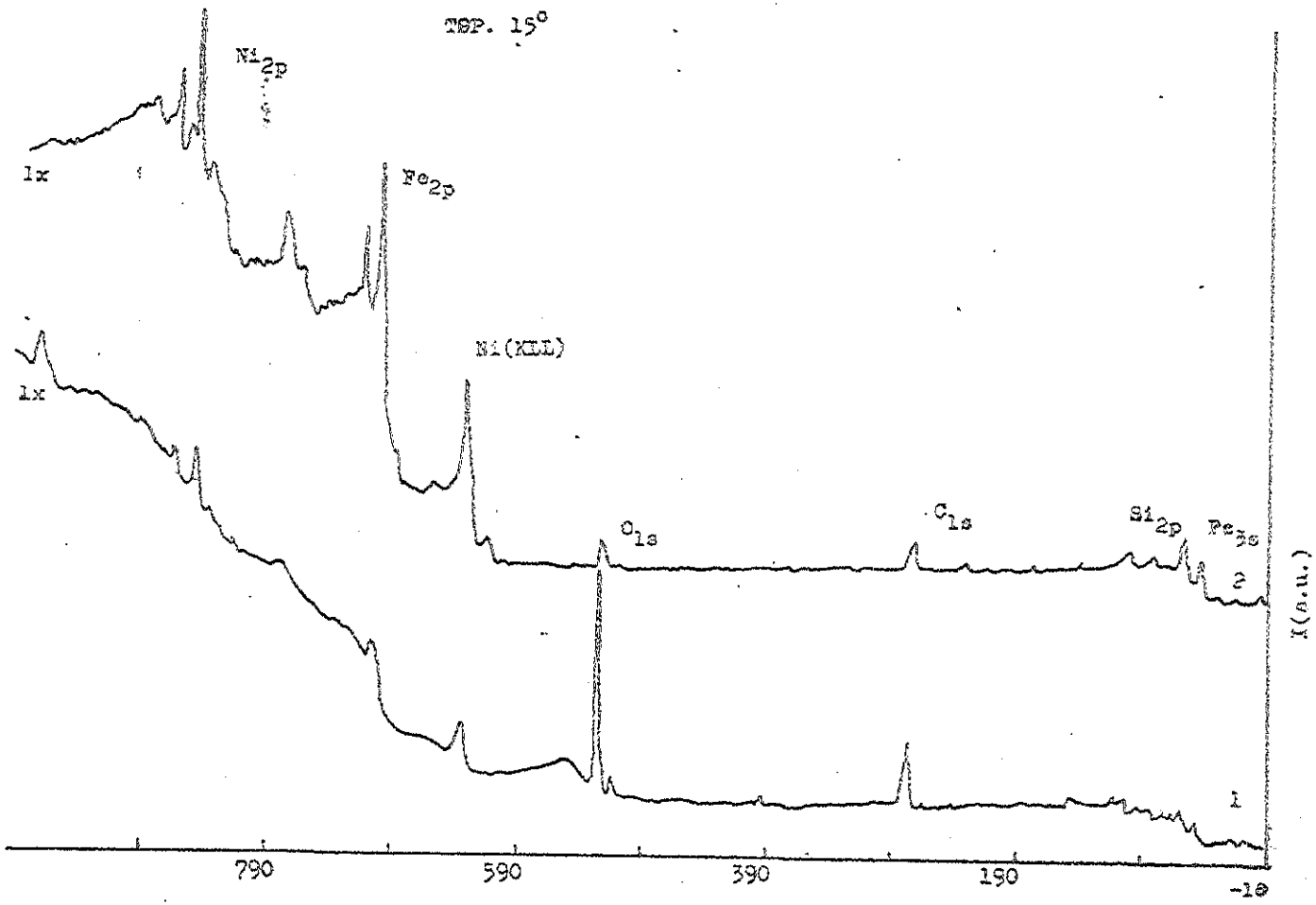
TEP. 15°
Ni 2p
Fe 2p
Ni(KLL)
O 1s
C 1s
Si 2p
Fe 3s
1x
1x
2
1
I(a.u.)
790
590
390
190
-10
BE (eV)

FIG 82.

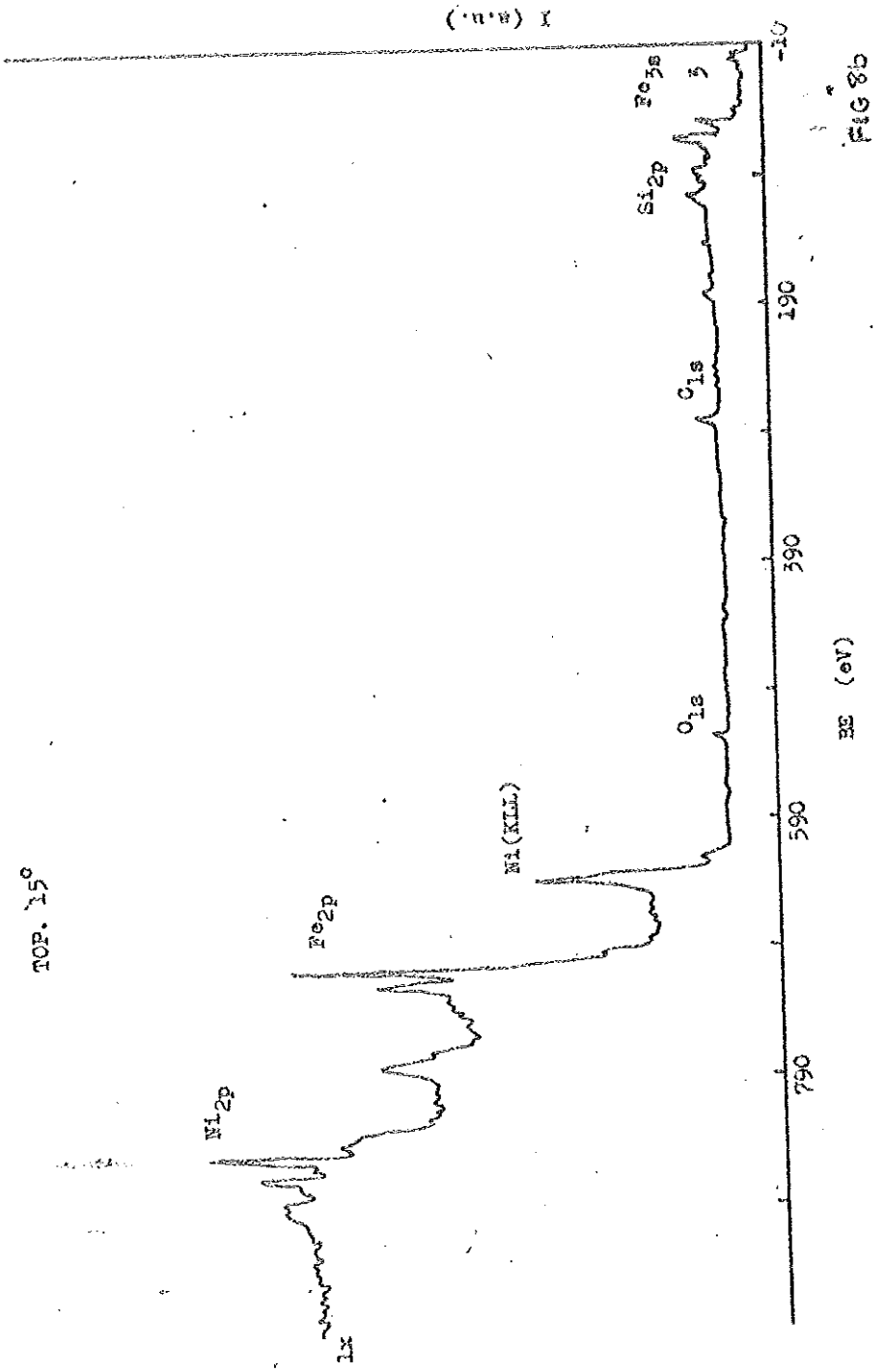
I (a.u.)
-10
Fe3s
Si2p
190
O1s
390
O1s
Ni(KLL)
590
Fe2p
Ni2p
790
1x
TOP. 15°
BE (eV)

FIG 8b

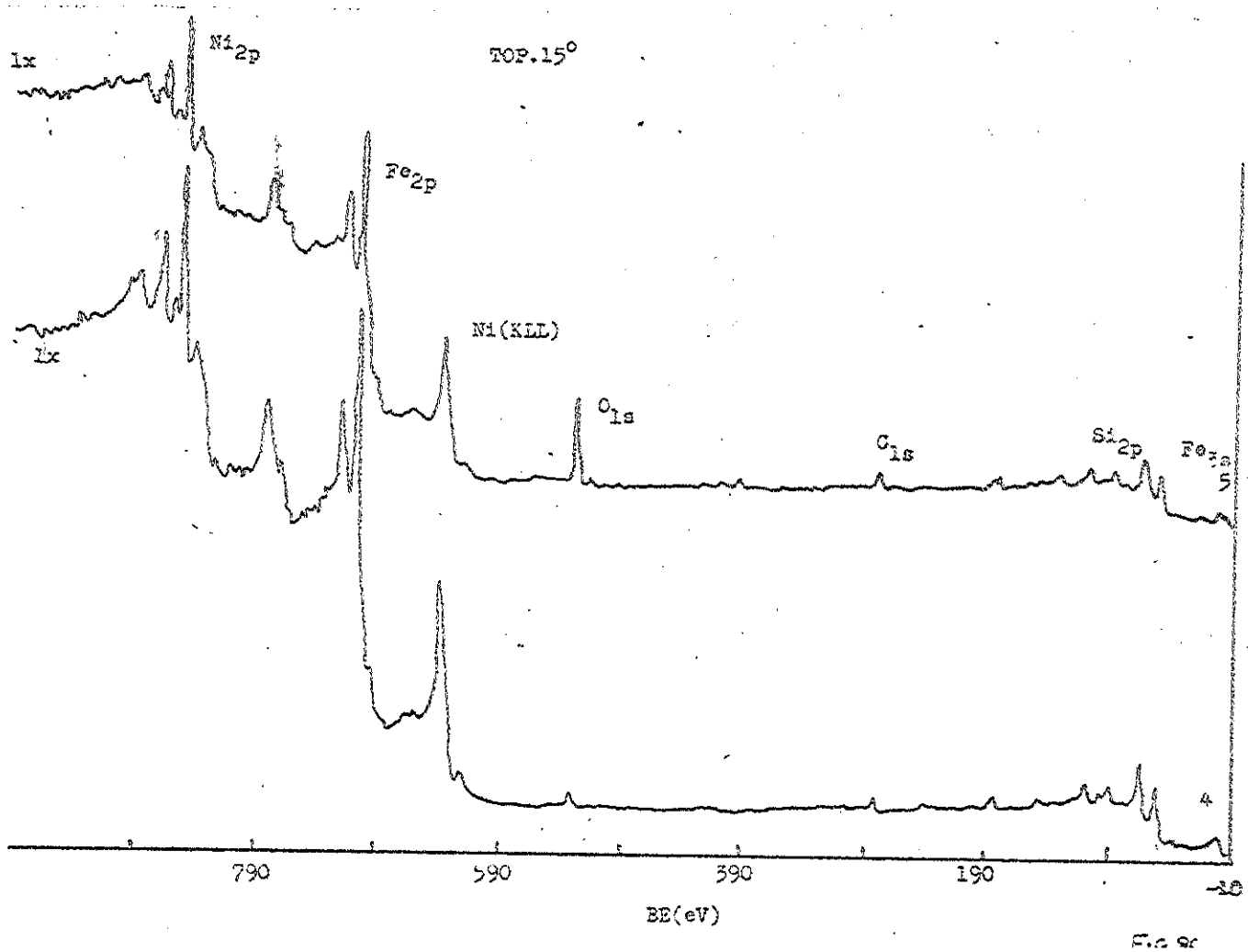
1x
Ni2p
TOP.15°
Fe2p
1x
Ni(KLL)
O1s
C1s
Si2p
Fe3p
5
4
I(a.u.)
790
590
390
190
BE(eV)

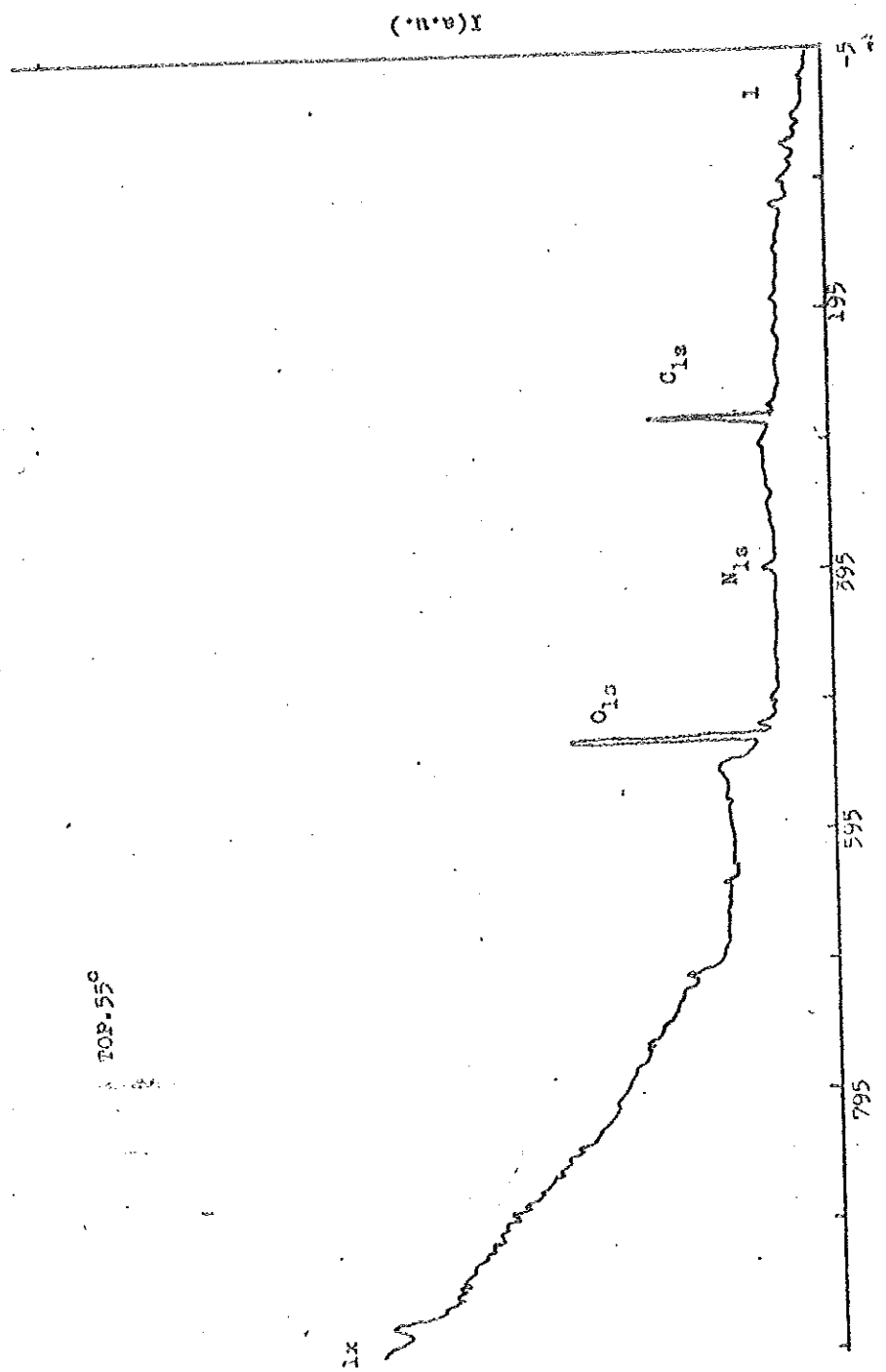
I(a.u.)
I
C_{1s}
N_{1s}
O_{1s}
1x
θ_{TOA}=55°
795
595
595
395
-5 eV

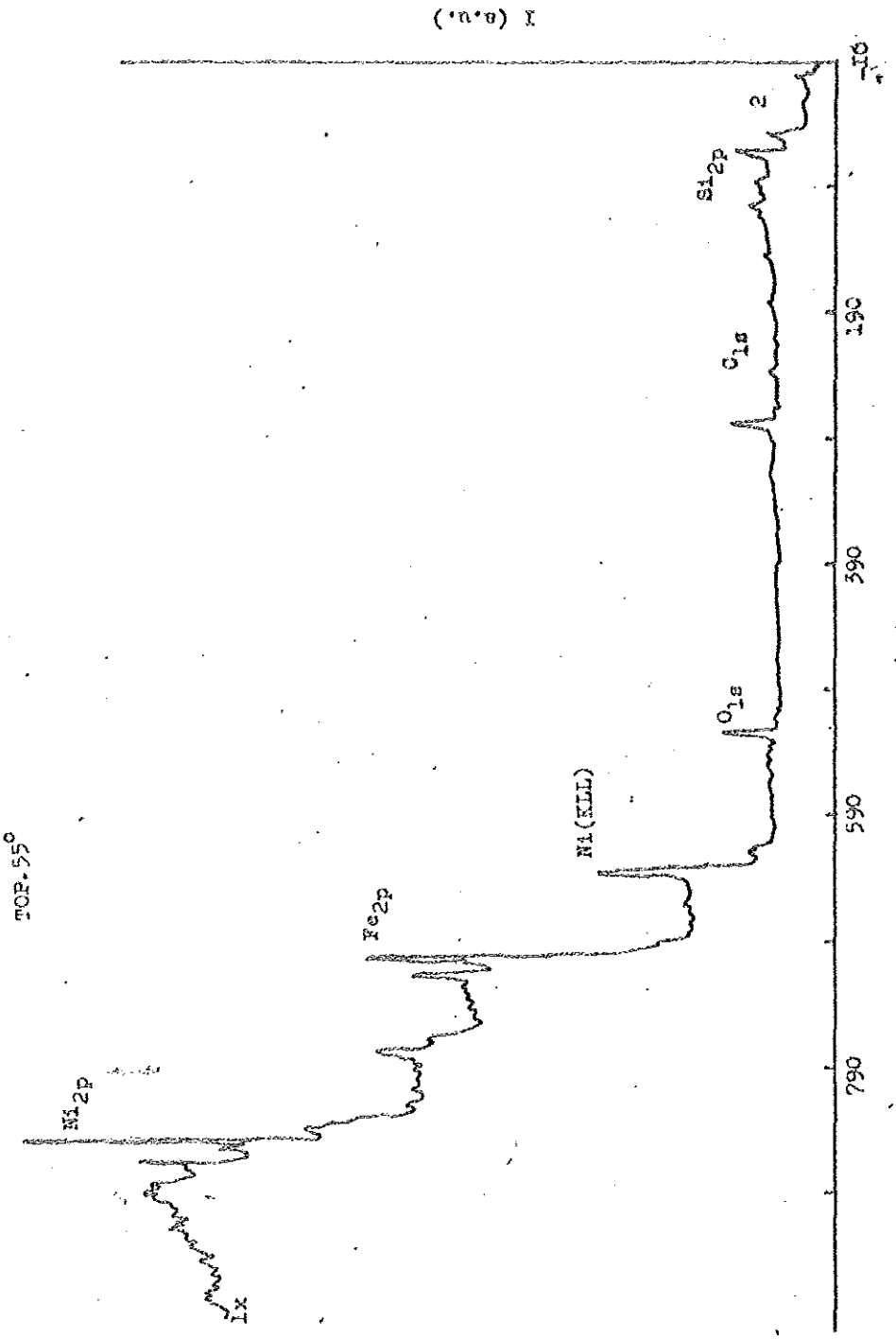
I (a.u.)
TOP.55°
Ni2p
Ix
Fe2p
N1(KLL)
O1s
C1s
Si2p
2
790
590
390
190
-10
BE (eV)

Fig 8e

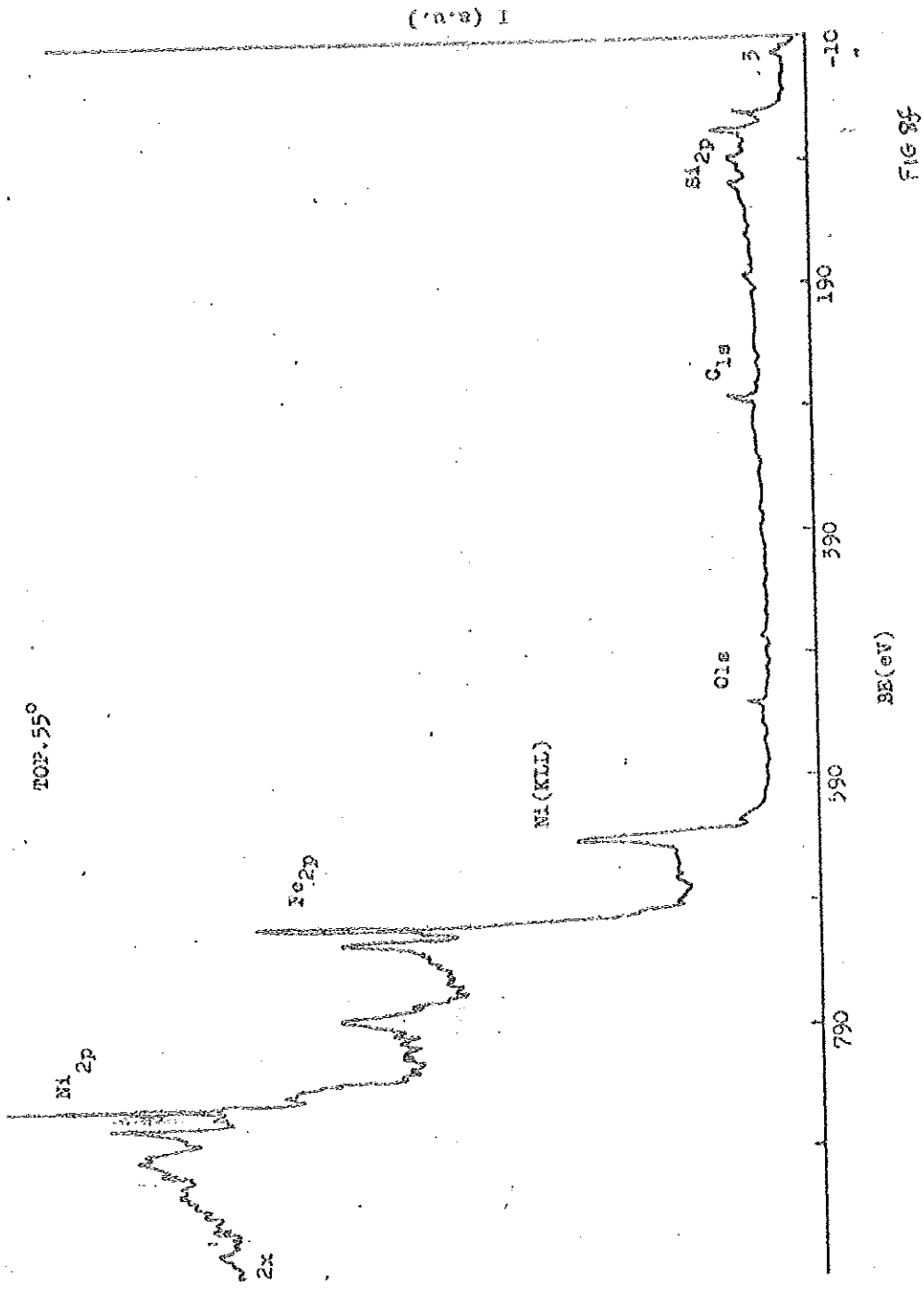
I (a.u.)
TOP-55°
Ni 2p
2x
Fe2p
Ni(KLL)
O1s
C1s
Si2p
790
590
390
190
-10
BE(eV)

FIG 8f

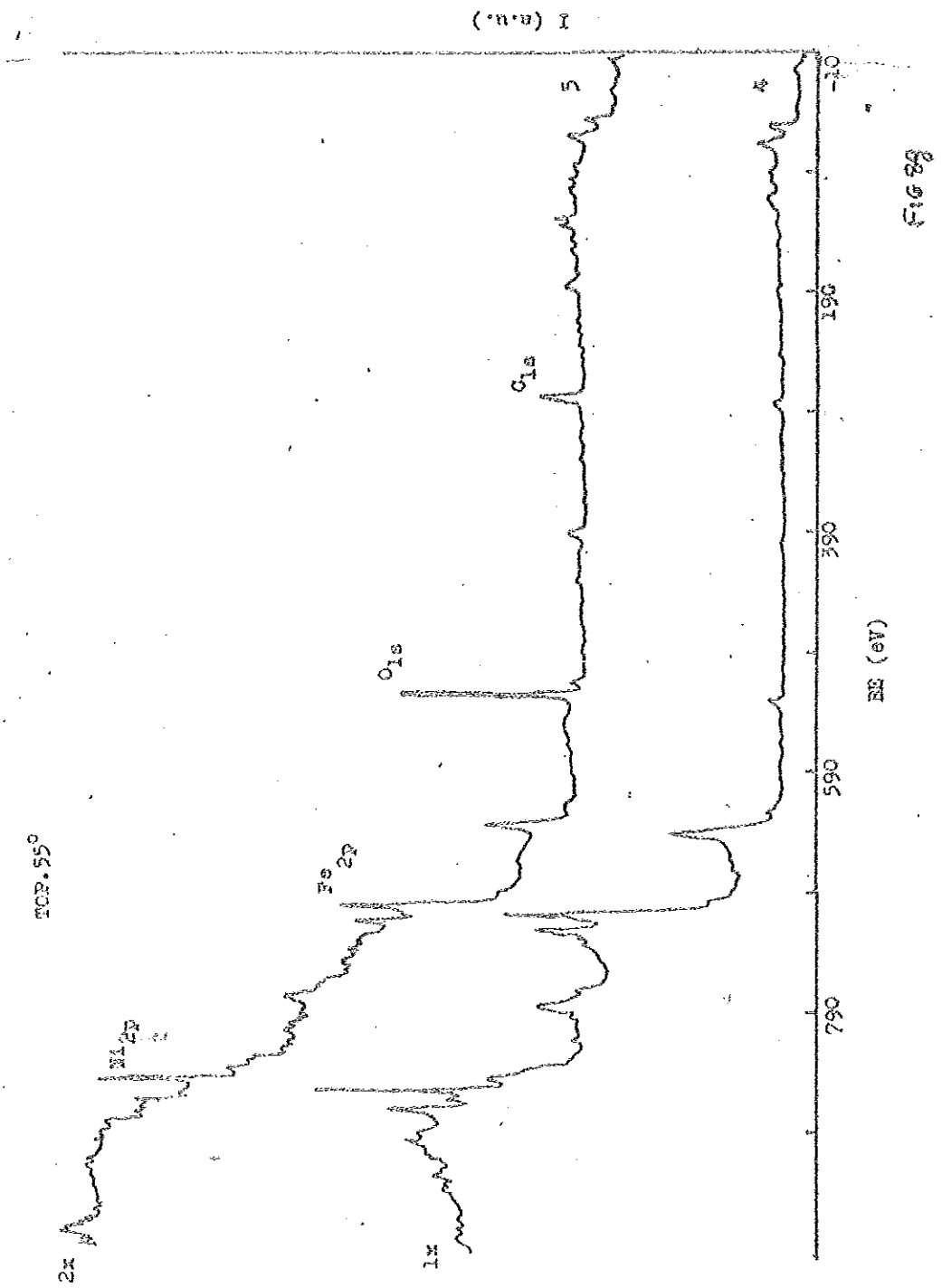

Fig 88

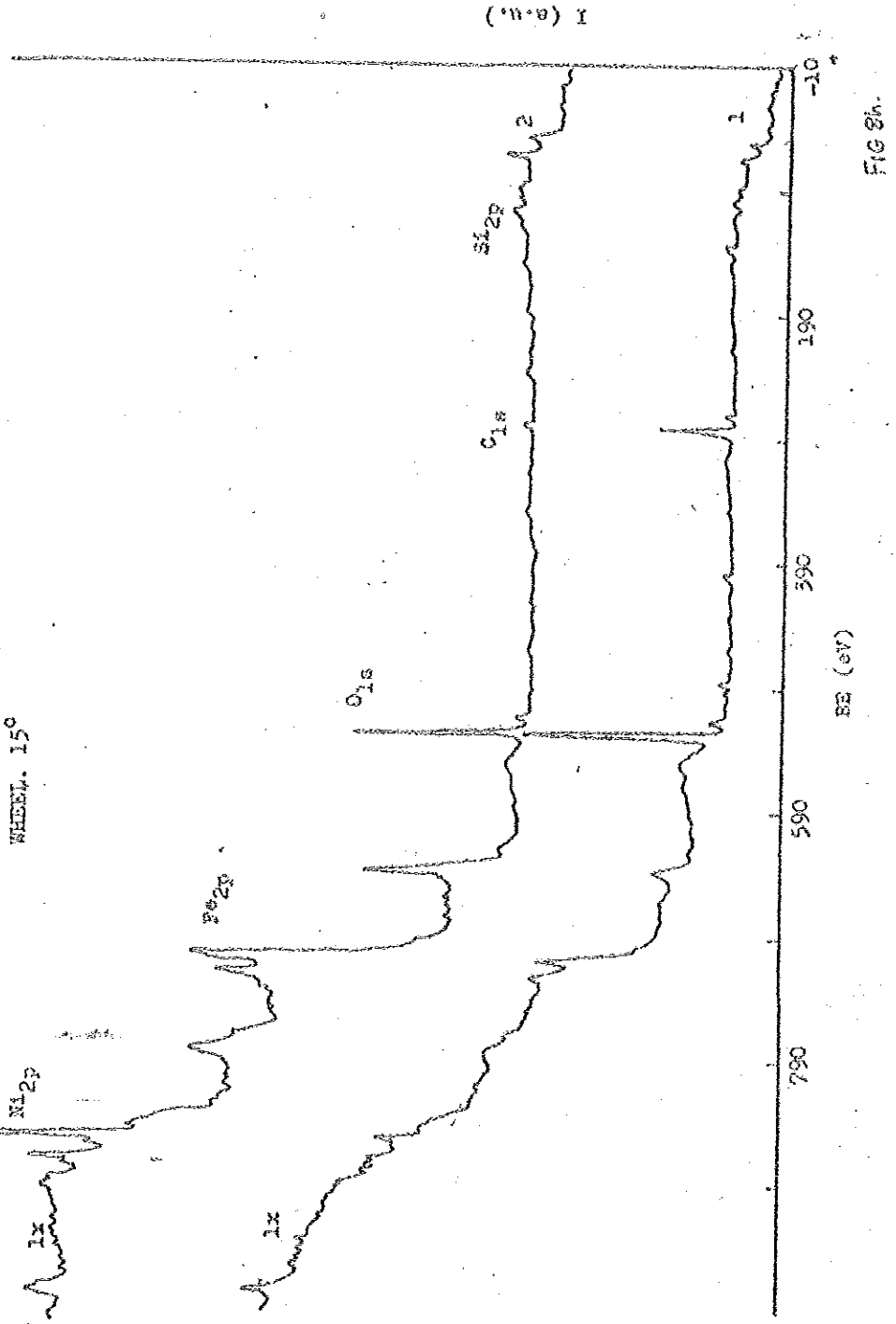
I (a.u.)
-10
190
390
590
790
BE (eV)
WHEEM. 15°
Ni2p
Ni2p*
O1s
Si2p
O1s*
1
2
1x
1x

FIG 8h.

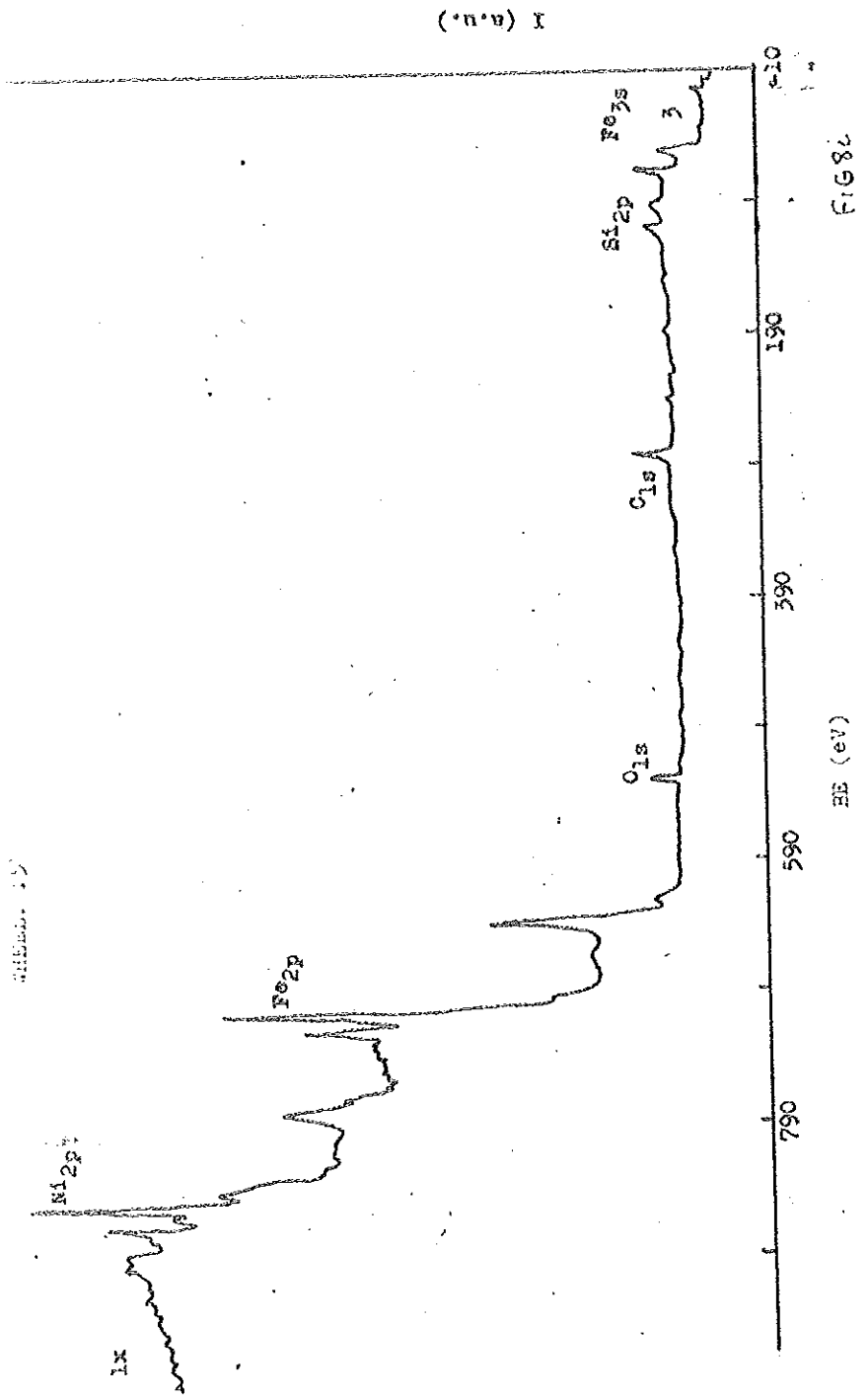

FIG 8.

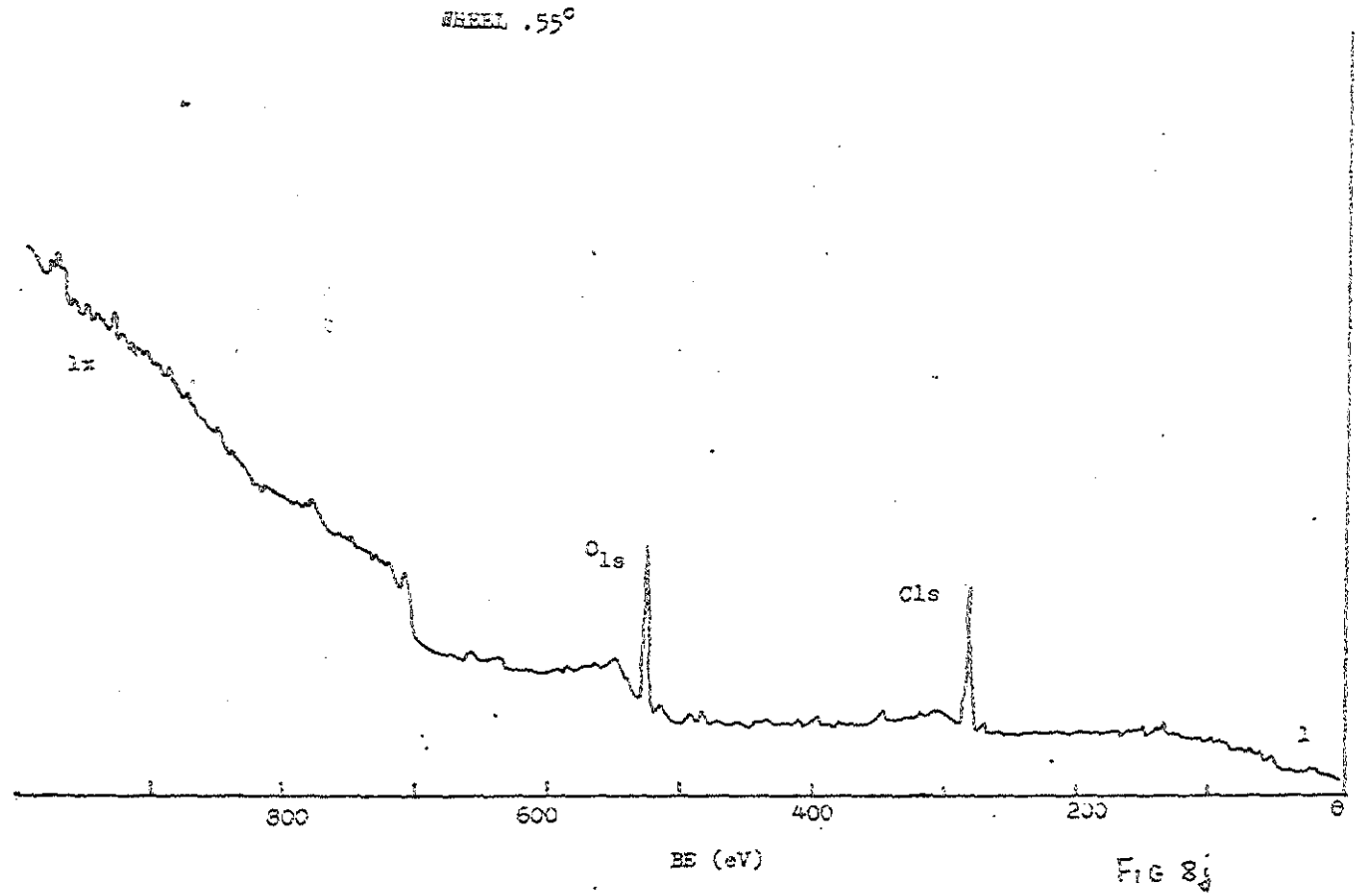

FIG 8j

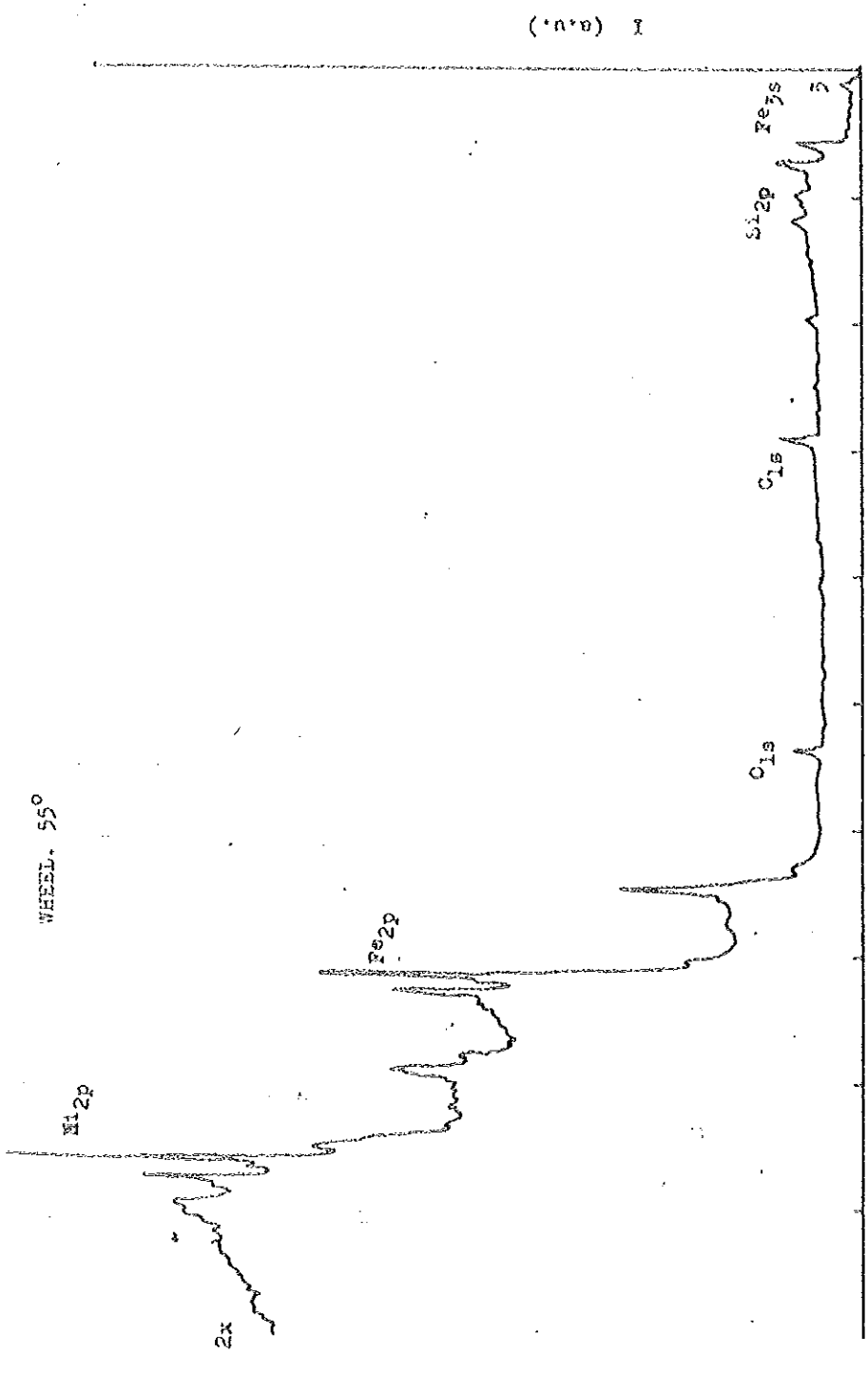
I (a.u.)
WHEEL. 55°
Ni2p
2x
Fe2p
O1s
C1s
Si2p
Fe3s
3
0
200
400
600
800
BE(eV)

FIG 8K

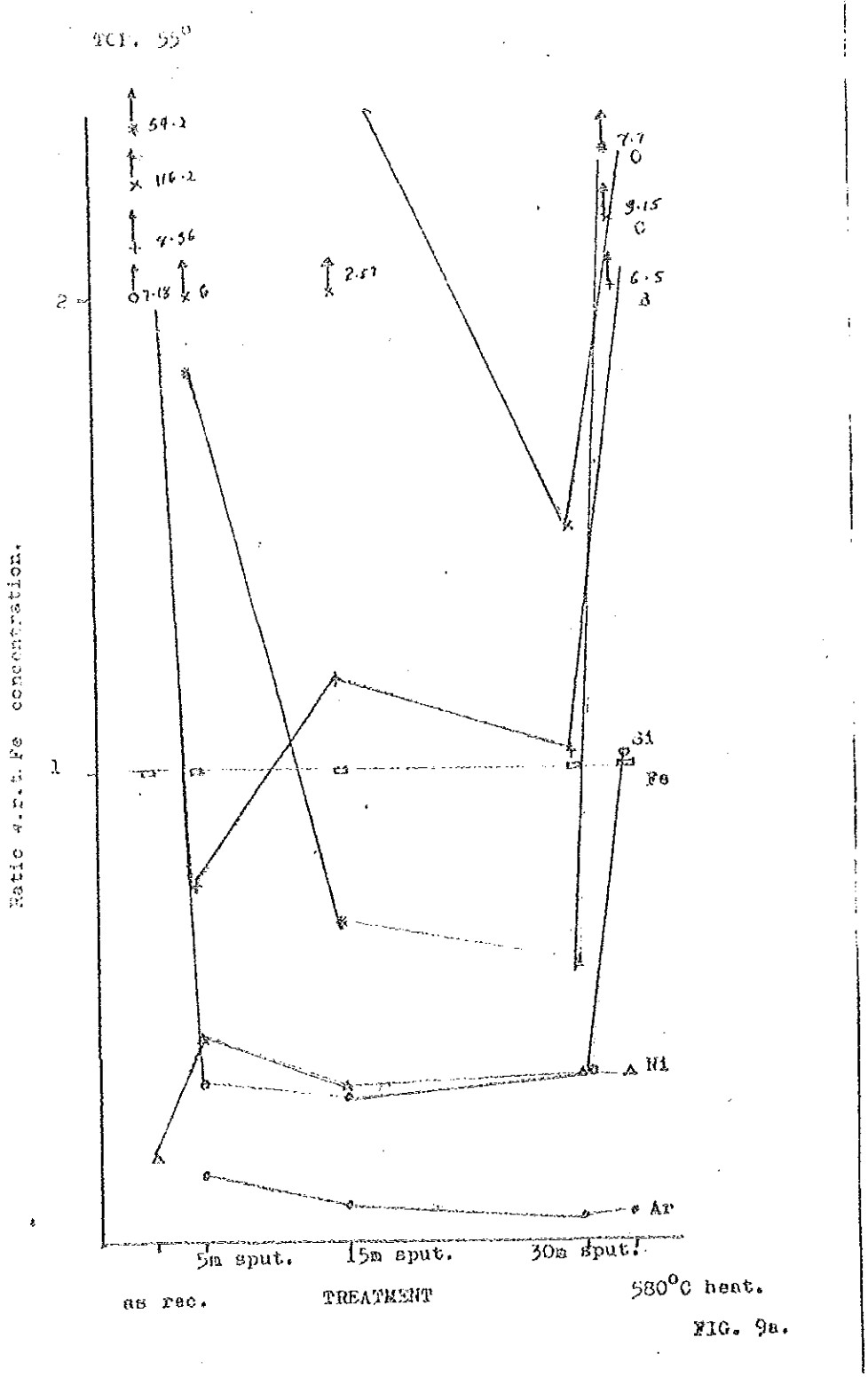
HCl. 55°
59·2
116·2
4·56
7·18
6
2·57
7·7
O
9·15
C
6·5
S
2
1
Ratio a.n.a. Fe concentration.
Si
Fe
Ni
Ar
as rec.
5m sput.
15m sput.
30m sput.
TREATMENT
580°C heat.

FIG. 9a.

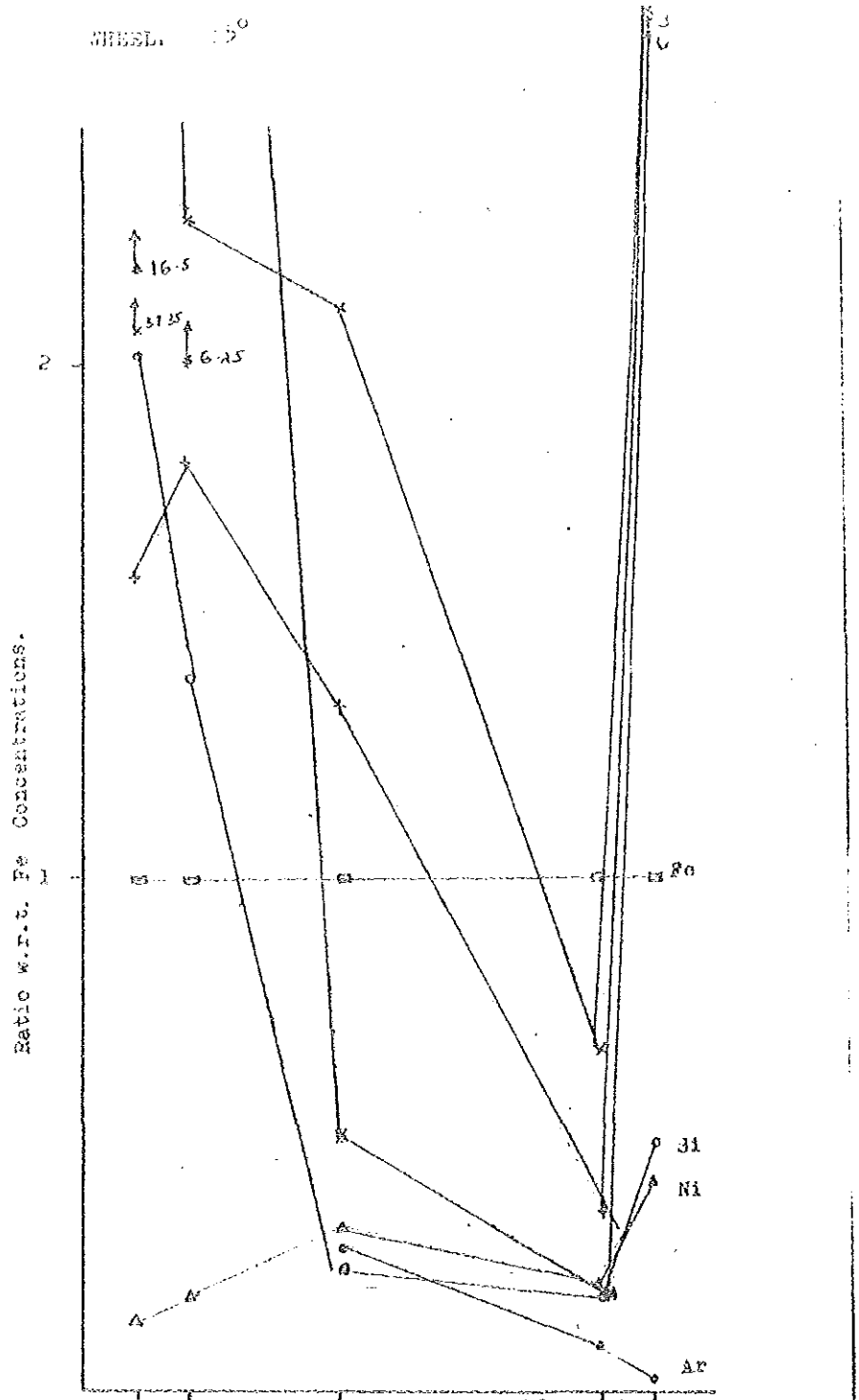
WHEEL. 15°
16·5
31·25
6·25
2
1
Ratio w.r.t. Fe Concentrations.
Fe
Si
Ni
Ar
5mi.sput.
15m.sput.
30m.sput.
as rec.
TREATMENT
580°C heat.

FIG.9b.

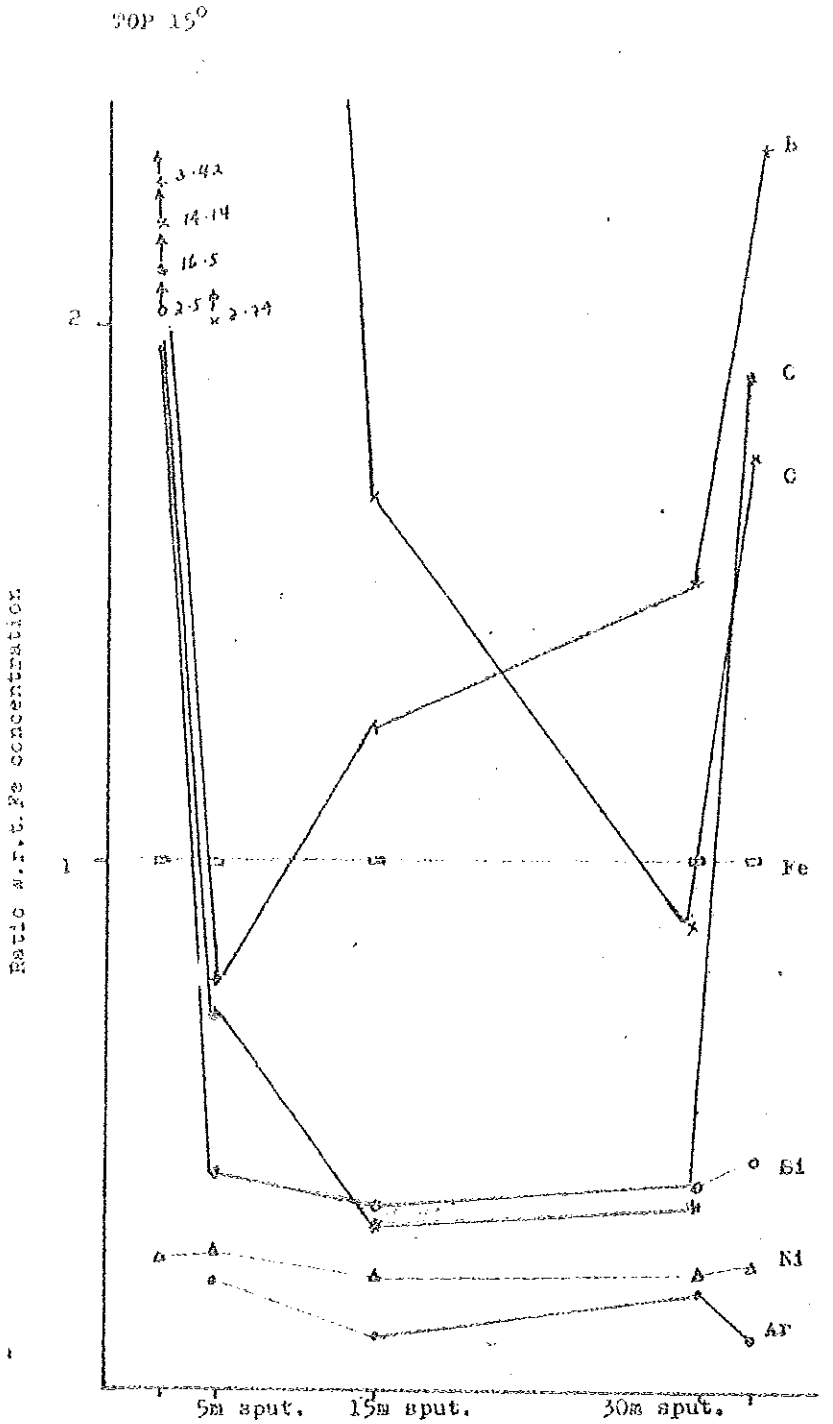
TOP 15°
3·42
14·14
16·5
2·5
2·74
2
1
Ratio a.r.t.Fe concentration
B
C
C
Fe
Si
Ni
Ar
5m sput.
15m sput.
30m sput.
as rec.
TREATMENT
580°C heat.

FIG.9c.

WHEEL. 15°

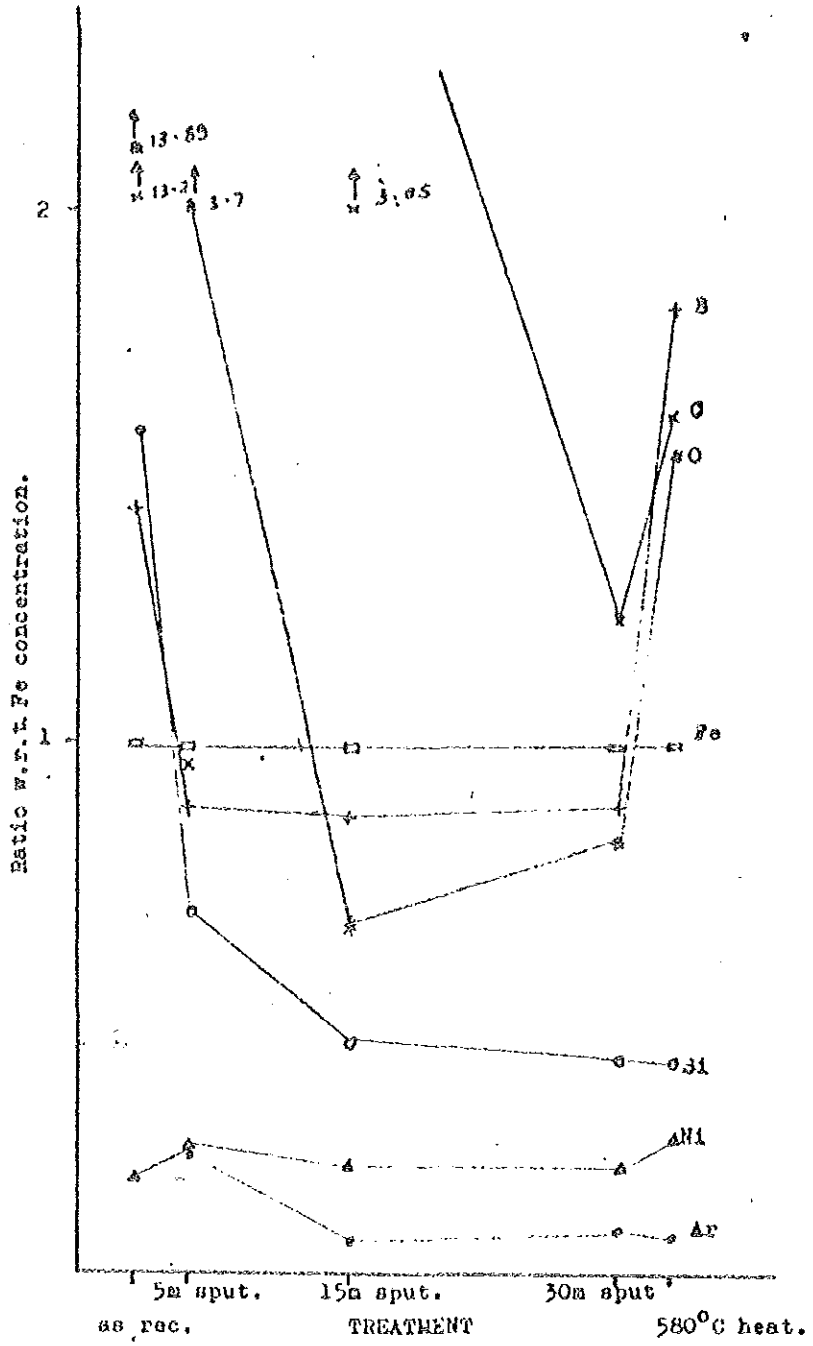

FIG. 9d.

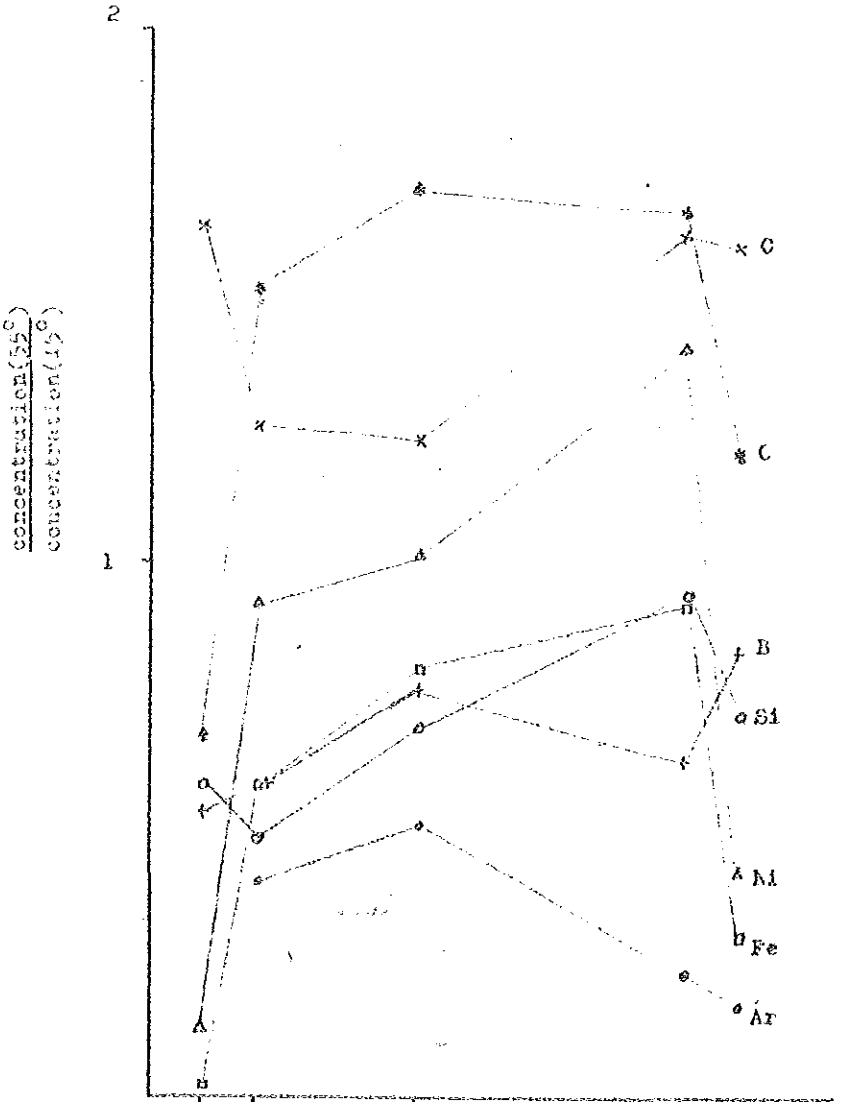
TOP
2
1
concentration(52°)
concentration(15°)
C
C
B
Si
Al
Fe
Ar
5m sput.
15m sput
30m sput.
as rec.
TREATMENT
580°C heat.

FIG. 9b.

WHEEL.

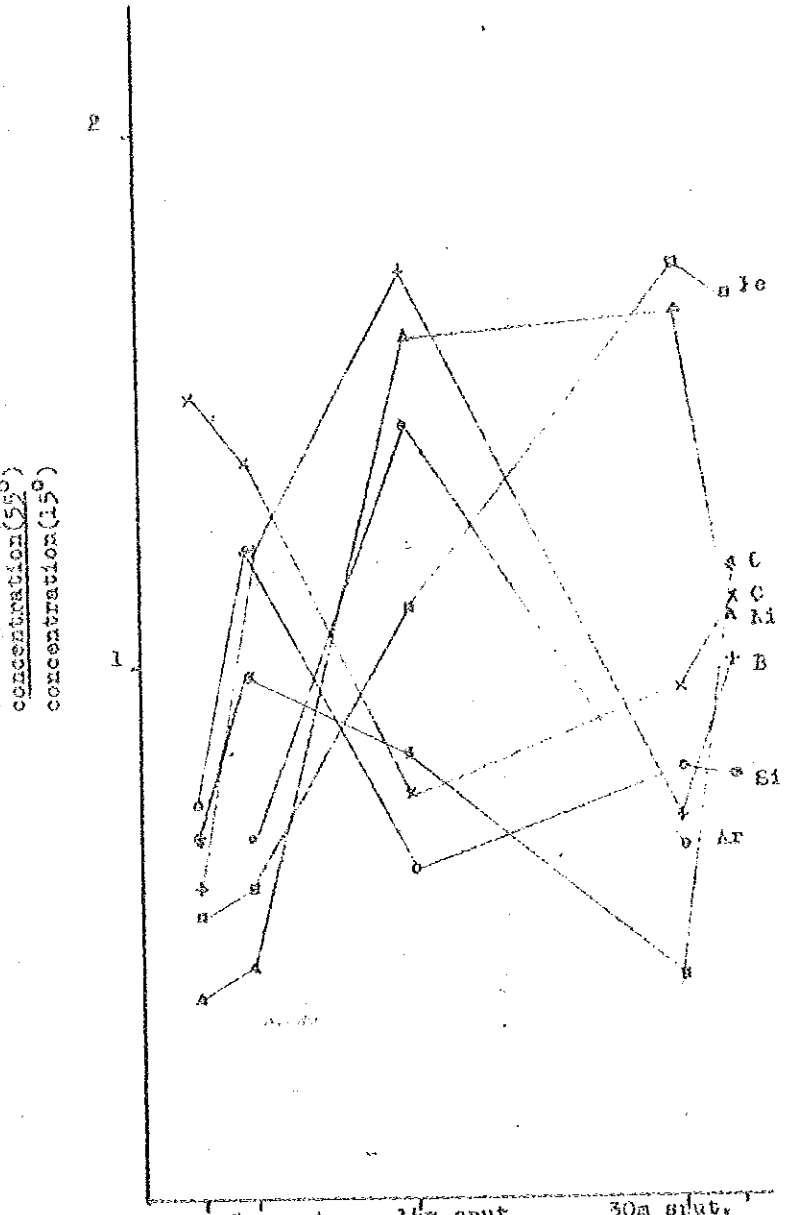
2
1
concentration(52°)
concentration(15°)
Fe
C
C
Mi
B
Si
Ar
5m sput.
15m sput
30m sput.
as rec
TREATMENT
580°C heat.

FIG. 9f.

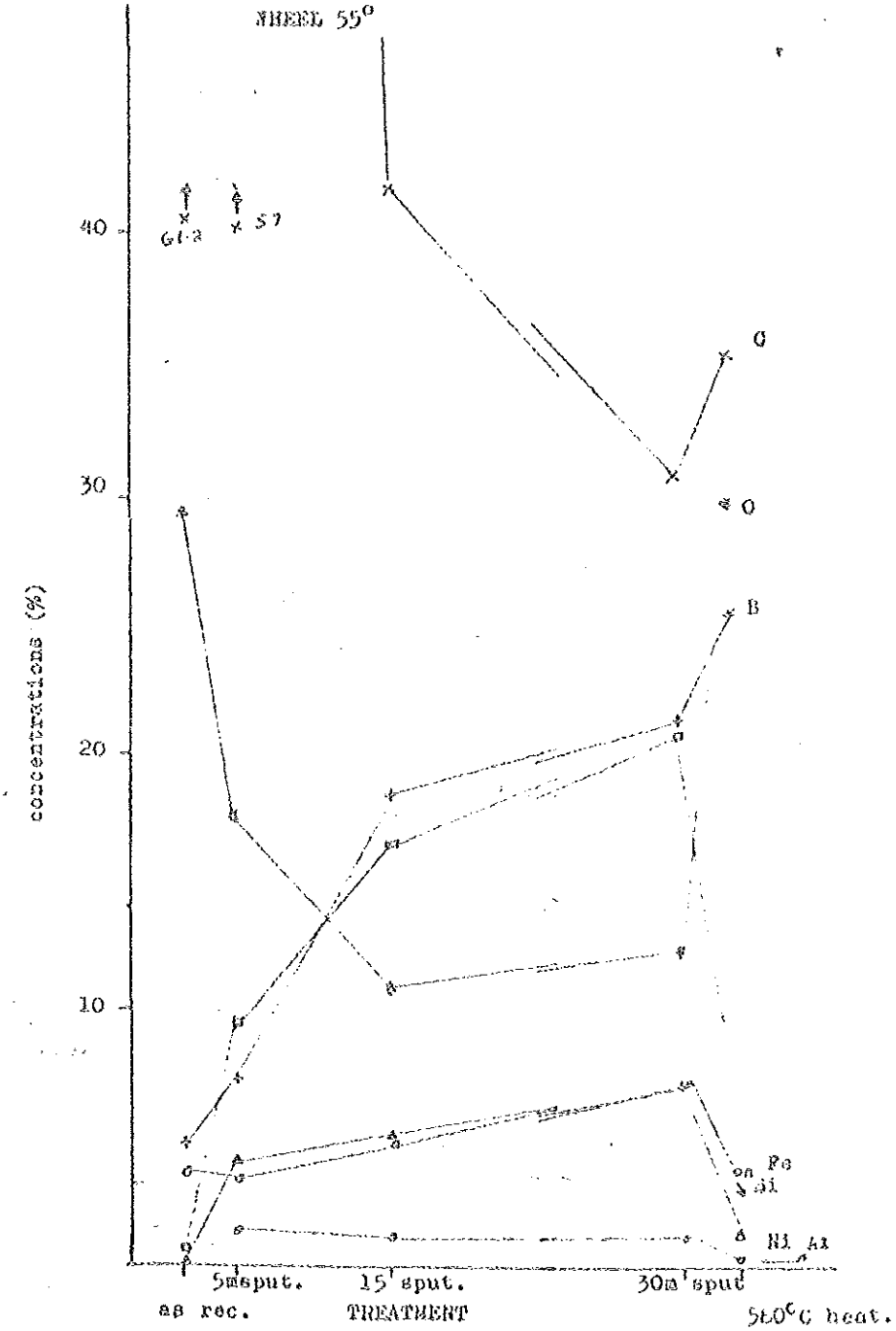
WHEEL 55°
Ga
Si
40
30
20
10
concentrations (%)
C
O
B
Fe
Si
Ni Al
as rec.
5m sput.
15' sput.
30m' sput
TREATMENT
560°C heat.

FIG.9c.

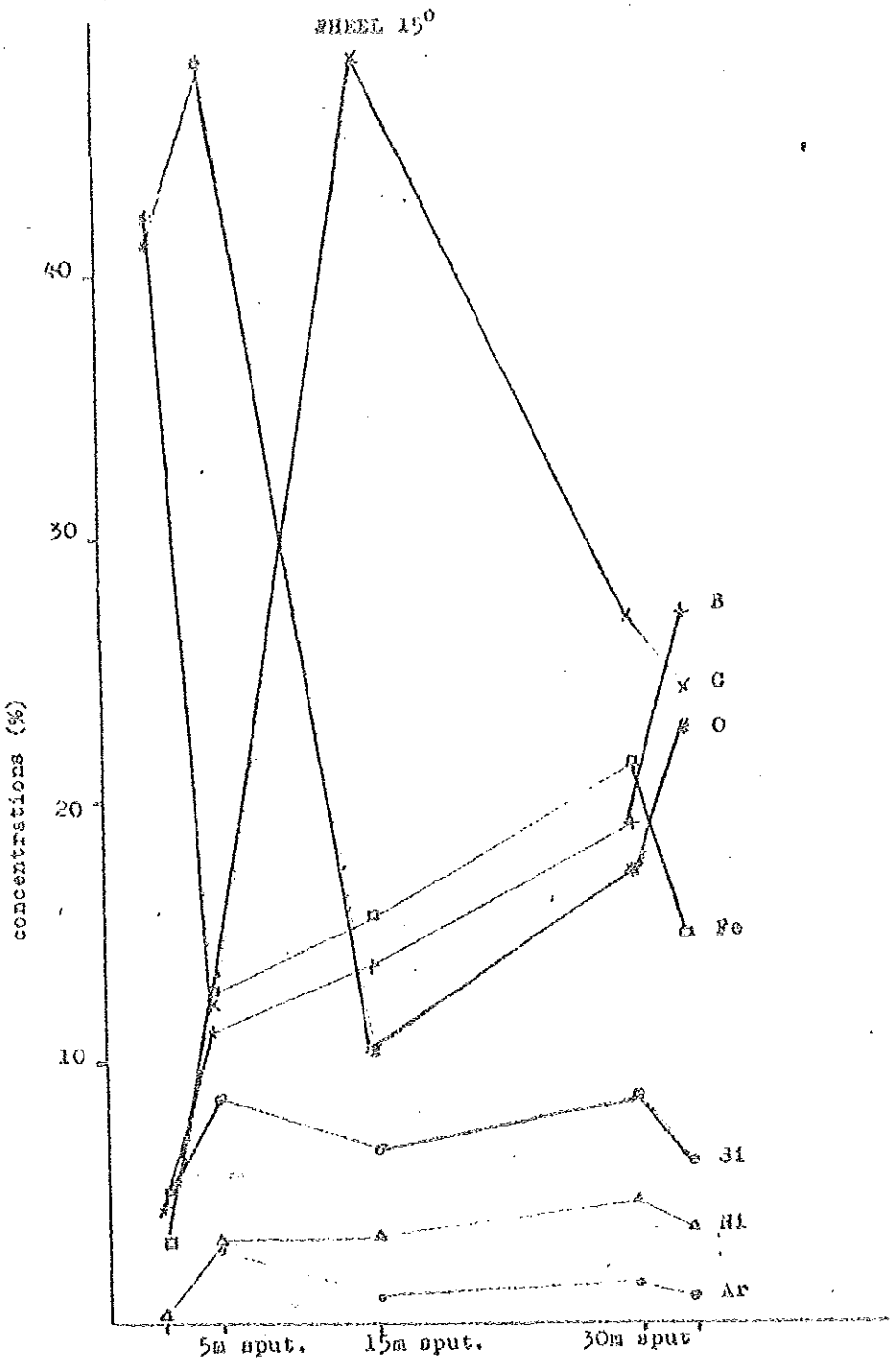
WHEEL 15°
40
30
20
10
concentrations (%)
B
C
O
Fe
Si
Al
Ar
5m sput.
15m sput.
30m sput
as rec.
TREATMENT
580°C heat.

FIG. 9h.

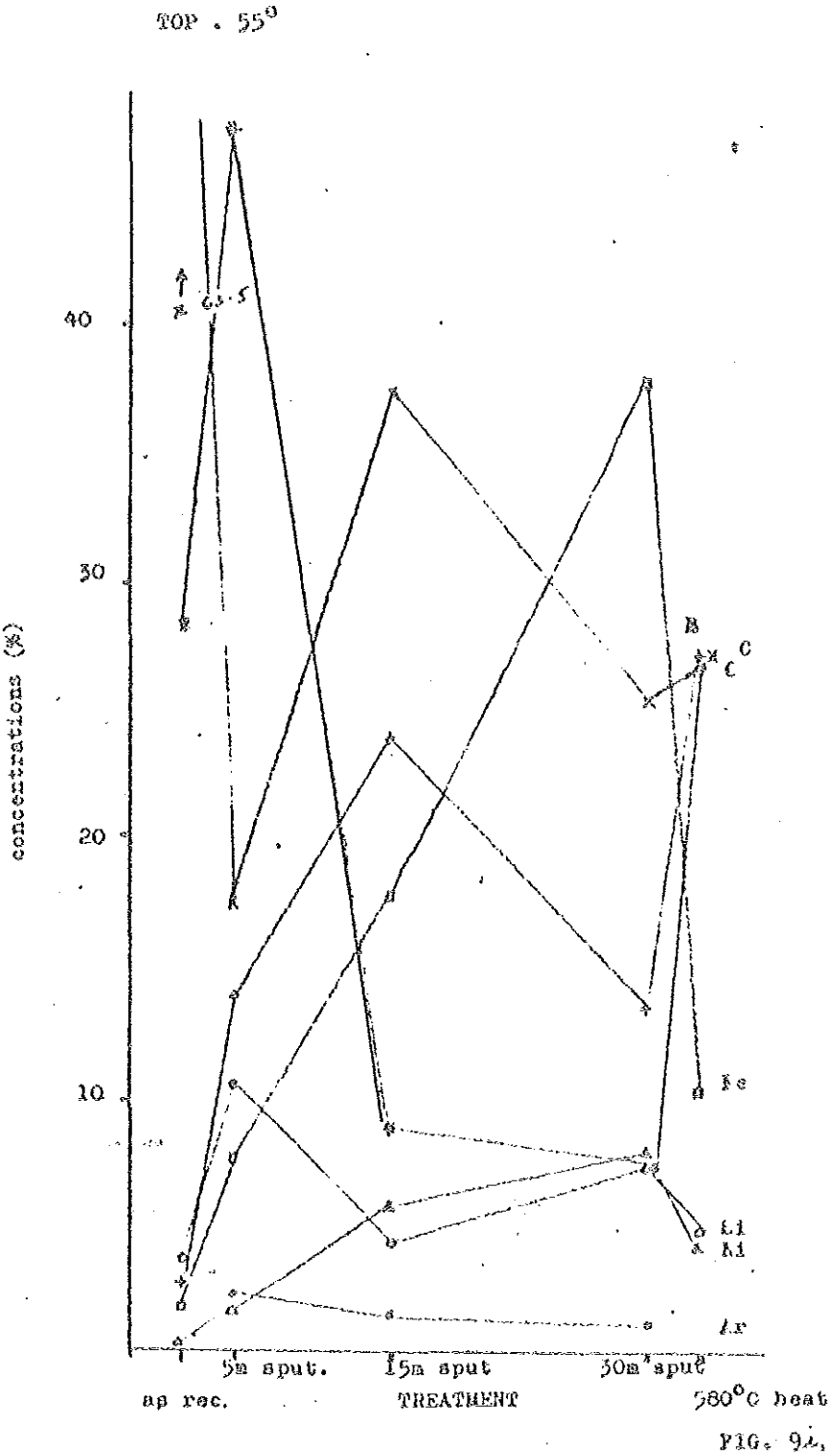
TOP . 55°
63.5
40
30
20
10
concentrations (%)
B
C
C
Fe
Ni
Mi
Cr
5m sput.
15m sput
30m sput
ap rec.
TREATMENT
580°C heat

FIG. 9.

TOP. 15°

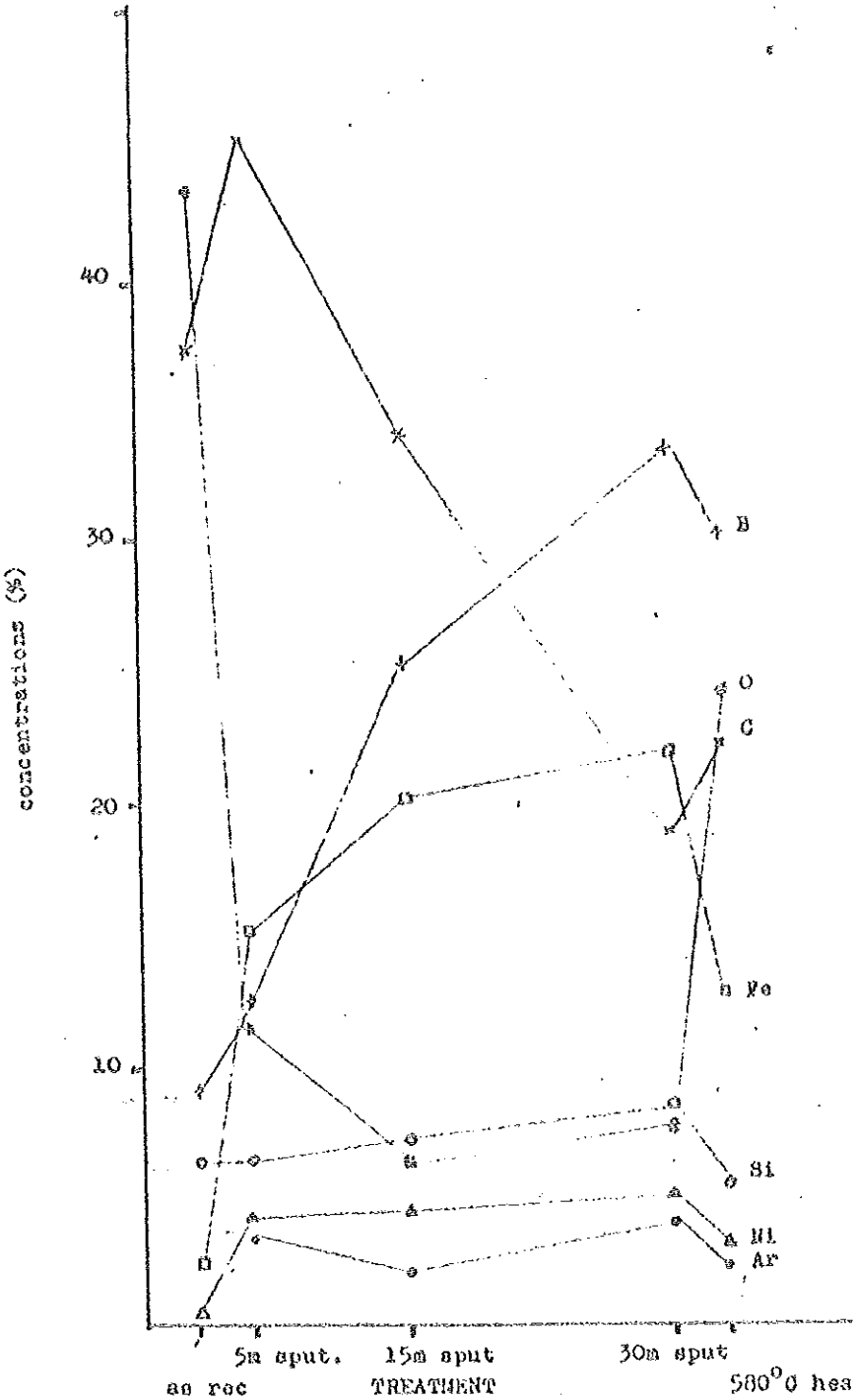
40
30
20
10
concentrations (%)
B
O
C
N Ve
Si
Al
Ar
5m aput.
15m aput
30m aput
an roc
TREATMENT
580°C hea

Fig 9j

APPENDIX B

CONCENTRATION TABLES

TABLE 1a.

CORE LEVEL BINDING ENERGIES OF THE TOP SIDE AT 55° IN eV.

	Fe							Ni				
TREATMENT	2p3	Δ E	$\Delta E_{sat.}$	2p1	Δ E	$\Delta E_{sat.}$	3s	2p3	$\Delta E_{sat.}$	2p1	$\Delta E_{sat.}$	3s
As rec.	707.5	3.4	8	720.6			92.7	852.8	7.4	870.0		111.2
Ar^+5min.	707.0		5.2	720.0			91.5	852.6	7.0	870.0	5.0	110.8
Ar^+15min.	707.1		5.1	720.1			91.4	852.8	7.4	870.1	5.5	111.1
Ar^+30min.	707.1		5.3	720.1			91.0	852.9	7.3	870.0	5.8	110.6
580°Cheat.	707.0		5.2	720.0		14.0	91.2	852.6	7.4	870.0	5.4	110.6

	Si		B		Ar		C	O
TREATMENT	2p	Δ E	1s	Δ E	2p3	2p1	1s	1s
As rec.	99.1	3.3	188.2	4.2	-	-	285.3	531.9
Ar^+5min.	99.1	2.7	187.7	4.0	241.3	243.3	284.2	531.5
Ar^+15min.	99.4	3.3	187.8	4.3	241.5	243.2	283.9	531.7
Ar^+30min.	98.9		187.8		241.3	243.1	283.5	531.4
580°C heat.	99.2	3.4	187.7	4.7	240.9	243.9	284.5	532.4

TABLE 1b.

CORE LEVEL BINDING ENERGIES OF THE TOP SIDE AT 15° IN eV.

	Fe							Ni				
TREATMENT	2p3	ΔE	$\Delta E_{sat.}$	2p1	ΔE	$\Delta E_{sat.}$	3s	2p3	$\Delta E_{sat.}$	2p1	$\Delta E_{sat.}$	3s
As rec.	706.9	4.1		719.6	4.5		91.8	852.5	7.0	869.8	5.9	110.5
Ar^+5min.	706.8	4.4		720.0			91.2	852.5	7.0	869.9	5.1	110.7
Ar^+15min.	706.9		5.2	720.1		14.0	91.2	852.5	6.8	870.0	5.0	110.9
Ar^+30min.	706.7		4.8	720.1		14.9	91.2	852.2	6.7	869.6	5.2	110.5
580°C heat.	706.7		5.4	719.9		13.1	91.1	852.6	6.9	870.0	5.2	110.8

	Si		B		Ar		C	O
TREATMENT	2p	ΔE	1s	ΔE	2p3	2p1	1s	1s
As rec.	99.0	2.9	187.5	4.3	-	-	285.2	531.5
Ar^+5min.	99.0	2.2	187.8	3.9	241.0	242.9	284.0	531.3
Ar^+15min.	99.0	3.2	187.7	4.0	241.1	243.0	283.8	531.4
Ar^+30min.	98.9		187.6	4.0	241.1	243.1	283.5	531.1
580°C heat.	99.0	3.7	187.5	4.7	240.9	242.3	284.3	532.2

TABLE 1c.

CORE LEVEL BINDING ENERGIES OF THE WHEEL SIDE AT 15° IN eV.

	Fe							Ni				
TREATMENT	2p3	ΔE	$\Delta E_{sat.}$	2p1	ΔE	$\Delta E_{sat.}$	3s	2p3	$\Delta E_{sat.}$	2p1	$\Delta E_{sat.}$	3s
As rec.	706.7	4.0		720.0	4.0		93.0	852.4	8.2	870.1	4.9	110.3
Ar^+5min.	706.6	3.6		719.7	3.4		91.6	852.3	6.8	869.7	5.7	110.5
Ar^+15min.	706.4		5.1	719.5		12.0	91.0	852.5	6.7	869.9	6.0	110.5
Ar^+30min.	706.7		4.6	719.9		13.0	91.3	852.4	7.3	869.6	5.8	110.8
580°C heat.	706.6		4.9	719.8		12.0	91.1	852.4	7.3	869.6	5.8	110.8

	Si		B		Ar		C	O
TREATMENT	2p	ΔE	1s	ΔE	2p3	2p1	1s	1s
As rec.	98.6	2.7	187.7	3.8	-	-	284.6	530.6
Ar^+5min.	99.0	3.0	187.4	4.6	241.3	243.4	284.1	531.3
Ar^+15min.	99.1	2.2	187.4	2.6	240.9	242.9	284.2	531.6
Ar^+30min.	99.0		187.6		241.1	242.3	283.4	531.4
580°C heat.	99.0	3.4	187.4	5.0	241.1	243.1	284.0	532.2

TABLE Id.

CORE LEVEL BINDING ENERGIES OF THE WHEEL SIDE AT 55° IN eV.

	Fe							M1				
TREATMENT	2p3	ΔE	$\Delta E_{sat.}$	2p1	ΔE	$\Delta E_{sat.}$	3s	2p3	$\Delta E_{sat.}$	2p1	$\Delta E_{sat.}$	3s
As rec.		3.6	8.5		4.2	13.1	93.0	852.2	8.2			110.3
Ar^+5min.	707.0	3.1	7.0	720.0	3.4	9.7	92.1	852.4	6.3	869.7	5.2	110.3
Ar^+15min.	706.0		5.2	719.3			92.0	852.4	7.0	869.7	5.5	111.6
Ar^+30min.	706.5		5.5	719.6		11.4	91.0	852.4	6.8	869.7	5.3	110.8
580°C heat.	706.4		5.2	719.6			91.0	852.2	7.1	869.6	6.0	110.8

	Si		B		Ar		C	O
TREATMENT	2p	ΔE	1s	ΔE	2p3	2p1	1s	1s
As rec.	101.4		187.4	3.7 4.8	-	-	284.6	531.1
Ar^+5min.	99.6	2.4	187.0	4.3 5.3	241.3	242.7	284.4	531.3
Ar^+15min.	99.0		187.4		240.9	242.8	283.4	531.2
Ar^+30min.	98.9	3.3	187.6		240.9	243.2	283.3	531.2
580°C heat.	98.8	3.6	187.4	5.0	-	-	283.9	532.2

TABLE 2a.

VALENCE BAND BINDING ENERGIES IN eV MEASURED WITH RESPECT TO E_F

WHEEL-SIDE 55°

TREATMENT	E_F	1	2	3	4	5	6
As rec.	-0.6	3.2				22.5	25.6
Ar^+5min.	-0.1	1.2	6.2				26.5
Ar^+15min.	0	1.0					24.1
Ar^+30min.	-0.5	1.5					24.1
580°C heat.	-0.2	1.3			17.8	20.4	25.3

WHEEL-SIDE 15°

TREATMENT	E_F	1	2	3	4	5	6
As rec.	-0.5	2.5	7.5			23	26.1
Ar^+5min.	-0.4	1.2	8.9				26.1
Ar^+15min.	-0.3	1.6					24.7
Ar^+30min.	-0.1	1.1					24.8
580°C heat.	0	1.4			18.0	20.9	25.4

TABLE 2b.

VALENCE BAND BINDING ENERGIES IN eV MEASURED WITH RESPECT TO E_F

TOP-SIDE 55°

TREATMENT	E_F	1	2	3	4	5	6
As rec.	0	1.7	5.6	10.9	18.5		23.5
Ar^+5min.	-0.5	1.4	6.5	13.1			25.0
Ar^+15min.	-0.1	1.4					24.6
Ar^+30min.	0	1.5					24.0
580°C heat.	-0.5	1.5	6.7		17.8		25.7

TOP-SIDE 15°

TREATMENT	E_F	1	2	3	4	5	6
As rec.	-0.4	1.4		10.4			24.4
Ar^+ 5min.	-0.6	1.3		13.4			24.6
Ar^+15min.	-0.4	1.5					24.9
Ar^+30min.	-0.2	1.2					24.2
580°C heat.	-0.4	1.4		9.8	17.9	20.6	25.6

TABLE 3a;

CONCENTRATION OF THE TOP-SIDE AT 15°

			As rec.				5min.sputt.				15min sputt.				30min sputt.				580°C heating			
ELEMENT	$\sqrt{E}_{kin}$[1]	σ[2]	N[3]	S[4]	Ar[5]	n	N	S	Ar	n	N	S	Ar	n	N	S	Ar	n	N	S	Ar	n
Fe2p	27.7	16.4	32	2	0.19	20.5	8	4	0.28	240.8	8	4	0.39	334.0	4	4	0.24	414.0	8	2	0.27	116.6
Ni2p	24.8	22.2	16	2	0.03	3.7	8	4	0.18	104.9	8	4	0.19	112.0	4	2	0.26	149.0	8	2	0.14	41.3
Fe3s	37.2	0.75	32	0.5	0.11	83.9	32	1	0.18	287.7	16	0.5	0.22	356.5	8	0.5	0.15	470.0	16	0.5	0.15	233.4
Ni3s	37.2	0.89	32	0.5	0.02	43.4	32	1	0.28	372.5	16	0.5	0.28	379.2	8	0.5	0.17	445.9	16	0.5	0.19	253.6
Si2p	37.2	0.82	32	0.5	0.20	147.2	32	1	0.06	83.1	16	0.5	0.07	102.0	8	0.5	0.05	145.8	16	0.5	0.08	120.9
B1s	36.01	0.49	32	0.5	0.16	183.8	64	1	0.16	183.9	50	1	0.26	400.6	16	0.5	0.18	426.0	16	0.5	0.32	758.0
C1s	34.7	1.00	4	1	0.26	2321.	8	1	0.33	1445.	8	0.5	0.39	860.4	8	0.5	0.28	622.0	8	1	0.24	1067.0
O1s	30.8	2.93	4	2	0.21	1113.	8	1	0.33	443.6	8	0.5	0.33	222.5	4	0.5	0.18	247.3	4	1	0.38	906.0
Ar2p	35.2	3.04	-	-	-	-	16	0.5	0.10	36.7	16	0.5	0.07	25.9	16	0.5	0.06	22.2	32	0.5	0.04	7.7

[1] $\sqrt{E}$ = (eV)$^{\frac{1}{2}}$

[2] σ in units of 20,000 barns

[3] N is the sweep number

[4] S is the digital scale in kilobytes. 1k.b = 1024

[5] Ar is the area x 10^2 cm^2

TABLE 3b.

CONCENTRATION OF THE TOP SIDE AT 55°

		As rec.					5min.sputt.				15min. sputt.				30min. sputt.				580°C heating			
ELEMENT	$\sqrt{E}_{kin.}$[1]	σ[2]	N[3]	S[4]	Ar[5]	n	N	S	Ar.	n	N	S	Ar.	n	N	S	Ar.	n	N	S	Ar.	n
Fe2p	27.7	16.4	16	4	0.35	152.8	4	4	0.31	533.6	4	4	0.34	580.2	2	2	0.40	686.0	8	8	0.27	473.0
Ni2p	24.8	22.2	8	2	0.14	40.4	4	2	0.25	144.4	4	4	0.23	130.1	2	1	0.28	161.6	4	2	0.20	116.9
Fe3s	37.2	0.75	32	1	0.22	351.7	16	1	0.22	697.0	16	1	0.23	748.0	8	1	0.15	927.0	8	.5	0.20	639.0
Ni3s	37.2	0.82	32	1	0.28	369.8	16	1	0.34	921.3	16	1	0.34	204.0	8	1	0.20	1068.	8	.5	0.29	785.0
Si2p	37.2	0.89	32	1	0.26	383.4	16	1	0.06	218.6	16	1	0.07	899.9	8	1	0.05	268.2	8	.5	0.07	204.0
Bls	36.01	0.49	32	1	0.22	523.9	32	1	0.18	414.9	32	2	0.15	725.5	8	0.5	0.22	1043.	8	.5	0.24	1114.
Cls	34.7	1.00	4	1	0.24	2161.	8	1	0.34	1494.	8	.5	0.44	980.5	8	0.5	0.27	593.6	4	.5	0.19	831.0
Cls	30.7	2.93	2	2	0.24	2527.	8	1	0.28	379.0	8	.5	0.28	190.8	8	0.5	0.36	239.9	4	1	0.34	900.6
Ar2p	35.2	3.04	-	-	-	-	8	0.5	0.16	119.9	16	.5	0.19	68.48	11	0.5	0.24	131.4	32	1	0.14	49.9

[1] $\sqrt{E} = (eV)^{1/2}$

[2] σ in units of 20,000 barns

[3] N is the number of sweeps

[4] S is the digital scale in kilobytes, 1k.b.= 1024

[5] Ar area. $\times 10^{2}$ cm^{2}

TABLE 3c.

CONCENTRATIONS OF THE WHEEL-SIDE AT 55°

		As rec.					5min.sputt.				15min.sputt.				30min.sputt.				580°C heating			
ELEMENT	$\sqrt{E}_{kin.}$	σ [2]	N [3]	S [4]	Ar [5]	n	N	S	Ar	n	N	S	Ar	n	N	S	Ar	n	N	S	Ar	n
Fe2p	27.7	16.4	8	4	0.26	222.7	8	4	0.64	584.2	4	4	0.37	632.0	4	4	0.39	683.0	4	4	0.30	519.8
NI2p	24.8	22.2	16	4	0.15	42.9	4	2	0.24	138.1	8	4	0.25	144.4	4	2	0.26	151.3	4	2	0.24	136.4
Fe3s	37.2	0.75	16	1	0.11	351.7	16	1	0.19	604.3	8	1	0.13	799.0	4	0.5	0.17	869.6	8	0.5	0.26	815.3
Ni3s	37.2	0.82	16	1	0.10	280.4	16	1	0.26	699.6	8	1	0.18	950.6	4	0.5	0.22	1158.	8	0.5	0.33	861.0
Si2p	37.2	0.89	16	1	0.12	349.9	16	1	0.13	379.0	8	1	0.05	274.0	4	0.5	0.05	285.7	8	0.5	0.08	218.0
B1s	36.0	0.49	64	2	0.14	322.4	16	0.5	0.20	479.0	16	1	0.16	545.3	8	0.5	0.19	602.2	8	0.5	0.20	948.0
C1s	34.7	1.00	8	2	0.33	2952.	8	0.5	0.24	529.0	4	1	0.22	1920.	4	0.5	0.19	844.8	8	1	0.19	844.
O1s	30.7	2.93	2	2	0.28	2871.	4	2	0.38	2037.	8	1	0.31	422	4	1	0.21	556.1	4	1	0.30	803.0
Ar2p	35.2	3.04	-	-	-	-	8	0.5	0.19	136.9	16	1	0.07	49.6	8	0.5	0.77	57.0	16	0.5	0.11	39.6

[1] $E = (eV)^{1/2}$

[2] σ in units of 20,000 barns

[3] N is the number of sweeps

[4] S is the digital scale in kilobytes, 1k.b=1024

[5] Ar = area. x 10^2 cm2

TABLE 3d.

CONCENTRATION OF THE WHEEL-SIDE AT 15°

							As rec.					5min. sputt.					15min. sputt					30min. sputt.					580°C heating				
ELEMENT	$\sqrt{E}_{kin.}$[1]	σ[2]	N[3]	S[4]	Ar[5]	n	N	S	Ar	n	N	S	Ar	n	N	S	Ar	n	N	S	Ar	n	N	S	Ar	n	N	S	Ar	n
Fe2p	27.7	16.4	64	4	0.29	31.4	8	2	0.51	218.8	8	4	0.51	438.6	8	4	0.40	340.0	8	2	0.29	128.2								
Ni2p	24.8	22.1	64	4	0.06	4.4	8	2	0.15	42.9	8	4	0.25	142.7	8	2	0.26	73.3	8	2	0.19	53.0								
Fe3s	37.2	0.75	64	1	0.07	55.9	16	0.5	0.15	239.8	16	0.5	0.29	455.6	16	0.5	0.14	183.8	32	0.5	0.27	215.8								
Ni3s	37.2	0.89	64	1	0.04	26.7	16	0.5	0.15	196.3	16	0.5	0.38	508.7	16	0.5	0.18	239.0	32	0.5	0.29	190.2								
Si2p	37.2	0.82	64	1	0.09	69.24	16	0.5	0.21	300.3	16	0.5	0.07	106.4	16	0.5	0.05	65.6	32	0.5	0.08	61.9								
B1s	36.01	0.49	64	0.5	0.08	49.9	16	0.5	0.12	277.4	32	2	0.13	588.0	16	0.5	0.05	125.6	16	0.5	0.15	343.7								
C1s	34.7	1.0	8	1	0.26	1173.	16	1	0.23	500.2	8	1	0.21	933.0	16	0.5	0.21	227.8	16	0.5	0.31	345.0								
C1s	30.7	2.93	8	1	0.38	518.8	13	4	0.41	1369.	8	0.5	0.35	235.2	16	0.5	0.20	67.2	16	0.5	0.26	342.0								
Ar2p	35.17	3.04	-	-	-	-	16	0.5	0.17	62.93	23	0.5	0.17	43.8	32	0.5	0.07	12.2	-	-	-	-								

[1] $\sqrt{E}$ = $(eV)^{\frac{1}{2}}$

[2] σ in units of 20,000barns

[3] N is the number of sweeps

[4] S is the digital scale in kilobytes 1k.b = 1024

[5] Ar = area $x10^2$ cm^2

TABLE 4a.

CONCENTRATION WITH RESPECT TO Fe CONCENTRATION OF THE TOP-SIDE.

	55°					15°				
ELEMENT	As rec.	5min. Sputt.	15min. Sputt.	30min. Sputt.	580°C heating	As rec.	5min. Sputt.	15min. Sputt.	30min. Sputt.	580°C heating
Fe	1	1	1	1	1	1	1	1	1	1
Ni	0.18	0.43	0.33	0.35	0.35	0.26	0.27	0.22	0.23	0.24
Si	7.18	0.34	0.30	0.35	1.03	2.50	0.41	0.35	0.39	0.43
B	8.96	0.76	1.19	1.03	6.50	3.42	0.77	1.25	1.52	2.35
C	113.20	6.00	2.57	1.50	9.15	14.14	2.79	1.68	0.86	1.75
O	54.29	1.84	0.67	0.59	7.70	16.50	0.71	0.32	0.35	1.90
Ar	-	0.15	0.07	0.05	0.06	-	0.22	0.11	0.19	0.11

TABLE 4b.

CONCENTRATION WITH RESPECT TO Fe CONCENTRATION OF THE WHEEL-SIDE.

	55°					15°				
ELEMENT	As rec.	5min. Sputt.	15min. Sputt.	30min. Sputt.	580°C heating	As rec.	5min. Sputt.	15min. Sputt.	30min Sputt.	580°C heating
Fe	1	1	1	1	1	1	1	1	1	1
Ni	0.14	0.19	0.32	0.21	0.41	0.19	0.25	0.22	0.22	0.26
Si	2.20	1.38	0.24	0.19	0.48	1.57	0.69	0.43	0.41	0.41
B	1.58	1.82	1.34	0.36	2.58	1.44	0.87	0.86	0.88	1.82
C	37.35	2.28	2.12	0.67	2.69	13.20	0.96	3.03	1.23	1.62
O	16.52	6.25	0.50	0.19	2.66	12.89	3.71	0.66	0.81	1.54
Ar	-	0.28	0.09	0.03	-	-	0.24	0.07	0.08	0.07

TABLE 5a.

CONCENTRATION IN % OF THE TOP-SIDE

	55°					15°				
ELEMENT	As rec.	5min. Sputt.	15min. Sputt.	30min. Sputt.	580°C heating	As rec.	5min. Sputt.	15min. Sputt.	30min. Sputt.	580°C heating
Fe	0.54	9.50	16.30	20.53	3.87	2.60	16.20	20.20	22.00	12.80
Ni	0.09	4.08	5.38	7.18	1.35	0.68	4.37	4.46	5.06	3.08
Si	3.85	3.23	4.89	7.18	3.99	6.60	6.60	7.09	8.5	5.5
B	4.84	7.22	19.40	21.14	25.2	9.00	12.40	25.35	33.50	30.20
C	61.25	57.00	41.90	30.80	35.40	37.40	45.20	34.00	18.90	22.20
O	29.30	17.49	10.90	12.10	29.80	43.60	11.50	6.40	7.7	24.40
Ar	-	1.42	1.14	1.02	0.23	-	3.56	2.23	4.10	1.30
$\sum R_i^*$	184.81	10.52	6.13	4.87	25.79	37.82	6.17	4.93	4.54	7.77

* SUM OF CONCENTRATIONS WITH RESPECT TO Fe CONCENTRATION.

TABLE 5b.

CONCENTRATION IN % OF THE WHEEL-SIDE.

	55°					15°				
ELEMENT	As rec.	5min. Sputt.	15min. Sputt.	30min. Sputt.	580°C heating	As rec.	5min. Sputt.	15min. Sputt.	30min. Sputt.	580°C heating.
Fe	1.70	7.75	17.50	37.70	10.10	3.30	12.90	15.50	21.50	14.80
Ni	0.23	1.43	5.70	7.92	4.13	0.63	3.24	3.50	4.75	3.80
Si	3.74	10.40	4.27	7.16	4.84	5.18	8.90	6.80	8.85	6.10
B	2.68	13.70	23.88	13.50	27.00	4.75	11.20	13.70	19.00	27.00
C	63.53	17.20	37.00	25.30	27.10	43.60	12.40	48.30	26.50	24.10
O	28.00	47.30	8.90	7.16	26.80	42.85	48.00	10.50	17.40	22.90
Ar	-	2.12	1.60	1.13	-	-	3.10	1.10	1.70	1.04
$\sum R_i^*$	58.74	13.20	5.61	2.65	9.92	31.29	7.72	6.27	4.63	6.72

* SUM OF CONCENTRATIONS WITH RESPECT TO Fe CONCENTRATION.

TABLE 6

CONCENTRATION IN % AT 55°

CONCENTRATION IN % AT 15°

	TOP-SIDE					WHEEL-SIDE				
ELEMENT	As rec.	Ar^+ 5min.	Ar^+ 15min.	Ar^+ 30min.	580°C heat.	As rec.	Ar^+ 5min.	Ar^+ 15min.	Ar^+ 30min.	580°C heat.
Ni	0.13	0.93	1.20	1.40	0.43	0.38	0.44	1.62	1.66	1.08
Fe	0.20	0.58	0.80	0.93	0.30	0.53	0.58	1.11	1.75	0.68
Si	0.58	0.48	0.69	0.84	0.72	0.74	1.22	0.62	0.80	0.79
B	0.53	0.58	0.76	0.63	0.83	0.58	1.22	1.74	0.71	1.00
C	1.63	1.26	1.23	1.62	1.59	1.50	1.38	0.76	0.95	1.12
O	0.67	1.52	1.70	1.66	1.22	0.68	0.98	0.84	0.41	1.17
Ar	-	0.40	0.51	0.24	0.17	-	0.68	1.45	0.66	-